Physical Solutions of the Nature of the Atom, Photon, and Their Interactions to Form Excited and Predicted Hydrino States

Randell L. Mills, BlackLight Power, Inc., 493 Old Trenton Road, Cranbury, NJ 08512

(609) 490-1090, rmills@blacklightpower.com, www.blacklightpower.com

Starting with the same essential physics as Bohr, Schrödinger, and Dirac of e^- moving in the Coulombic field of the proton and the wave equation as originally sought by Schrödinger, advancements in the understanding of the stability of the bound electron to radiation are applied to solve for the exact nature of the electron. Rather than using the postulated Schrödinger boundary condition: "$\Psi \to 0$ as $r \to \infty$", which leads to a purely mathematical model of the electron, the constraint is based on experimental observation. Using Maxwell's equations, *the classical wave equation is solved with the constraint that the bound* $n = 1$*-state electron cannot radiate energy*. Although it is well known that an accelerated *point* particle radiates, an *extended distribution* modeled as a superposition of accelerating charges does not have to radiate. A simple invariant physical model obeying the two-dimensional wave equation plus time arises naturally wherein the results are extremely straightforward, internally consistent, and predictive of conjugate parameters for the first time, requiring minimal math as in the case of the most famous exact equations (no uncertainty) of Newton, Maxwell, Einstein, de Broglie, and Planck on which the model is based. No new physics is needed; only the known physical laws based on direct observation are used. Together with the solution of the nature of the photon, many problems are solved uniquely and exactly in closed-form equations involving fundamental constants only such as the ionization energies of multielectron atoms, excited states of hydrogen

and helium, the anomalous magnetic moment of the electron, the Lamb Shift, the fine structure and hyperfine structure of the hydrogen atom, the hyperfine structure intervals of positronium and muonium, photon, inelastic electron scattering from helium, and the nature of the chemical bond. Beyond revealing the physics of known results, new states of the hydrogen atom are predicted in Sec. II that extend the Rydberg series to lower levels. A large body of experimental evidence supports the predictions.

Several departures from the nonphysical methodology of standard quantum mechanics (SQM) are used and some results arise that are missed or are not anticipated by critics [1] which are given in detail in this paper: (1) the nonradiation condition requires that the three-dimensional wave equation plus time be reduced to the two-dimensional wave equation plus time corresponding to a radial Dirac delta function; this boundary constraint was missed by a critic [1], and critic's errors [1] in this wave equation and analysis of the angular solutions were identified, (2) the electron is not a point-particle probability wave, rather it is a two-dimensional membrane of charge, mass, and current and the de Broglie wavelength arises from first principles rather than a postulated wave-particle duality; nothing is waving in contradiction to critic's misunderstanding [1], (3) in the bound state, the current is perpendicular to the radius such that it obeys the two-dimensional wave equation; yet it is relativistically invariant in contradiction to critic's claims [1], (4) using the solved two-dimensional nature of the electron, the radii and the energies of the n=1 and excited states of hydrogen atom are solved from a force balance between the field of the electron and that of the nucleus plus any photons of excited states in contradiction to critic's claims [1], (5) the central field of trapped photons given by Maxwell's equations that superimposes the proton's field can be positive or negative to increase as well as decrease the binding energy of the electron, respectively, (6) in contradiction to

critic's claims [1], the latter case corresponds to excited states wherein the central field is a reciprocal integer times that of the proton and the corresponding radii are each an integer times that of the n=1 state, and the former case corresponds to predicted hydrino states wherein the field is an integer times that of the proton and the corresponding radii are each a reciprocal integer times that of the n=1 state, and (7) based on Maxwell's equations, the excited states involve photons directly and the hydrino states require a first nonradiative energy transfer to a catalyst followed by a radiative or resonant energy transfer in contradiction to critic's speculation [1].

Key words: Maxwell's equations, nonradiation, quantum theory, special and general relativity, particle masses, cosmology, wave equation

I. Classical Quantum Theory of the Atom Based on Maxwell's Equations

In this paper, the old view that the electron is a zero or one-dimensional point in an all-space probability wave function $\Psi(x)$ is not taken for granted. The theory of classical quantum mechanics (CQM), derived from first principles, must successfully and consistently apply physical laws on all scales [2-11]. Stability to radiation was ignored by all past atomic models. Historically, the point at which SQM broke with classical laws can be traced to the issue of nonradiation of the one electron atom. Bohr just postulated orbits stable to radiation with the further postulate that the bound electron of the hydrogen atom does not obey Maxwell's equations—rather it obeys different physics [2-11]. Later physics was replaced by "pure mathematics" based on the notion of the inexplicable wave-particle duality nature of electrons which lead to the Schrödinger equation wherein the consequences of radiation predicted by Maxwell's equations were ignored. Ironically, Bohr, Schrödinger, and Dirac used the Coulomb potential, and Dirac used the vector potential of Maxwell's equations. But, all ignored electrodynamics and the corresponding radiative consequences. Dirac originally attempted to solve the bound electron physically with stability with respect to radiation according to Maxwell's equations with the further constraints that it was relativistically invariant and gave rise to electron spin [12]. He and many founders of QM such as Sommerfeld, Bohm, and Weinstein wrongly pursued a planetary model, were unsuccessful, and resorted to the current mathematical-probability-wave model that has many problems [2-11, 13-16]. Consequently, Feynman for example, attempted to use first principles including Maxwell's equations to discover new physics to replace quantum mechanics [17].

Physical laws may indeed be the root of the observations thought to be "purely quantum mechanical", and it may have been a mistake to make the assumption that Maxwell's

electrodynamic equations must be rejected at the atomic level. Thus, in the present approach, the classical wave equation is solved with the constraint that a bound $n=1$-state electron cannot radiate energy.

Herein, derivations consider the electrodynamic effects of moving charges as well as the Coulomb potential, and the search is for a solution representative of the electron wherein there is acceleration of charge motion without radiation. The mathematical formulation for zero radiation based on Maxwell's equations follows from a derivation by Haus [18]. The function that describes the motion of the electron must not possess spacetime Fourier components that are synchronous with waves traveling at the speed of light. Similarly, nonradiation is demonstrated based on the electron's electromagnetic fields and the Poynting power vector.

It was shown previously [2-7, 9-10] that CQM gives closed form solutions for the atom including the stability of the $n=1$ state and the instability of the excited states, the equation of the photon and electron in excited states, the equation of the free electron, and photon which predict the wave particle duality behavior of particles and light. The current and charge density functions of the electron may be directly physically interpreted. For example, spin angular momentum results from the motion of negatively charged mass moving systematically, and the equation for angular momentum, $\mathbf{r}\times\mathbf{p}$, can be applied directly to the wave function (a current density function) that describes the electron. The magnetic moment of a Bohr magneton, Stern Gerlach experiment, g factor, Lamb shift, resonant line width and shape, selection rules, correspondence principle, wave particle duality, excited states, reduced mass, rotational energies, and momenta, orbital and spin splitting, spin-orbital coupling, Knight shift, and spin-nuclear coupling, and elastic electron scattering from helium atoms, are derived in closed form equations based on Maxwell's equations. The calculations agree with experimental observations.

In contrast to the failure of the Bohr theory and the nonphysical, unpredictive, adjustable-parameter approach of quantum mechanics, multielectron atoms [3, 7] and the nature of the chemical bond [4, 7] are given by exact closed-form solutions containing fundamental constants only. Using the nonradiative wave equation solutions that describe each bound electron having conserved momentum and energy, the radii are determined from the force balance of the electric, magnetic, and centrifugal forces that correspond to the minimum of energy of the atomic or ionic system. The ionization energies are then given by the electric and magnetic energies at these radii. The spreadsheets to calculate the energies from exact solutions of one through twenty-electron atoms are available from the internet [19]. For 400 atoms and ions the agreement between the predicted and experimental results are remarkable. Other problems exactly solved as further tests of CQM are the anomalous magnetic moment of the electron, the Lamb Shift, the fine structure and hyperfine structure of the hydrogen atom, the hyperfine structure intervals of positronium and muonium. The agreement between observations and predictions based on closed-form equations with fundamental constants only matches to the limit permitted by the error in the measured fundamental constants.

The solution of the nature of the electron and photon for the first time also allow for exact solutions of excited states. For over 100 excited states of the helium atom, the r-squared value is 0.999994, and the typical average relative difference is about 5 significant figures which is within the error of the experimental data. Using only the Coulomb energy at the calculated radii, the agreement is remarkable. These results demonstrate the predictive power of CQM that further provides the nature of and conditions to form lower-energy states of hydrogen which is also based on electron-photon interactions. Extensive supporting data is reviewed.

A. One-Electron Atoms

The physics of numerous phenomena in electricity and magnetism, optics, celestial and orbital mechanics, heat, hydrodynamics, aerodynamics, elasticity, and others obey equations containing the Laplacian:

$$\nabla^2\phi = 0 \qquad \text{is Laplace's equation} \qquad (1)$$

$$\nabla^2\phi = \frac{1}{a^2}\frac{\delta^2\phi}{\delta t^2} \qquad \text{is the wave equation} \qquad (2)$$

$$\nabla^2\phi = \frac{1}{a^2}\frac{\delta\phi}{\delta t} \qquad \text{is the diffusion or heat-conduction equation} \qquad (3)$$

The time-dependent Schrödinger equation (SE) has the form of Eq. (3) and is not a true wave equation. The current standard quantum theory (SQM) based on the time dependent and time independent SE has many problems, is not based on physical laws, and is not predictive as discussed previously [6]. SQM has never dealt with the nature or structure of fundamental particles. They are treated as zero-dimensional points that occupy no volume and are everywhere at once. This view is impossible since occupying no volume would preclude their existence; the inherent infinities are not observed nor are they possible, and the possibility of a particle being everywhere at once violates all physical laws including conservation of energy and causality. Now, a physical approach is followed. Since the hydrogen atom is stable and nonradiative, the electron has constant energy. Furthermore, it is time dynamic. The wave equation is useful to describe orbiting bodies as well as electric and magnetic fields. It can

provide for conservation of energy and angular momentum. Thus, it is the logical choice to solve for the nature of the bound electron. Once the nature of the electron is solved, all problems involving electrons can be solved in principle. Thus, in the case of one-electron atoms, the electron radius, binding energy, and other parameters are solved after solving for the nature of the bound electron.

One-electron atoms include the hydrogen atom, He^{+}, Li^{2+}, Be^{3+}, and so on. The mass-energy and angular momentum of the electron are constant; this requires that the equation of motion of the electron be temporally and spatially harmonic. Thus, the classical wave equation applies and

$$\left[\nabla^2 - \frac{1}{v^2}\frac{\partial^2}{\partial t^2}\right]\rho(r,\theta,\phi,t) = 0 \tag{4}$$

where $\rho(r,\theta,\phi,t)$ is the time dependent charge density function of the electron in time and space, and v is the velocity of the charge-density wave. (It is shown *infra.* that the motion is azimuthal to the radius which constitutes an inertial frame that is relativistically invariant in contradiction to expectations [1].) In general, the wave equation has an infinite number of solutions. To arrive at the solution which represents the electron, a suitable boundary condition must be imposed. It is well known from experiments that each single atomic electron of a given isotope radiates to the same stable state. Thus, the physical boundary condition of nonradiation of the bound electron was imposed on the solution of the wave equation for the time dependent charge density function of the electron [2-7, 9-10]. The condition for radiation by a moving point charge given by Haus [18] is that its spacetime Fourier transform does possess components that are synchronous with waves traveling at the speed of light. Conversely, it is proposed that

the condition for nonradiation by an ensemble of moving point charges that comprises a current density function is

For non-radiative states, the current-density function must NOT possess spacetime Fourier components that are synchronous with waves traveling at the speed of light.

The time, radial, and angular solutions of the wave equation are separable. The motion is time harmonic with frequency ω_n. A constant angular function is a solution to the wave equation. Solutions of the Schrödinger wave equation comprising a radial function radiate according to Maxwell's equation as shown previously by application of Haus' condition [18]. In fact, it was found that any function which permitted radial motion gave rise to radiation. A radial function which does satisfy the boundary condition is a radial delta function:

$$f(r) = \frac{1}{r^2}\delta(r - r_n) \tag{5}$$

This function is not a radial solution of Eq. 4; rather, it defines a constant charge density on a spherical shell of a fixed radius, not yet determined, and Eq. (4) becomes the two-dimensional wave equation plus time with separable time and angular functions. Given time harmonic motion and a radial delta function, the relationship between an allowed radius and the electron wavelength is given by

$$2\pi r_n = \lambda_n \tag{6}$$

where the integer subscript n here and in Eq. (5) is *determined during photon absorption* as given in the Sec. I.L and the Excited States of the One-Electron Atom (Quantization) section of Ref. [7]. It is shown in these sections that the force balance between the electric fields of the

electron and proton plus any resonantly absorbed photons gives the result that $r_n = nr_1$ wherein n is an integer in an excited state.

a. Classical Physics of the de Broglie Relation

It is shown in the Free Electron section (Sec. I.X) that the free electron is a two-dimension lamina of charge with an azimuthal current with a corresponding angular momentum of $\hbar$. It is shown in Chp. 3 of Ref. [7] that the linear velocity of the free electron can be considered to be due to absorption of photons that excite surface currents corresponding to a decreased electron de Broglie wavelength:

$$\lambda_o = \frac{h}{m_e v_z} = 2\pi\rho_o \tag{7}$$

The relationship between the electron wavelength, it radius, ρ_0, and its linear velocity is

$$\frac{\lambda}{2\pi} = \rho_o = \frac{\hbar}{m_e v_z} = k^{-1} = \frac{v_z}{\omega_z} \tag{8}$$

In this case, the angular frequency ω_z is given by

$$\omega_z = \frac{\hbar}{m_e \rho_0^2} \tag{9}$$

which conserves the photon's angular momentum of $\hbar$ with that of the electron.

It is further shown [7] that the total energy, E_T, is given by the sum of the change in the free-electron translational kinetic energy, T, the rotational energy, E_{rot}, corresponding to the azimuthal current, and the potential energy, E_{mag}, due to a radiation reaction force $\mathbf{F}_{mag}$, the magnetic attractive force due to the relative azimuthal current motion:

$$
\begin{aligned}
E_T &= T + E_{rot} + E_{mag} \\
&= \frac{1}{2}\frac{\hbar^2}{m_e\rho_0^2} + \frac{5}{4}\frac{\hbar^2}{m_e\rho_0^2} - \frac{5}{4}\frac{\hbar^2}{m_e\rho_0^2} \\
&= \frac{1}{2}\frac{\hbar^2}{m_e\rho_0^2}
\end{aligned}
\tag{10}
$$

Thus, the total energy, E_T, of the excitation of a free-electron transitional state by a photon having $\hbar$ of angular momentum and an energy given by Planck's equation of $\hbar\omega$ is

$$
E_T = T = \frac{1}{2}m_e v_z^2 = \frac{1}{2}\frac{h^2}{m_e\lambda^2} = \frac{1}{2}\hbar\omega_z \tag{11}
$$

where λ is the de Broglie wavelength. The angular momentum of the free electron of $\hbar$ is unchanged. The energies in the currents in the plane lamina are balanced so that the total energy is unchanged. The radius ρ_0 decrease to match the de Broglie wavelength and frequency at an increased velocity. At this velocity, the kinetic energy matches the energy provided by the photon wherein the de Broglie frequency matches the photon frequency and both the electron-kinetic energy and the photon energy are given by Planck's equation.

The correspondence principle is the basis of the de Broglie wavelength relationship. The de Broglie relationship is not an independent fundamental property of matter in conflict with physical laws as formalized in the wave-particle-duality-related postulates of quantum mechanics and the corresponding Schrödinger wave equation. The Stern-Gerlach experimental results and the double-slit interference pattern of electrons are also predicted classically [7]. A simulation is given at Ref [19].

Furthermore, the free electron is equivalent to a continuum excited state with conservation of the parameters of the bound electron. Thus, the de Broglie relationship applied to the bound electron is again due to conservation of the free electron's angular momentum of $\hbar$.

Using the classically predicted and experimentally confirmed de Broglie relationship for the electron mass where the coordinates are spherical,

$$\lambda_n = \frac{h}{p_n} = \frac{h}{m_e v_n} \tag{12}$$

and the magnitude of the velocity for *every* point on the orbitsphere is

$$v_n = \frac{\hbar}{m_e r_n} \tag{13}$$

The sum of the $|\mathbf{L}_i|$, the magnitude of the angular momentum of each infinitesimal point of the orbitsphere of mass m_i, must be constant. The constant is $\hbar$.

$$\sum |\mathbf{L}_i| = \sum |\mathbf{r} \times m_i \mathbf{v}| = m_e r_n \frac{\hbar}{m_e r_n} = \hbar \tag{14}$$

Thus, a bound electron is a constant two-dimensional spherical surface of charge (zero thickness and total charge = $-e$), called *an electron orbitsphere shown in Figure 1, that can exist in a bound state at only specified distances from the nucleus determined by an energy minimum for the n=1 states and integer multiples of this radius due to the action of resonant photons as shown in Secs. I.I and I.L, respectively*.

It is well known that the field of a spherical shell of charge is zero inside the shell and that of a point charge at the origin outside the shell [20]. See Figure 2. The corresponding uniform current function which gives rise to the phenomenon of *spin* is derived in the Spin Function section (Sec. I.B). (See the Orbitsphere Equation of Motion for $\ell = 0$ of Ref. [7] at Chp. 1.)

Nonconstant functions are also solutions for the angular functions. To be a harmonic

solution of the wave equation in spherical coordinates, these angular functions must be spherical harmonic functions [21]. A zero of the spacetime Fourier transform of the product function of two spherical harmonic angular functions, a time harmonic function, and an unknown radial function is sought. The solution for the radial function which satisfies the boundary condition is also a delta function given by Eq. (5). Thus, bound electrons are described by a charge-density (mass-density) function which is the product of a radial delta function, two angular functions (spherical harmonic functions), and a time harmonic function.

$$\rho(r,\theta,\phi,t) = f(r)A(\theta,\phi,t) = \frac{1}{r^2}\delta(r-r_n)A(\theta,\phi,t); \qquad A(\theta,\phi,t) = Y(\theta,\phi)k(t) \tag{15}$$

In these cases, the spherical harmonic functions correspond to a traveling charge density wave confined to the spherical shell which gives rise to the phenomenon of orbital angular momentum. The orbital functions which modulate the constant "spin" function shown graphically in Figure 3 are given in the Sec. I.H.

B. Spin Function

It is known from the Stern-Gerlach experiment that a beam of silver atoms is split into two components when passed through an inhomogeneous magnetic field. This implies that the electron is a spin 1/2 particle with an intrinsic angular momentum in the direction of the applied field (spin axis) of $\pm\frac{\hbar}{2}$, and the magnitude of the angular momentum vector which precesses about the spin axis is $\sqrt{\frac{3}{4}}\hbar$. Furthermore, the magnitude of the splitting implies a magnetic moment of μ_B, a full Bohr magneton, given by Eq. (50) corresponding to $\hbar$ of total angular momentum on the axis of the applied field. Thus, the electron has a measured magnetic field and

corresponding magnetic moment of a Bohr magneton and behaves as a spin 1/2 particle or fermion. For any magnetic field, the solution for the corresponding current from Maxwell's equations is unique. Thus, the electron field requires a unique current according to Maxwell's equations that matches the boundary condition imposed by the results of the Stern-Gerlach experiment.

The algorithm to generate the spin function designated as $Y_0^0(\theta,\phi)$ (part of Eqs. (30-31)) and called the electron orbitsphere is developed in this section. The magnitude of the angular momentum over the orbitsphere must be constant. The constant is $\hbar$ as given by Eq. (14). It is shown in this section that the projection of the intrinsic orbitsphere angular momentum onto the spin axis is $\pm\frac{\hbar}{2}$, and the projection onto **S**, the axis which precesses about the spin axis, is $\hbar$ with a precessing component in the perpendicular plane of $\sqrt{\frac{3}{4}}\hbar$ and a component on the spin axis of $\pm\frac{\hbar}{2}$. Thus, the mystery of an intrinsic angular momentum of $\pm\frac{\hbar}{2}$ and a total angular momentum in a resonant radio frequency (RF) experiment of $\mathbf{L_z} = \hbar$ is resolved since the sum of the intrinsic and spin-axis projection of the precessing component is $\hbar$. The Stern-Gerlach experiment implies a magnetic moment of one Bohr magneton and an associated angular momentum quantum number of 1/2. Historically, this quantum number is called the spin quantum number, s ($s = \frac{1}{2};\ m_s = \pm\frac{1}{2}$), and that designation is maintained.

The orbitsphere spin function comprises a constant charge (current) density function with moving charge confined to a two-dimensional spherical shell. The magnetostatic current pattern of the orbitsphere spin function comprises an infinite series of correlated orthogonal great circle

current loops wherein each point charge (current) density element moves time harmonically with constant angular velocity

$$\omega_n = \frac{\hbar}{m_e r_n^2} \tag{16}$$

The uniform current density function $Y_0^0(\theta,\phi)$ that gives rise to the spin of the electron is generated from a basis set current-vector field defined as the orbitsphere current-vector field ("orbitsphere-cvf"). The orbitsphere-cvf comprises a continuum of correlated orthogonal great circle current loops. The current pattern comprising two components is generated over the surface by two sets (*Steps One and Two*) of rotations of two orthogonal great circle current loops that serve as basis elements about each of the $\left(\mathbf{i_x}, \mathbf{i_y}, 0\mathbf{i_z}\right)$ and $\left(-\frac{1}{\sqrt{2}}\mathbf{i_x}, \frac{1}{\sqrt{2}}\mathbf{i_y}, \mathbf{i_z}\right)$-axes, respectively, by π radians. In Appendix III of Ref. [7], the *continuous* uniform electron current density function $Y_0^0(\theta,\phi)$ having the same angular momentum components as that of the orbitsphere-cvf is then exactly generated from this orbitsphere-cvf as a basis element by a convolution operator comprising an autocorrelation-type function.

The orthogonal great circle basis set for Step One is shown in Figure 4. One half of the orbitsphere-cvf, the orbitsphere-cvf component of STEP ONE, is generated by the rotation of two orthogonal great circles about the $\left(\mathbf{i_x}, \mathbf{i_y}, 0\mathbf{i_z}\right)$-axis by π wherein one basis-element great circle initially is initially in the yz-plane and the other is in the xz-plane:

Step One

$$\begin{bmatrix} x' \\ y' \\ z' \end{bmatrix} = \begin{bmatrix} \frac{1}{2}+\frac{\cos\theta}{2} & \frac{1}{2}-\frac{\cos\theta}{2} & -\frac{\sin\theta}{\sqrt{2}} \\ \frac{1}{2}-\frac{\cos\theta}{2} & \frac{1}{2}+\frac{\cos\theta}{2} & \frac{\sin\theta}{\sqrt{2}} \\ \frac{\sin\theta}{\sqrt{2}} & -\frac{\sin\theta}{\sqrt{2}} & \cos\theta \end{bmatrix} \bullet \left(\begin{bmatrix} 0 \\ r_n \cos\phi \\ r_n \sin\phi \end{bmatrix} + \begin{bmatrix} r_n \cos\phi \\ 0 \\ r_n \sin\phi \end{bmatrix} \right) \tag{17}$$

The first component of the orbitsphere-cvf given by Eq. (17) can also be generated by each of rotating a great circle basis element initially in the yz or the xz-planes about the $\left(\mathbf{i}_x, \mathbf{i}_y, 0\mathbf{i}_z\right)$-axis by 2π radians as shown in Figures 5 and 6, respectively.

The orthogonal great circle basis set for Step Two is shown in Figure 7. The second half of the orbitsphere-cvf, the orbitsphere-cvf component of STEP TWO, is generated by the rotation of two orthogonal great circles about the $\left(-\frac{1}{\sqrt{2}}\mathbf{i}_x, \frac{1}{\sqrt{2}}\mathbf{i}_y, \mathbf{i}_z\right)$-axis by π wherein one basis-element great circle is initially in the plane that bisects the xy-quadrant and is parallel to the z-axis and the other is in the xy-plane:

Step Two

$$\begin{bmatrix} x' \\ y' \\ z' \end{bmatrix} = \begin{bmatrix} \frac{1}{4}\left(1+3\cos\theta\right) & \frac{1}{4}\left(-1+\cos\theta+2\sqrt{2}\sin\theta\right) & \frac{1}{4}\left(-\sqrt{2}+\sqrt{2}\cos\theta-2\sin\theta\right) \\ \frac{1}{4}\left(-1+\cos\theta-2\sqrt{2}\sin\theta\right) & \frac{1}{4}\left(1+3\cos\theta\right) & \frac{1}{4}\left(\sqrt{2}-\sqrt{2}\cos\theta-2\sin\theta\right) \\ \frac{1}{2}\left(\frac{-1+\cos\theta}{\sqrt{2}}+\sin\theta\right) & \frac{1}{4}\left(\sqrt{2}-\sqrt{2}\cos\theta+2\sin\theta\right) & \cos^2\frac{\theta}{2} \end{bmatrix}$$
$$\bullet \left(\begin{bmatrix} \frac{r_n\cos\phi}{\sqrt{2}} \\ \frac{r_n\cos\phi}{\sqrt{2}} \\ r_n\sin\phi \end{bmatrix} + \begin{bmatrix} r_n\cos\phi \\ r_n\sin\phi \\ 0 \end{bmatrix} \right) \tag{18}$$

The second component of the orbitsphere-cvf given by Eq. (18) can also be generated by each of rotating a great circle basis element that is initially in the plane that bisects the xy-quadrant and is parallel to the z-axis or is in the xy-plane about the $\left(-\frac{1}{\sqrt{2}}\mathbf{i}_x, \frac{1}{\sqrt{2}}\mathbf{i}_y, \mathbf{i}_z\right)$-axis by 2π radians as shown in Figures 8 and 9, respectively.

The orbitsphere-cvf is given by the superposition of the components from Step One and from Step Two. The current pattern of the orbitsphere-cvf generated by the rotations of the orthogonal great circle current loops is a continuous and total coverage of the spherical surface, but it is shown as visual representations using 6 degree increments θ in Figures 10A-C.

a. Angular Momentum Projections of the Orbitsphere Current-Vector Field

Due to the resulting self dot product with the convolution to form $Y_0^0(\theta,\phi)$, the total of each projection, $\mathbf{L}_{xy}$ and $\mathbf{L}_z$, is the integral as a function of θ of the magnitude of the resultant vector of the two orthogonal angular momentum component vectors corresponding to the two

orthogonal great circles. For Step One, the vector projection of the angular momentum onto the xy-plane is given by sum of the vector contributions from each great circle:

$$\begin{aligned}\mathbf{L}_{xy} &= \sqrt{\frac{2}{\pi}\int_0^{\frac{\pi}{2}}\left[\frac{\hbar}{4}\cos\theta\right]^2+\left[\frac{\hbar}{4}\cos\theta\right]^2 d\theta} - \sqrt{\frac{2}{\pi}\int_{\frac{\pi}{2}}^{\pi}\left[\frac{\hbar}{4}\cos\theta\right]^2+\left[\frac{\hbar}{4}\cos\theta\right]^2 d\theta} \\ &= \frac{\hbar}{2\sqrt{2}}\ \frac{1}{\sqrt{2}} - \frac{\hbar}{2\sqrt{2}}\ \frac{1}{\sqrt{2}} = 0\end{aligned} \tag{19a}$$

where each angular integral is normalized by, $\frac{\pi}{2}$, the angular range of θ. Similarly, the vector projection of the angular momentum onto the z-axis as shown in Figure 11 is

$$\mathbf{L}_z = \sqrt{\frac{1}{\pi}\int_0^{\pi}\left[\frac{\hbar}{4}\sin\theta\right]^2+\left[\frac{\hbar}{4}\sin\theta\right]^2 d\theta} = \frac{\hbar}{2\sqrt{2}}\ \frac{1}{\sqrt{2}} = \frac{\hbar}{4} \tag{19b}$$

where each angular integral is normalized by, π, the angular range of θ. Thus, from the initial $\frac{\hbar}{4}$ of angular momentum along each of the x and y-axes, $\frac{\hbar}{4}$ canceled in the xy-plane and $\frac{\hbar}{4}$ was projected onto the z-axis as the angular momentum was spread over one half of the surface of the sphere with Step One.

For Step Two, the orthogonal great-circle basis set rotates about the $\left(-\frac{1}{\sqrt{2}}\mathbf{i}_x, \frac{1}{\sqrt{2}}\mathbf{i}_y, \mathbf{i}_z\right)$-axis. The resultant angular momentum vector of the orthogonal great circle current loops of magnitude $\frac{\hbar}{2\sqrt{2}}$ of Step Two (black vector) is stationary since it is along the $\left(-\frac{1}{\sqrt{2}}\mathbf{i}_x, \frac{1}{\sqrt{2}}\mathbf{i}_y, \mathbf{i}_z\right)$-axis. Thus, the projections of the resultant vector for Step Two are the constant initial projections of

$$\mathbf{L}_{xy} = \frac{\hbar}{4} \tag{20a}$$

and

$$\mathbf{L}_{z} = \frac{\hbar}{4} \tag{20b}$$

The total vector projection of the angular momentum onto the xy-plane given by the sum of Eqs. (19a) and (20a) is

$$\mathbf{L}_{xy} = 0 + \frac{\hbar}{4} = \frac{\hbar}{4} \tag{21}$$

The total vector projection of the angular momentum into the z-axis given by the sum of Eqs. (19b) and (20b) is

$$\mathbf{L}_{z} = \frac{\hbar}{4} + \frac{\hbar}{4} = \frac{\hbar}{2} \tag{22}$$

The current pattern gives rise to the phenomenon corresponding to the spin quantum number. The details of the derivation of the spin function are given in Ref. [2] and Chp. 1 of Ref. [7].

b. Convolution Operator

The resultant angular momentum projections of $\mathbf{L}_{xy} = \frac{\hbar}{4}$ and $\mathbf{L}_{z} = \frac{\hbar}{2}$ meet the boundary condition for the unique current having an angular velocity magnitude at each point on the surface given by Eq. (13) and give rise to the Stern Gerlach experiment as shown in Ref. [7]. The further constraint that the current density is uniform such that the charge density is uniform, corresponding to an equipotential, minimum energy surface is satisfied by using the orbitsphere-cvf as a basis element to generate $Y_0^0(\theta,\phi)$ using a convolution operator as given in Appendix III of Ref. [7]. The orbitsphere-cvf comprises two components corresponding to each of STEP

ONE and STEP TWO. The convolution operator comprises an autocorrelation-type function that that treats each component defined as a primary component corresponding to STEPS ONE and TWO separately and results in the replacement of each great circle of the primary component orbitsphere-cvf with a secondary component orbitsphere-cvf of matching angular momentum, orientation, and phase. The convolution is given by rotating a matched basis-element secondary about the same axis as that which generated the primary from the basis-element current loop to exactly give rise to a spherically-symmetric uniform current density. The superposition of the two resulting uniform densities gives $Y_0^0(\theta,\phi)$. The resulting exact uniform current distribution has the same angular momentum distribution, resultant, $\mathbf{L_R}$, and components of $\mathbf{L}_{xy} = \frac{\hbar}{4}$ and $\mathbf{L}_z = \frac{\hbar}{2}$.

As shown in Appendix III of Ref. 3, STEP TWO can be generated by a 2π-rotation of a single basis-element current loop about the $\left(-\frac{1}{\sqrt{2}}\mathbf{i_x}, \frac{1}{\sqrt{2}}\mathbf{i_y}, \mathbf{i_z}\right)$-axis or a π-rotation of two orthogonal current loops such that the angular momentum vector is stationary on the $\left(-\frac{1}{\sqrt{2}}\mathbf{i_x}, \frac{1}{\sqrt{2}}\mathbf{i_y}, \mathbf{i_z}\right)$-axis as the component orbitsphere-cvf is generated. In the general case that the resultant angular momentum of each pair of orthogonal great circle current loops of the component orbitsphere-cvf is along the 2π-rotational axis (defined as the rotational axis which generates the component orbitsphere-cvf from a basis-element great circle), a secondary nth component orbitsphere-cvf can serve as a basis element to match the angular momentum of any given nth great circle of a primary component orbitsphere-cvf. The replacement of each great circle of the primary orbitsphere-cvf with a secondary orbitsphere-cvf of matching angular

momentum, orientation, and phase comprises an autocorrelation-type function that exactly gives rise to the spherically-symmetric current density, $Y_0^0(\theta,\phi)$.

The orbitsphere-cvf comprises the superposition or sum of the components corresponding to STEP ONE and STEP TWO. Thus, the convolution is performed on each component designated a primary component. The convolution of a secondary component orbitsphere-cvf element with the each great circle current loop of each primary orbitsphere-cvf is designated as the convolution operator, $A(\theta,\phi)$, given by

$$\begin{aligned} A(\theta,\phi) &= \frac{1}{2r_n^2}\lim_{\Delta\theta_2\to 0}\sum_{m'=1}^{m'=\frac{2\pi}{|\Delta\theta_2|}}\lim_{\Delta\theta_1\to 0}\sum_{m=1}^{m=\frac{2\pi}{|\Delta\theta_1|}} 2°O(\theta,\phi)\otimes\begin{pmatrix}1°_1 O(\theta,\phi)\delta(\theta-m\Delta\theta_1,\phi-\phi')\\ +1°_2 O(\theta,\phi)\delta(\theta-m'\Delta\theta_2,\phi-\phi'')\end{pmatrix} \\ &= \frac{1}{2r_n^2}\lim_{\Delta\theta_2\to 0}\sum_{m'=1}^{m'=\frac{2\pi}{|\Delta\theta_2|}}\lim_{\Delta\theta_1\to 0}\sum_{m=1}^{m=\frac{2\pi}{|\Delta\theta_1|}} 2°O(\theta,\phi)\otimes\begin{pmatrix}GC_{STEPONE}(m\Delta\theta_1,\phi')\\ +GC_{STEPTWO}(m'\Delta\theta_2,\phi'')\end{pmatrix} \end{aligned} \tag{23}$$

wherein (1) the secondary component orbitsphere-cvf that is matched to the basis element of the primary is defined by the symbol $2°O(\theta,\phi)$, (2) the primary component orbitsphere-cvf of STEP M is defined by the symbol $1°_M O(\theta,\phi)$, (3) each rotated great circle of the primary component orbitsphere-cvf of STEP M is selected by the Dirac delta function $\delta(\theta-m\Delta\theta_M,\phi-\phi',)$; the product $1°_M O(\theta,\phi)\delta(\theta-m\Delta\theta_M,\phi-\phi')$ is zero except for the great circle at the angle $\theta=m\Delta\theta_M$ about the 2π-rotational axis; each selected great circle having $0\le\phi'\le 2\pi$ is defined by $GC_{STEPM}(m\Delta\theta_M,\phi')$, and (4) $\frac{1}{2r_n^2}$ is the normalization constant. In Eq. (23), the angular momentum of each secondary component orbitsphere-cvf is equal in magnitude and direction as that of the current loop with which it is convolved. With the magnitude of the angular momentum of the secondary component orbitsphere-cvf matching that

of the current loop which it replaces during the convolution and the loop then serving as a unit vector, the angular momentum self dot product resulting from the convolution operation is inherently normalized to that of the primary component orbitsphere-cvf.

The convolution of a sum is the sum of the convolutions. Thus, the convolution operation may be performed on each of STEP ONE and STEP TWO separately, and the result may be superposed in terms of the current densities and angular momenta. Factoring out the secondary component orbitsphere-cvf which is a constant at each position of $GC_{STEPM}\left(m\Delta\theta_M,\phi'\right)$ gives

$$A(\phi,\theta)=\frac{1}{2r_n^2}2°O(\theta,\phi)\left(\begin{array}{l}\lim\limits_{\Delta\theta_2\to 0}\sum\limits_{m'=1}^{m'=\frac{2\pi}{|\Delta\theta_2|}} GC_{STEPONE}\left(m\Delta\theta_1,\phi'\right)\\ +\lim\limits_{\Delta\theta_1\to 0}\sum\limits_{m=1}^{m=\frac{2\pi}{|\Delta\theta_1|}} GC_{STEPTWO}\left(m'\Delta\theta_2,\phi''\right)\end{array}\right) \tag{24}$$

The summation is the operator that generates the primary component orbitsphere-cvf of STEP M, $1°_M O(\theta,\phi)$. Thus, the current-density function is given by the dot product of each primary orbitsphere-cvf with itself. The result is the scalar sum of the square of each of the STEP ONE and STEP TWO primary component orbitsphere-cvfs:

$$A(\theta,\phi)=\frac{1}{2r_n^2}\left(\left(1°_1 O(\theta,\phi)\right)^2+\left(1°_2 O(\theta,\phi)\right)^2\right) \tag{25}$$

where the dot-product scalar is valid over the entire spherical surface. The orbitsphere-cvf squared given in Eq. (25) is the equation of a uniform sphere. The superposition of the uniform distributions from STEP ONE and STEP TWO is the exact uniform current density function $Y_0^0(\theta,\phi)$ that is an equipotential, minimum energy surface shown in Figure 12. The angular

momentum is identically $\mathbf{L}_{xy} = \frac{\hbar}{4}$ and $\mathbf{L}_z = \frac{\hbar}{2}$ given by Eqs. (21-22).

c. STEP-ONE Matrices to Visualize the Currents of $Y_0^0(\phi,\theta)$

Consider the case that the STEP-ONE primary component orbitsphere-cvf is given by Eq. (17). The yz-plane great circle current loop that served as a basis element that was initially in the yz-plane is shown as red. The current is counterclockwise; thus, the angular momentum is along the x-axis. The secondary component orbitsphere-cvf shown in Figure 13 that is matched for angular momentum, orientation, and phase is given the matrix:

$$\begin{bmatrix} x' \\ y' \\ z' \end{bmatrix} = \begin{bmatrix} \cos\left(\frac{\pi}{4}\right) & -\sin\left(\frac{\pi}{4}\right) & 0 \\ \sin\left(\frac{\pi}{4}\right)\cos\theta & \cos\left(\frac{\pi}{4}\right)\cos\theta & \sin\theta \\ -\sin\left(\frac{\pi}{4}\right)\sin\theta & -\cos\left(\frac{\pi}{4}\right)\sin\theta & \cos\theta \end{bmatrix} \begin{bmatrix} 0 \\ r_n\cos\phi \\ r_n\sin\phi \end{bmatrix} \tag{26}$$

The secondary component orbitsphere-cvf is aligned on the yz-plane and the resultant angular momentum vector, $\mathbf{L_R}$, is also along the x-axis.

Then, the uniform current distribution is given from Eq. (23) as a infinite sum of the convolved elements comprising the secondary component orbitsphere-cvf given by Eq. (26) rotated according to Eq. (17), the matrix which generated the primary component orbitsphere-cvf. The resulting constant function is exact as given by Eq. (25). A representation (Figure 14) that shows the current elements can be generated by showing the basis-element secondary component orbitsphere-cvf as a sum of N great circles using Eq. (26) and by showing the continuous convolution as a sum of M discrete incremental rotations of the position of the

secondary component orbitsphere-cvf about the $\left(\mathbf{i}_x, \mathbf{i}_y, 0\mathbf{i}_z\right)$-axis using Eq. (23):

$$\begin{bmatrix} x' \\ y' \\ z' \end{bmatrix} = \sum_{m=1}^{m=M} \begin{bmatrix} \frac{1}{2} + \frac{\cos\left(\frac{m2\pi}{M}\right)}{2} & \frac{1}{2} - \frac{\cos\left(\frac{m2\pi}{M}\right)}{2} & -\frac{\sin\left(\frac{m2\pi}{M}\right)}{\sqrt{2}} \\ \frac{1}{2} - \frac{\cos\left(\frac{m2\pi}{M}\right)}{2} & \frac{1}{2} + \frac{\cos\left(\frac{m2\pi}{M}\right)}{2} & \frac{\sin\left(\frac{m2\pi}{M}\right)}{\sqrt{2}} \\ \frac{\sin\left(\frac{m2\pi}{M}\right)}{\sqrt{2}} & -\frac{\sin\left(\frac{m2\pi}{M}\right)}{\sqrt{2}} & \cos\left(\frac{m2\pi}{M}\right) \end{bmatrix}$$

$$\bullet \sum_{n=1}^{n=N} \begin{bmatrix} \cos\left(\frac{\pi}{4}\right) & -\sin\left(\frac{\pi}{4}\right) & 0 \\ \sin\left(\frac{\pi}{4}\right)\cos\left(\frac{n2\pi}{N}\right) & \cos\left(\frac{\pi}{4}\right)\cos\left(\frac{n2\pi}{N}\right) & \sin\left(\frac{n2\pi}{N}\right) \\ -\sin\left(\frac{\pi}{4}\right)\sin\left(\frac{n2\pi}{N}\right) & -\cos\left(\frac{\pi}{4}\right)\sin\left(\frac{n2\pi}{N}\right) & \cos\left(\frac{n2\pi}{N}\right) \end{bmatrix} \begin{bmatrix} 0 \\ r_n \cos\phi \\ r_n \sin\phi \end{bmatrix} \tag{27}$$

The similar result for STEP TWO is superimposed on that of STEP ONE wherein the uniform distribution is normalized.

C. Angular Functions

The time, radial, and angular solutions of the wave equation are separable. Also based on the radial solution, the angular charge and current-density functions of the electron, $A(\theta,\phi,t)$, must be a solution of the wave equation in two dimensions (plus time),

$$\left[\nabla^2 - \frac{1}{v^2}\frac{\partial^2}{\partial t^2}\right] A(\theta,\phi,t) = 0 \tag{28}$$

where $\rho(r,\theta,\phi,t) = f(r)A(\theta,\phi,t) = \frac{1}{r^2}\delta(r-r_n)A(\theta,\phi,t)$ and $A(\theta,\phi,t) = Y(\theta,\phi)k(t)$

$$\left[\frac{1}{r^2\sin\theta}\frac{\partial}{\partial\theta}\left(\sin\theta\frac{\partial}{\partial\theta}\right)_{r,\phi} + \frac{1}{r^2\sin^2\theta}\left(\frac{\partial^2}{\partial\phi^2}\right)_{r,\theta} - \frac{1}{v^2}\frac{\partial^2}{\partial t^2}\right]A(\theta,\phi,t) = 0 \tag{29}$$

where v is the linear velocity of the electron[1]. The charge-density functions including the time-function factor are

$\ell = 0$

$$\rho(r,\theta,\phi,t) = \frac{e}{8\pi r^2}[\delta(r-r_n)]\left[Y_0^0(\theta,\phi) + Y_\ell^m(\theta,\phi)\right] \tag{30}$$

$\ell \neq 0$

$$\rho(r,\theta,\phi,t) = \frac{e}{4\pi r^2}[\delta(r-r_n)]\left[Y_0^0(\theta,\phi) + \mathrm{Re}\left\{Y_\ell^m(\theta,\phi)e^{i\omega_n t}\right\}\right] \tag{31}$$

where $Y_\ell^m(\theta,\phi)$ are the spherical harmonic functions that spin about the z-axis with angular

---

[1] Eq. (31) is a solution to the two-dimensional wave equation plus time as shown in Box 1.1 of Ref. [7]. Rathke is in error by giving the two-dimensional wave equation as

$$\left[\frac{1}{r^2}\Delta_{\theta,\phi} + \frac{1}{v^2}\frac{\partial^2}{\partial t^2}\right]A(\theta,\phi,t) = 0 \tag{FN1.1}$$

at his Eq. (9) of Ref. [1] (the sign before the second term should be negative). The correct form is given in the cited reference 24. His subsequent statements regarding incurable flaws and inconsistencies in CQM are consequently also in error and misplaced.

frequency ω_n with $Y_0^0(\theta,\phi)$ the constant function. $\mathrm{Re}\left\{Y_\ell^m(\theta,\phi)e^{i\omega_n t}\right\} = P_\ell^m(\cos\theta)\cos\left(m\phi+\omega_n' t\right)$ where to keep the form of the spherical harmonic as a traveling wave about the z-axis, $\omega_n' = m\omega_n$.

D. Acceleration without Radiation

a. Special Relativistic Correction to the Electron Radius for Motion on a Great Circle

The electron moves in an orbit relative to the laboratory frame. Muons and electrons are both leptons. Time dilation of muonic decay due to relativistic motion in a cyclotron orbit relative to a stationary laboratory frame provides strong confirmation of special relativity and confirms that the electron's frame is an inertial frame. eB/m bunching of electrons in a gyrotron [22] occurs because the cyclotron frequency is inversely proportional to the relativistic electron mass. This further demonstrates that the electron frame is an inertial frame and that electron mass and time dilation occur. The special relativistic relationship in polar coordinates is derived. The result of the treatment of the electron motion relative to the laboratory frame is in excellent agreement with numerous experimental observables such as the electron g factor, the invariance of the electron magnetic moment of μ_B and angular momentum of $\hbar$, the Lamb shift, the fine structure and hyperfine structure of the hydrogen atom, the hyperfine structure intervals of positronium and muonium and the relativistically corrected ionization energies of one and two electron atoms given previously [3, 5-6], *infra*., and in the Chp. 1 (Determination of Orbitsphere Radii, Energy Calculations, Special Relativistic Correction to the Ionization Energies sections), Chp. 2 (Excited States of the One-Electron Atom (Quantization)) and Chp. 7 (The Two-Electron Atom) of Ref. [7].

The relationship between the electron wavelength and its radius is given by Eq. (6) where λ is the de Broglie wavelength. For each current density element of the spin function, the distance along each great circle in the direction of instantaneous motion undergoes length contraction and time dilation. Using a phase matching condition, the wavelengths of the electron and laboratory inertial frames are equated, and the corrected radius is given by

$$r_n = r_n^{'}\left[\sqrt{1-\left(\frac{v}{c}\right)^2}\,\sin\left[\frac{\pi}{2}\left(1-\left(\frac{v}{c}\right)^2\right)^{3/2}\right]+\frac{1}{2\pi}\cos\left[\frac{\pi}{2}\left(1-\left(\frac{v}{c}\right)^2\right)^{3/2}\right]\right] \tag{32}$$

where the electron velocity is given by Eq. (13). (See Ref. [7] Chp. 1, Special Relativistic Correction to the Ionization Energies section). $\frac{e}{m_e}$ of the electron, the electron angular momentum of $\hbar$, and μ_B are invariant, but the mass and charge densities increase in the laboratory frame due to the relativistically contracted electron radius. As $v \to c$, $r/r' \to \frac{1}{2\pi}$ and $r = \lambda$ as shown in Figure 15.

b. Nonradiation Based on the Spacetime Fourier Transform of the Electron Current

The Fourier transform of the electron charge density function given by Eq. (15) is a solution of the three-dimensional wave equation in frequency space ($\mathbf{k}, \omega$ *space*) as given in Chp 1, Spacetime Fourier Transform of the Electron Function section of Ref. [7]. Then the corresponding Fourier transform of the current density function $K(s,\Theta,\Phi,\omega)$ is given by multiplying by the constant angular frequency.

$$K(s,\Theta,\Phi,\omega) = 4\pi\omega_n \frac{\sin(2s_n r_n)}{2s_n r_n} \otimes 2\pi \sum_{\upsilon=1}^{\infty} \frac{(-1)^{\upsilon-1}\left(\pi \sin\Theta\right)^{2(\upsilon-1)}}{(\upsilon-1)!(\upsilon-1)!} \frac{\Gamma\left(\frac{1}{2}\right)\Gamma\left(\upsilon+\frac{1}{2}\right)}{\left(\pi\cos\Theta\right)^{2\upsilon+1} 2^{\upsilon+1}} \frac{2\upsilon!}{(\upsilon-1)!} s^{-2\upsilon}$$
$$\otimes 2\pi \sum_{\upsilon=1}^{\infty} \frac{(-1)^{\upsilon-1}\left(\pi \sin\Phi\right)^{2(\upsilon-1)}}{(\upsilon-1)!(\upsilon-1)!} \frac{\Gamma\left(\frac{1}{2}\right)\Gamma\left(\upsilon+\frac{1}{2}\right)}{\left(\pi\cos\Phi\right)^{2\upsilon+1} 2^{\upsilon+1}} \frac{2\upsilon!}{(\upsilon-1)!} s^{-2\upsilon} \frac{1}{4\pi}[\delta(\omega-\omega_n)+\delta(\omega+\omega_n)] \tag{33}$$

$\mathbf{s}_n \bullet \mathbf{v}_n = \mathbf{s}_n \bullet \mathbf{c} = \omega_n$ implies $r_n = \lambda_n$ which is given by Eq. (32) in the case that k is the lightlike k^0. In this case, Eq. (33) vanishes. Consequently, spacetime harmonics of $\frac{\omega_n}{c} = k$ or $\frac{\omega_n}{c}\sqrt{\frac{\varepsilon}{\varepsilon_o}} = k$ for which the Fourier transform of the current-density function is nonzero do not exist. Radiation due to charge motion does not occur in any medium when this boundary condition is met. Nonradiation is also determined directly from the fields based on Maxwell's equations as given in Sec. I.D.c.

c. Nonradiation Based on the Electron Electromagnetic Fields and the Poynting Power Vector

A point charge undergoing periodic motion accelerates and as a consequence radiates according to the Larmor formula:

$$P = \frac{1}{4\pi\varepsilon_0}\frac{2e^2}{3c^3}a^2 \tag{34}$$

where e is the charge, a is its acceleration, ε_0 is the permittivity of free space, and c is the speed of light. Although an accelerated *point* particle radiates, an *extended distribution* modeled as a superposition of accelerating charges does not have to radiate [12, 18, 23-25]. In Ref. [2]

and Appendix I, Chp. 1 of Ref. [7], the electromagnetic far field is determined from the current distribution in order to obtain the condition, if it exists, that the electron current distribution must satisfy such that the electron does not radiate. The current follows from Eqs. (30-31). The currents corresponding to Eq. (30) and first term of Eq. (31) are static. Thus, they are trivially nonradiative. The current due to the time dependent term of Eq. (31) corresponding to p, d, f, etc. orbitals is

$$\begin{aligned}\mathbf{J} &= \frac{\omega_n}{2\pi}\frac{e}{4\pi r_n^2} N[\delta(r-r_n)]\,\mathrm{Re}\left\{Y_\ell^m(\theta,\phi)\right\}\left[\mathbf{u}(t)\times\mathbf{r}\right] \\ &= \frac{\omega_n}{2\pi}\frac{e}{4\pi r_n^2} N'[\delta(r-r_n)]\left(P_\ell^m(\cos\theta)\cos\left(m\phi+\omega_n' t\right)\right)\left[\mathbf{u}\times\mathbf{r}\right] \\ &= \frac{\omega_n}{2\pi}\frac{e}{4\pi r_n^2} N'[\delta(r-r_n)]\left(P_\ell^m(\cos\theta)\cos\left(m\phi+\omega_n' t\right)\right)\sin\theta\hat{\phi}\end{aligned} \tag{35}$$

where to keep the form of the spherical harmonic as a traveling wave about the z-axis, $\omega_n' = m\omega_n$ and N and N' are normalization constants. The vectors are defined as

$$\hat{\phi} = \frac{\hat{u}\times\hat{r}}{\left|\hat{u}\times\hat{r}\right|} = \frac{\hat{u}\times\hat{r}}{\sin\theta}; \qquad \hat{u} = \hat{z} = orbital\ axis \tag{36}$$

$$\hat{\theta} = \hat{\phi}\times\hat{r} \tag{37}$$

"^" denotes the unit vectors $\hat{u} \equiv \frac{\mathbf{u}}{|\mathbf{u}|}$, non-unit vectors are designed in bold, and the current function is normalized. For the electron source current given by Eq. (35), each comprising a multipole of order (ℓ, m) with a time dependence $e^{i\omega_n t}$, the far-field solutions to Maxwell's equations are considered.

As shown in Appendix I of Ref. [7], for time-varying electromagnetic fields, Jackson [26] gives a generalized expansion in vector spherical waves that are convenient for electromagnetic boundary-value problems possessing spherical symmetry properties and for analyzing multipole

radiation from a localized source distribution. The Green function $G(\mathbf{x}', \mathbf{x})$ which is appropriate to the equation

$$\left(\nabla^2 + k^2\right) G(\mathbf{x}', \mathbf{x}) = -\delta(\mathbf{x}' - \mathbf{x}) \tag{38}$$

in the infinite domain with the spherical wave expansion for the outgoing wave Green function is

$$G(\mathbf{x}', \mathbf{x}) = \frac{e^{-ik|\mathbf{x}-\mathbf{x}'|}}{|\mathbf{x}-\mathbf{x}'|} = ik \sum_{\ell=0}^{\infty} j_\ell(kr_<) h_\ell^{(1)}(kr_>) \sum_{m=-\ell}^{\ell} Y_{\ell,m}^*(\theta', \phi') Y_{\ell,m}(\theta, \phi) \tag{39}$$

Jackson [26] further gives the general multipole field solution to Maxwell's equations in a source-free region of empty space with the assumption of a time dependence $e^{i\omega_n t}$:

$$\begin{aligned} \mathbf{B} &= \sum_{\ell,m} \left[a_E(\ell, m) f_\ell(kr) \mathbf{X}_{\ell.m} - \frac{i}{k} a_M(\ell, m) \nabla \times g_\ell(kr) \mathbf{X}_{\ell.m} \right] \\ \mathbf{E} &= \sum_{\ell,m} \left[\frac{i}{k} a_E(\ell, m) \nabla \times f_\ell(kr) \mathbf{X}_{\ell.m} + a_M(\ell, m) g_\ell(kr) \mathbf{X}_{\ell.m} \right] \end{aligned} \tag{40}$$

where the cgs units used by Jackson are retained in this section. The radial functions $f_\ell(kr)$ and $g_\ell(kr)$ are of the form:

$$g_\ell(kr) = A_\ell^{(1)} h_\ell^{(1)} + A_\ell^{(2)} h_\ell^{(2)} \tag{41}$$

$\mathbf{X}_{\ell.m}$ is the vector spherical harmonic defined by

$$\mathbf{X}_{\ell,m}(\theta, \phi) = \frac{1}{\sqrt{\ell(\ell+1)}} \mathbf{L} Y_{\ell,m}(\theta, \phi) \tag{42}$$

where

$$\mathbf{L} = \frac{1}{i}(\mathbf{r} \times \nabla) \tag{43}$$

The coefficients $a_E(\ell, m)$ and $a_M(\ell, m)$ of Eq. (40) specify the amounts of electric (ℓ, m) multipole and magnetic (ℓ, m) multipole fields, and are determined by sources and boundary

conditions as are the relative proportions in Eq. (41). Jackson gives the result of the electric and magnetic coefficients from the sources as

$$a_E(\ell,m)=\frac{4\pi k^2}{i\sqrt{\ell(\ell+1)}}\int Y_\ell^{m*}\left\{\rho\frac{\delta}{\delta r}\left[rj_\ell(kr)\right]+\frac{ik}{c}(\mathbf{r}\cdot\mathbf{J})\,j_\ell(kr)-ik\nabla\cdot(r\times\boldsymbol{M})\,j_\ell(kr)\right\}d^3x \quad (44)$$

and

$$a_M(\ell,m)=\frac{-4\pi k^2}{\sqrt{\ell(\ell+1)}}\int j_\ell(kr)Y_\ell^{m*}\mathbf{L}\cdot\left(\frac{\mathbf{J}}{c}+\nabla\times\boldsymbol{M}\right)d^3x \quad (45)$$

respectively, where the distribution of charge $\rho(\mathbf{x},t)$, current $\mathbf{J}(\mathbf{x},t)$, and intrinsic magnetization $\boldsymbol{M}(\mathbf{x},t)$ are harmonically varying sources: $\rho(\mathbf{x})e^{-\omega_n t}$, $\mathbf{J}(\mathbf{x})e^{-\omega_n t}$, and $\boldsymbol{M}(\mathbf{x})e^{-\omega_n t}$. The currents corresponding to Eq. (30) and first term of Eq. (31) are static. Thus, they are trivially nonradiative. From Eq. (35), the charge and intrinsic magnetization terms are zero. Also, the current $\mathbf{J}(\mathbf{x},t)$ is in the $\hat{\phi}$ direction; thus, the $a_E(\ell,m)$ coefficient given by Eq. (44) is zero since $\mathbf{r}\cdot\mathbf{J}=0$. Substitution of Eq. (35) into Eq. (45) gives the magnetic multipole coefficient $a_M(\ell,m)$:

$$a_M(\ell,m)=\frac{-ek^2}{c\sqrt{\ell(\ell+1)}}\frac{\omega_n}{2\pi}Nj_\ell(kr_n)\Theta\sin(mks) \quad (46)$$

For the electron source current given by Eq. (35), each comprising a multipole of order (ℓ,m) with a time dependence $e^{i\omega_n t}$, the far-field solutions to Maxwell's equations given by Eq. (40) are

$$\begin{aligned}\mathbf{B}&=-\frac{i}{k}a_M(\ell,m)\nabla\times g_\ell(kr)\mathbf{X}_{\ell.m}\\ \mathbf{E}&=a_M(\ell,m)\,g_\ell(kr)\mathbf{X}_{\ell.m}\end{aligned} \quad (47)$$

and the time-averaged power radiated per solid angle $\frac{dP(\ell,m)}{d\Omega}$ is

$$\frac{dP(\ell,m)}{d\Omega} = \frac{c}{8\pi k^2}\left|a_M(\ell,m)\right|^2 \left|\mathbf{X}_{\ell.m}\right|^2 \tag{48}$$

where $a_M(\ell,m)$ is given by Eq. (46). In the case that k is the lightlike k^0, then $k = \omega_n / c$, in Eq. (46), and Eqs. (47-48) vanish for

$$s = vT_n = R = r_n = \lambda_n \tag{49}$$

There is no radiation.

E. Magnetic Field Equations of the Electron

The orbitsphere is a shell of negative charge current comprising correlated charge motion along great circles. For ℓ = 0, the orbitsphere gives rise to a magnetic moment of 1 Bohr magneton [27]. (The details of the derivation of the magnetic parameters including the electron g factor are given in Ref. [2] and Chp. 1 of Ref. [7].)

$$\mu_B = \frac{e\hbar}{2m_e} = 9.274\ X\ 10^{-24}\ JT^{-1} \tag{50}$$

The magnetic field of the electron shown in Figures 16A and B is given by

$$\mathbf{H} = \frac{e\hbar}{m_e r_n^3}(\mathbf{i}_r \cos\theta - \mathbf{i}_\theta \sin\theta) \qquad \text{for } r < r_n \tag{51}$$

$$\mathbf{H} = \frac{e\hbar}{2m_e r^3}(\mathbf{i}_r 2\cos\theta + \mathbf{i}_\theta \sin\theta) \quad \text{for } r > r_n \tag{52}$$

The energy stored in the magnetic field of the electron is

$$E_{mag} = \frac{1}{2}\mu_o \int_0^{2\pi}\int_0^{\pi}\int_0^{\infty} H^2 r^2 \sin\theta dr d\theta d\Phi \tag{53}$$

$$E_{mag\ \text{total}} = \frac{\pi\mu_o e^2\hbar^2}{m_e{}^2 r_1^3} = \frac{4\pi\mu_o\mu_B^2}{r_1^3} \tag{54}$$

F. Stern-Gerlach Experiment

The Stern-Gerlach experiment implies a magnetic moment of one Bohr magneton and an associated angular momentum quantum number of 1/2. Historically, this quantum number is called the spin quantum number, s ($s = \frac{1}{2};\ m_s = \pm\frac{1}{2}$). The superposition of the vector projection of the orbitsphere angular momentum on the z-axis is $\frac{\hbar}{2}$ with an orthogonal component of $\frac{\hbar}{4}$. Excitation of a resonant Larmor precession gives rise to $\hbar$ on an axis $\mathbf{S}$ that precesses about the z-axis called the spin axis at the Larmor frequency at an angle of $\theta = \frac{\pi}{3}$ to give a perpendicular projection of

$$\mathbf{S}_{\perp} = \hbar \sin\frac{\pi}{3} = \pm\sqrt{\frac{3}{4}}\hbar\ \mathbf{i}_{Y_R} \tag{55}$$

and a projection onto the axis of the applied magnetic field of

$$\mathbf{S}_{\parallel} = \hbar \cos\frac{\pi}{3} = \pm\frac{\hbar}{2}\mathbf{i}_z \tag{56}$$

The superposition of the $\frac{\hbar}{2}$, z-axis component of the orbitsphere angular momentum and the $\frac{\hbar}{2}$, z-axis component of $\mathbf{S}$ gives $\hbar$ corresponding to the observed electron magnetic moment of a Bohr magneton, μ_B.

G. Electron g Factor

As given in the Electron g Factor section of Ref. [7] and Ref. [2], conservation of angular momentum of the orbitsphere permits a discrete change of its "kinetic angular momentum" $(\mathbf{r} \times m\mathbf{v})$ by the applied magnetic field of $\frac{\hbar}{2}$, and concomitantly the "potential angular

momentum" $(\mathbf{r}\times e\mathbf{A})$ must change by $-\frac{\hbar}{2}$.

$$\Delta\mathbf{L}=\frac{\hbar}{2}-\mathbf{r}\times e\mathbf{A} \tag{57}$$

$$=\left[\frac{\hbar}{2}-\frac{e\phi}{2\pi}\right]\hat{z} \tag{58}$$

In order that the change of angular momentum, $\Delta\mathbf{L}$, equals zero, ϕ must be $\Phi_0=\frac{h}{2e}$, the magnetic flux quantum. The magnetic moment of the electron is parallel or antiparallel to the applied field only. During the spin-flip transition, power must be conserved. Power flow is governed by the Poynting power theorem,

$$\nabla\bullet(\mathbf{E}\times\mathbf{H})=-\frac{\partial}{\partial t}\left[\frac{1}{2}\mu_o\mathbf{H}\bullet\mathbf{H}\right]-\frac{\partial}{\partial t}\left[\frac{1}{2}\varepsilon_o\mathbf{E}\bullet\mathbf{E}\right]-\mathbf{J}\bullet\mathbf{E} \tag{59}$$

Eq. (60) gives the total energy of the flip transition which is the sum of the energy of reorientation of the magnetic moment (1st term), the magnetic energy (2nd term), the electric energy (3rd term), and the dissipated energy of a fluxon treading the orbitsphere (4th term), respectively,

$$\Delta E_{mag}^{spin}=2\left(1+\frac{\alpha}{2\pi}+\frac{2}{3}\alpha^2\left(\frac{\alpha}{2\pi}\right)-\frac{4}{3}\left(\frac{\alpha}{2\pi}\right)^2\right)\mu_B B \tag{60}$$

$$\Delta E_{mag}^{spin}=g\mu_B B \tag{61}$$

where the stored magnetic energy corresponding to the $\frac{\partial}{\partial t}\left[\frac{1}{2}\mu_o\mathbf{H}\bullet\mathbf{H}\right]$ term increases, the stored electric energy corresponding to the $\frac{\partial}{\partial t}\left[\frac{1}{2}\varepsilon_o\mathbf{E}\bullet\mathbf{E}\right]$ term increases, and the $\mathbf{J}\bullet\mathbf{E}$ term is

dissipative. The spin-flip transition can be considered as involving a magnetic moment of g times that of a Bohr magneton.

The magnetic moment, m, of Eq. (60) is twice that from the gyromagnetic ratio as given by

$$m = \frac{\text{charge} \cdot \text{angular momentum}}{2 \cdot \text{mass}} \tag{62}$$

The magnetic moment of the electron is the sum of the component corresponding to the kinetic angular momentum, $\frac{\hbar}{2}$, and the component corresponding to the vector potential angular momentum, $\frac{\hbar}{2}$, (Eq. (57). The spin-flip transition can be considered as involving a magnetic moment of g times that of a Bohr magneton. The g factor is redesignated the fluxon g factor as opposed to the anomalous g factor, and it is given by Eq. (60).

$$\frac{g}{2} = 1 + \frac{\alpha}{2\pi} + \frac{2}{3}\alpha^2\left(\frac{\alpha}{2\pi}\right) - \frac{4}{3}\left(\frac{\alpha}{2\pi}\right)^2 \tag{63}$$

For $\alpha^{-1} = 137.03604(11)$ [28]

$$\frac{g}{2} = 1.001\ \ 159\ \ 652\ \ 120 \tag{64}$$

The experimental value [29] is

$$\frac{g}{2} = 1.001\ \ 159\ \ 652\ \ 188(4) \tag{65}$$

The calculated and experimental values are within the propagated error of the fine structure constant. Different values of the fine structure constant have been recorded from different experimental techniques, and α^{-1} depends on a circular argument between theory and experiment [30]. One measurement of the fine structure constant based on the electron g factor

is $\alpha_{g_e}^{-1} = 137.036006(20)$ [31]. This value can be contrasted with equally precise measurements employing solid state techniques such as those based on the Josephson effect [32] ($\alpha_J^{-1} = 137.035963(15)$) or the quantized Hall effect [33] ($\alpha_H^{-1} = 137.035300(400)$). A method of the determination of α^{-1} that depends on the circular methodology between theory and experiment to a lesser extent is the substitution of the independently measured fundamental constants μ_0, e, c, and h into $\alpha = \frac{\mu_0 e^2 c}{2h}$. The following values of the fundamental constants are given by Weast [28]

$$\mu_o = 4\pi \; X \; 10^{-7} \, Hm^{-1} \tag{66}$$

$$e = 1.6021892(46) \; X \; 10^{-19} \, C \tag{67}$$

$$c = 2.99792458(12) \; X \; 10^{8} \, ms^{-1} \tag{68}$$

$$h = 6.626176(36) \; X \; 10^{-34} \, JHz^{-1} \tag{69}$$

For these constants,

$$\alpha^{-1} = 137.03603(82) \tag{70}$$

Substitution of the α^{-1} from Eq. (70) into Eq. (63) gives

$$\frac{g}{2} = 1.001\ 159\ 652\ 137 \tag{71}$$

The experimental value [29] is

$$\frac{g}{2} = 1.001\ 159\ 652\ 188(4) \tag{72}$$

The *postulated* QED theory of $\frac{g}{2}$ is based on the determination of the terms of a *postulated* power series in α/π where each *postulated* virtual particle is a source of *postulated* vacuum polarization that gives rise to a *postulated* term. The algorithm involves scores of *postulated* Feynman diagrams corresponding to thousands of matrices with thousands of integrations per matrix requiring decades to reach a consensus on the "appropriate" *postulated* algorithm to remove the intrinsic infinities. The remarkable agreement between Eqs. (71) and (72) demonstrates that $\frac{g}{2}$ may be derived in closed form from Maxwell's equations in a simple straightforward manner that yields a result with eleven figure agreement with experiment—the limit of the experimental capability of the measurement of α directly or the fundamental constants to determine α. In Sec. II of Ref. [5] and Chp. 1, Appendix II of Ref. [7], the Maxwellian result is contrasted with the QED algorithm of invoking virtual particles, zero point fluctuations of the vacuum, and negative energy states of the vacuum. Rather than an infinity of radically different QED models, an essential feature is that *Maxwellian solutions are unique and predictive of conjugate parameters*.

H. Spin and Orbital Parameters

The total function that describes the spinning motion of each electron orbitsphere is composed of two functions. One function, the spin function, is spatially uniform over the orbitsphere, spins with a quantized angular velocity, and gives rise to spin angular momentum. The other function, the modulation function, can be spatially uniform—in which case there is no orbital angular momentum and the magnetic moment of the electron orbitsphere is one Bohr magneton—or not spatially uniform—in which case there is orbital angular momentum. The modulation function also rotates with a quantized angular velocity.

The spin function of the electron corresponds to the nonradiative $n = 1$, $\ell = 0$ state of atomic hydrogen which is well known as an s state or orbital. (See Figure 1 for the charge function and Figures 10A-C and 14 for the current function.) In cases of orbitals of heavier elements and excited states of one electron atoms and atoms or ions of heavier elements with the ℓ quantum number not equal to zero and which are not constant as given by Eq. (30), the constant spin function is modulated by a time and spherical harmonic function as given by Eq. (31) and shown in Figure 3. The modulation or traveling charge density wave corresponds to an orbital angular momentum in addition to a spin angular momentum. These states are typically referred to as p, d, f, etc. orbitals. Application of Haus's [18] condition also predicts nonradiation for a constant spin function modulated by a time and spherically harmonic orbital function. There is acceleration without radiation as also shown in Sec. I.D.c. (Also see Abbott and Griffiths, Goedecke, and Daboul and Jensen [23-25]). However, in the case that such a state arises as an excited state by photon absorption, it is radiative due to a radial dipole term in its current density function since it possesses spacetime Fourier Transform components synchronous with waves traveling at the speed of light [18]. (See Sec. I.M and the Instability of

Excited States section of Ref. [7].)

a. Moment of Inertia and Spin and Rotational Energies

The moments of inertia and the rotational energies as a function of the ℓ quantum number for the solutions of the time-dependent electron charge density functions (Eqs. (30-31)) given in Sec. I.C are solved using the rigid rotor equation [21]. The details of the derivations of the results as well as the demonstration that Eqs. (30-31) with the results given *infra.* are solutions of the wave equation are given in Chp 1, Rotational Parameters of the Electron (Angular Momentum, Rotational Energy, Moment of Inertia) section of Ref. [7].

$\boldsymbol{\ell = 0}$

$$I_z = I_{spin} = \frac{m_e r_n^{\,2}}{2} \tag{73}$$

$$L_z = I\omega \mathbf{i}_z = \pm\frac{\hbar}{2} \tag{74}$$

$$E_{rotational} = E_{rotational,\,spin} = \frac{1}{2}\left[I_{spin}\left(\frac{\hbar}{m_e r_n^{\,2}}\right)^2 \right] = \frac{1}{2}\left[\frac{m_e r_n^{\,2}}{2}\left(\frac{\hbar}{m_e r_n^{\,2}}\right)^2 \right] = \frac{1}{4}\left[\frac{\hbar^2}{2I_{spin}} \right] \tag{75}$$

$$T = \frac{\hbar^2}{2m_e r_n^2} \tag{76}$$

$\boldsymbol{\ell \neq 0}$

$$I_{orbital} = m_e r_n^{\,2}\left[\frac{\ell(\ell+1)}{\ell^2+2\ell+1}\right]^{\frac{1}{2}} = m_e r_n^{\,2}\sqrt{\frac{\ell}{\ell+1}} \tag{77}$$

$$\mathbf{L} = I\omega\mathbf{i}_z = I_{orbital}\omega\mathbf{i}_z = m_e r_n^{\,2}\left[\frac{\ell(\ell+1)}{\ell^2+2\ell+1}\right]^{\frac{1}{2}}\omega\mathbf{i}_z = m_e r_n^{\,2}\frac{\hbar}{m_e r_n^{\,2}}\sqrt{\frac{\ell}{\ell+1}} = \hbar\sqrt{\frac{\ell}{\ell+1}} \tag{78}$$

$$L_{z\ total} = L_{z\ spin} + L_{z\ orbital} \tag{79}$$

$$E_{rotational\ \text{orbital}} = \frac{\hbar^2}{2I}\left[\frac{\ell(\ell+1)}{\ell^2+2\ell+1}\right] = \frac{\hbar^2}{2I}\left[\frac{\ell}{\ell+1}\right] = \frac{\hbar^2}{2m_e r_n^{\,2}}\left[\frac{\ell}{\ell+1}\right] \tag{80}$$

$$\left\langle L_{z\ orbital}\right\rangle = 0 \tag{81}$$

$$\left\langle E_{rotational\ \text{orbital}}\right\rangle = 0 \tag{82}$$

The orbital rotational energy arises from a spin function (spin angular momentum) modulated by a spherical harmonic angular function (orbital angular momentum). The time-averaged mechanical angular momentum and rotational energy associated with the wave-equation solution comprising a traveling charge-density wave on the orbitsphere is zero as given in Eqs. (81) and (82), respectively. Thus, the principal levels are degenerate except when a magnetic field is applied[2]. In the case of an excited state, the angular momentum of $\hbar$ is carried by the fields of

---

[2] SQM makes inescapable predictions that do not match observations. For example, at page 365 Margenau and Murphy [34] state:

" but with the term $\frac{\ell(\ell+1)\hbar^2}{2mr^2}$ added to the normal potential energy. What is the meaning of that term? In classical mechanics, the energy of a particle moving in three dimensions differs from that of a one-dimensional particle by the kinetic energy of rotation, $\frac{1}{2}mr^2\omega^2$. This is precisely the quantity $\frac{\ell(\ell+1)\hbar^2}{2mr^2}$, for we have seen that $\ell(\ell+1)\hbar^2$ is the *certain* value of the square of the angular momentum for the state Y_ℓ, in classical language

the trapped photon. The amplitudes that couple to external magnetic and electromagnetic fields are given by Eq. (78) and (80), respectively. The rotational energy due to spin is given by Eq. (75), and the total kinetic energy is given by Eq. (76).

I. Force Balance Equation

The radius of the nonradiative ($n=1$) state is solved using the electromagnetic force equations of Maxwell relating the charge and mass density functions wherein the angular momentum of the electron is given by $\hbar$ [7]. The reduced mass arises naturally from an electrodynamic interaction between the electron and the proton of mass m_p.

$$\frac{m_e}{4\pi r_1^2}\frac{v_1^2}{r_1} = \frac{e}{4\pi r_1^2}\frac{Ze}{4\pi\varepsilon_o r_1^2} - \frac{1}{4\pi r_1^2}\frac{\hbar^2}{m_p r_n^3} \tag{83}$$

$$r_1 = \frac{a_H}{Z} \tag{84}$$

$\left(mr^2\omega^2\right)^2$ which is divided by $2mr^2$, gives exactly the kinetic energy of rotation."

Zero rotational energy and zero angular momentum are predicted for the n=1 state which is impossible since the electron is bound in a Coulomb field and must have nonzero instantaneous motion. Thus, the Schrödinger equation solutions further predict that the ionized electron may have infinite angular momentum. The Schrödinger equation solutions also predict that the excited state rotational energy levels are nondegenerate as a function of the ℓ quantum number even in the absence of an applied magnetic field, and the predicted energy is over six orders of magnitude of the observed nondegenerate energy in the presence of a magnetic field. In the absence of a magnetic field, no preferred direction exists. In this case, the ℓ quantum number is a function of the orientation of the atom with respect to an arbitrary coordinate system. Therefore, the nondegeneracy is nonsensical and violates conservation of angular momentum of the photon.

where a_H is the radius of the hydrogen atom and the electron velocity is given by Eq. (13).

J. Energy Calculations

From Maxwell's equations, the potential energy V, kinetic energy T, electric energy or binding energy E_{ele} are

$$V = \frac{-Ze^2}{4\pi\varepsilon_o r_1} = \frac{-Z^2e^2}{4\pi\varepsilon_o a_H} = -Z^2\ X\ 4.3675\ X\ 10^{-18}\ J = -Z^2\ X\ 27.2\ eV \tag{85}$$

$$T = \frac{Z^2e^2}{8\pi\varepsilon_o a_H} = Z^2\ X\ 13.59\ eV \tag{86}$$

$$T = E_{ele} = -\frac{1}{2}\varepsilon_o \int_{\infty}^{r_1} \mathbf{E}^2 dv \quad \text{where } \mathbf{E} = -\frac{Ze}{4\pi\varepsilon_o r^2} \tag{87}$$

$$E_{ele} = -\frac{Ze^2}{8\pi\varepsilon_o r_1} = -\frac{Z^2e^2}{8\pi\varepsilon_o a_H} = -Z^2\ X\ 2.1786\ X\ 10^{-18}\ J = -Z^2\ X\ 13.598\ eV \tag{88}$$

The calculated Rydberg constant is $10,967,758\ m^{-1}$; the experimental Rydberg constant is $10,967,758\ m^{-1}$. For increasing Z, the velocity becomes a significant fraction of the speed of light; thus, special relativistic corrections were included in the calculation of the ionization energies of one-electron atoms that are given in Table I.

K. Source Current of Excited States

In a nonradiative state, there is no emission or absorption of radiation corresponding to the absence of radial motion wherein Eq. (44) is zero since $\nabla \bullet (\mathbf{E} \times \mathbf{H}) = -\frac{\delta}{\delta t}\left[\frac{1}{2}\mu_o \mathbf{H} \bullet \mathbf{H}\right] - \frac{\delta}{\delta t}\left[\frac{1}{2}\varepsilon_o \mathbf{E} \bullet \mathbf{E}\right] - \mathbf{J} \bullet \mathbf{E}$. The results of Sec. I.D.c show that the two-dimensional wave equation applies to the condition of radiative stability, and the three-

dimensional wave equation plus time is inappropriate since there is motion in the radial direction only when the energy of the system is changing. The same physical consequence can also be easily shown with a matter-wave dispersion relationship. Thus, radial motion corresponds to the emission or absorption of photons. The form of the radial solution during a transition is then a time-dependent radial Dirac delta function that connects the initial and final states as boundary conditions. The photon carries fields and corresponding angular momentum. This aspect is ignored in the ad hoc postulated SQM approach [5, 7-8, 10-11] where there is no physical basis for excited states[3]. The excited states are purely mathematical probability-wave eigenfunctions.

[3] Quantum mechanics is not a physical theory. It is based on the dubious application of statistics to a single particle and a single event. Consequently, the electron can be everywhere at once with an infinite number of positions and energies simultaneously including those that go to infinity in the positive as well as negative directions. SQM violates causality and can not be based in reality. Even more problematic is that according to SQM the electron has no physical form until it is measured. The success of SQM at reproducing numbers comes from the fact that it merely comprises internally inconsistent curve-fitting algorithms devoid of any physics. The solutions are not predictive, unique, or internally consistent. The ability of the founding equation, the Schrödinger equation (SE) and its solutions, to reproduce the Rydberg formula is touted as justifying the validity of quantum mechanics as representing the nature of physics on the atomic scale. This false confidence gives rise to the practice of curve fitting problems other than the principal energy levels of one electron atoms (the only problem for which a closed-form equation arises) with adjustable-parameters. But, the evaluation of the postulated Schrödinger equation for its basis in fundamental physics reveals that it is merely a complicated equivalent mathematical form of the Rydberg formula to which it reduces. It has no predictability, nor does it contain any physical truth. It misses stability to radiation, electron spin, the Lamb shift, fine structure, hyperfine structure, g factor and many other observables as detailed previously [2-11]. The lack of predictability confirms that is just a mathematical statement of an empirical relationship discovered a generation prior to it being postulated, and it is not a physical theory. The lack of physical insight and predictability is a general shortcoming of all applications of SQM.

Many inescapable problems and discrepancies with observations arise as discussed previously [2-11]. For example, they are not square integrable, but are infinite for n>>1 [34]. Zero rotational energy and zero angular momentum are predicted for the n=1 state which is impossible since the electron is bound in a Coulomb field and must have nonzero instantaneous motion (See FN 2). Furthermore, it must radiate in the n=1 state according to Maxwell's equations [7-8].

In contrast, the physical characteristics of the photon and the electron are the basis of physically solving for excited states according to Maxwell's equations. The vector potential of the current that connects the initial and final states of a transition, each having currents of the form given by Eq. (35) is

$$\mathbf{A}(r) = \frac{\mu_0}{2\pi}\frac{e\hbar}{m_e}\frac{1}{r_{n_i} - r_{n_f}}\frac{e^{-jk_r}}{4\pi r}\mathbf{i}_z \tag{89}$$

The magnetic and electric fields are derived from the vector potential and are used in the Poynting power vector to give the power. The transition probability or Einstein coefficient A_{ki} for intial state n_i and final state n_f of atomic hydrogen given by the power divided by the energy of the transition is

$$\frac{1}{\tau} = \frac{1}{m_e c^2}\frac{\eta}{24\pi}\left(\frac{e\hbar}{m_e a_0^2}\right)^2 \frac{1}{\left(n_f n_i\right)^2} = 2.67\ X\ 10^9 \frac{1}{\left(n_f n_i\right)^2} s^{-1} \tag{90}$$

which matches the NIST values for all transitions extremely well as shown in Ref. [7].

L. Excited States

CQM gives closed form solutions for the resonant photons and excited state electron functions. The angular momentum of the photon given by

$$\mathbf{m} = \frac{1}{8\pi}\mathrm{Re}\left[\mathbf{r}\times(\mathbf{E}\times\mathbf{B}^*)\right] \tag{91}$$

is conserved [26]. The change in angular velocity of the electron is equal to the angular frequency of the resonant photon. The energy is given by Planck's equation. The predicted energies, Lamb shift, hyperfine structure, resonant line shape, line width, selection rules, etc. are in agreement with observation.

The orbitsphere is a dynamic spherical resonator cavity which traps photons of discrete frequencies. The relationship between an allowed radius and the "photon standing wave" wavelength is

$$2\pi r = n\lambda \tag{92}$$

where n is an integer. The relationship between an allowed radius and the electron wavelength is

$$2\pi(nr_1) = 2\pi r_n = n\lambda_1 = \lambda_n \tag{93}$$

where $n = 1, 2, 3, 4, \ldots$. The radius of an orbitsphere increases with the absorption of electromagnetic energy. *The radii of excited states are solved using the electromagnetic force equations of Maxwell relating the field from the charge of the proton, the electric field of the photon, and charge and mass density functions of the electron wherein the angular momentum of the electron is given by $\hbar$ (Eq. (14))*[4]. The solutions to Maxwell's equations for modes that can be excited in the orbitsphere resonator cavity give rise to four quantum numbers, and the energies of the modes are the experimentally known hydrogen spectrum. The relationship

[4] This was missed by Rathke [1] and defines the seminal difference between CQM and SQM. The former is based on physics. The latter is based on postulates and methodology to reproduce the Rydberg formula as eigenvalues without any consideration of the physics which gives rise to the Rydberg states in the first place.

between the electric field equation and the "trapped photon" source charge-density function is given by Maxwell's equation in two dimensions.

$$\mathbf{n} \bullet \left(\mathbf{E}_1 - \mathbf{E}_2 \right) = \frac{\sigma}{\varepsilon_0} \tag{94}$$

The photon standing electromagnetic wave is phase matched with the electron

$$\mathbf{E}_{r\,photon\;\;n,l,m} = \frac{e\left(na_H\right)^{\ell}}{4\pi\varepsilon_o} \frac{1}{r^{(\ell+2)}} \left[-Y_0^0\left(\theta,\phi\right) + \frac{1}{n}\left[Y_0^0\left(\theta,\phi\right) + \mathrm{Re}\left\{ Y_\ell^m\left(\theta,\phi\right)\left[1+e^{i\omega_n t}\right]\right\}\right]\right] \tag{95}$$

$\omega_n = 0 \;\; for \; m = 0$

$\ell = 1, 2, ..., n-1$

$m = -\ell, -\ell+1, ..., 0, ..., +\ell$

$$\mathbf{E}_{r\,total} = \frac{e}{4\pi\varepsilon_o r^2} + \frac{e\left(na_H\right)^{\ell}}{4\pi\varepsilon_o} \frac{1}{r^{(\ell+2)}} \left[-Y_0^0\left(\theta,\phi\right) + \frac{1}{n}\left[Y_0^0\left(\theta,\phi\right) + \mathrm{Re}\left\{ Y_\ell^m\left(\theta,\phi\right)\left[1+e^{i\omega_n t}\right]\right\}\right]\right] \tag{96}$$

$\omega_n = 0$ for $m = 0$

For $r = na_H$ and $m = 0$, the total radial electric field is

$$\mathbf{E}_{r\,total} = \frac{1}{n} \frac{e}{4\pi\varepsilon_o \left(na_H\right)^2} \tag{97}$$

When an electron in the n=1 state absorbs a photon of energy sufficient to take it to a new resonant state, $n = 2, 3, 4, ...,$ force balance must be maintained with the reduction of the central field caused by the superposition of the electric field of the proton and the photon trapped in the orbitsphere, a spherical resonator cavity. According to Eq. (97), the central field is equivalent to that of a central charge of $\frac{e}{n}$, and the excited-state force balance equation is

$$\frac{m_e v_n^2}{r_n} = \frac{\hbar^2}{m_e r_n^3} = \frac{1}{n}\frac{e^2}{4\pi\varepsilon_o r_n^2} \tag{98}$$

where r_1 is the n=1 state radius of the electron, r_n is the nth excited state radius of the electron, and the electron velocity is given by Eq. (13). The radius of the nth excited state given by Eq. (98) is

$$r_n = na_H \tag{99}$$

The energy of the photon which excites a mode in the electron spherical resonator cavity from radius a_H to radius na_H is

$$E_{photon} = \frac{e^2}{4\pi\varepsilon_o a_H}\left[1 - \frac{1}{n^2}\right] = h\nu = \hbar\omega \tag{100}$$

The change in angular velocity of the orbitsphere for an excitation from $n = 1$ to $n = n$ is

$$\Delta\omega = \frac{\hbar}{m_e (a_H)^2} - \frac{\hbar}{m_e (na_H)^2} = \frac{\hbar}{m_e (a_H)^2}\left[1 - \frac{1}{n^2}\right] \tag{101}$$

The kinetic energy change of the transition is

$$\frac{1}{2} m_e (\Delta v)^2 = \frac{1}{2}\frac{e^2}{4\pi\varepsilon_0 a_H}\left[1 - \frac{1}{n^2}\right] = \frac{1}{2}\hbar\omega \tag{102}$$

The change in angular velocity of the electron orbitsphere is identical to the angular velocity of the photon necessary for the excitation, ω_{photon} . The *correspondence principle holds*. It can be demonstrated that the resonance condition between these frequencies is to be satisfied in order to have a net change of the energy field [39]. The excited states of hydrogen are given in Table II.

M. Instability of Excited States

For the excited energy states of the hydrogen atom, σ_{photon} , the two dimensional surface

charge due to the "trapped photons" at the electron orbitsphere, given by Eq. (94) and Eq. (95) is

$$\sigma_{photon} = \frac{e}{4\pi(r_n)^2}\left[Y_0^0(\theta,\phi) - \frac{1}{n}\left[Y_0^0(\theta,\phi) + \mathrm{Re}\left\{ Y_\ell^m(\theta,\phi) e^{i\omega_n t} \right\} \right] \right] \delta(r - r_n) \tag{103}$$

where $n = 2,3,4,...,$. Whereas, $\sigma_{electron}$, the two dimensional surface charge of the electron orbitsphere given by Eq. (31) is

$$\sigma_{electron} = \frac{-e}{4\pi(r_n)^2}\left[Y_0^0(\theta,\phi) + \mathrm{Re}\left\{ Y_\ell^m(\theta,\phi) e^{i\omega_n t} \right\} \right] \delta(r - r_n) \tag{104}$$

The superposition of σ_{photon} (Eq. (103)) and $\sigma_{electron}$ (Eq. (104)) is equivalent to the sum of a radial electric dipole represented by a doublet function and a radial electric monopole represented by a delta function:

$$\sigma_{photon} + \sigma_{electron} = \frac{e}{4\pi(r_n)^2}\left[Y_0^0(\theta,\phi)\dot{\delta}(r - r_n) - \frac{1}{n} Y_0^0(\theta,\phi)\delta(r - r_n) - \left(1 + \frac{1}{n}\right)\left[\mathrm{Re}\left\{ Y_\ell^m(\theta,\phi) e^{i\omega_n t} \right\} \right] \delta(r - r_n) \right] \tag{105}$$

where $n = 2,3,4,...,$. Due to the radial doublet, excited states are radiative since spacetime harmonics of $\frac{\omega_n}{c} = k$ or $\frac{\omega_n}{c}\sqrt{\frac{\varepsilon}{\varepsilon_o}} = k$ do exist for which the spacetime Fourier transform of the current density function is nonzero.

N. Selection Rules

The multipole fields of a radiating source can be used to calculate the energy and angular momentum carried off by the radiation [40]. For definiteness we consider a linear superposition of electric (ℓ, m) multipoles with different m values, but all having the same ℓ, and following Eq. (16.46) of Jackson [40], write the fields as

$$\mathbf{B}_\ell = \sum_m a_E(\ell, m)\mathbf{X}_{\ell m} h_\ell^{(1)}(kr) e^{i\omega t}$$
$$\mathbf{E}_\ell = \frac{i}{k}\nabla \times \mathbf{B}_\ell \tag{106}$$

For harmonically varying fields, the time-averaged energy density is

$$u = \frac{1}{16\pi}\left(\mathbf{E} \bullet \mathbf{E}^* + \mathbf{B} \bullet \mathbf{B}^*\right) \tag{107}$$

In the radiation zone, the two terms are equal. Consequently, the energy in a spherical shell between r and $(r + dr)$ $(for\ kr >> 1)$ is

$$dU = \frac{dr}{8\pi k^2} \sum_{m,m'} a_E^*(\ell, m') a_E(\ell, m) \int \mathbf{X}_{\ell m'}^* \bullet \mathbf{X}_{\ell m} d\Omega \tag{108}$$

where the asymptotic form (Eq. (16.13) of Jackson [40]) of the spherical Hankel function has been used. With the orthogonality integral (Eq. (16.44) of Jackson [40]) this becomes

$$\frac{dU}{dr} = \frac{1}{8\pi k^2} \sum_m \left|a_E(\ell, m)\right|^2 \tag{109}$$

independent of the radius. For a general superposition of electric and magnetic multipoles, the sum over m becomes a sum over ℓ and m and $|a_E|^2$ becomes $|a_E|^2 + |a_M|^2$. The total energy in a spherical shell in the radiation zone is thus an *incoherent sum* over all multipoles.

The time-averaged angular-momentum density is

$$\mathbf{m} = \frac{1}{8\pi c}\mathrm{Re}\left[\mathbf{r} \times \left(\mathbf{E} \times \mathbf{B}^*\right)\right] \tag{110}$$

The triple cross product can be expanded, and the electric field substituted to yield, for a superposition of electric multipoles,

$$\mathbf{m} = \frac{1}{8\pi\omega}\mathrm{Re}\left[\mathbf{B}^*\left(\mathbf{L} \bullet \mathbf{B}\right)\right] \tag{111}$$

Then the angular momentum in a spherical shell between r and $(r + dr)$ in the radiation zone is

$$d\mathbf{M} = \frac{dr}{8\pi\omega k^2} \mathrm{Re} \sum_{m,m'} a_E^*(\ell,m') a_E(\ell,m) \int \left(\mathbf{L} \bullet \mathbf{X}_{\ell m'}\right)^* \mathbf{X}_{\ell m} d\Omega \tag{112}$$

With the explicit form (Eq. (16.43) of Jackson [40]) for X_{lm}, Eq. (112) can be written

$$\frac{d\mathbf{M}}{dr} = \frac{1}{8\pi\omega k^2} \mathrm{Re} \sum_{m,m'} a_E^*(\ell,m') a_E(\ell,m) \int Y_{\ell m'}^* \mathbf{L} Y_{\ell m} d\Omega \tag{113}$$

From the properties of $LY_{\ell m}$ listed in Eq. (16.28) of Jackson [40] and the orthogonality of the spherical harmonics, we obtain the following expressions for the Cartesian components of $\frac{dM}{dr}$

$$\frac{d\mathbf{M}_x}{dr} = \frac{1}{16\pi\omega k^2} \mathrm{Re} \begin{bmatrix} \sqrt{(\ell-m)(\ell+m+1)}\, a_E^*(\ell,m+1) \\ +\sqrt{(\ell+m)(\ell-m+1)}\, a_E^*(\ell,m-1) \end{bmatrix} a_E(\ell,m) \tag{114}$$

$$\frac{d\mathbf{M}_y}{dr} = \frac{1}{16\pi\omega k^2} \mathrm{Im} \begin{bmatrix} \sqrt{(\ell-m)(\ell+m+1)}\, a_E^*(\ell,m+1) \\ -\sqrt{(\ell+m)(\ell-m+1)}\, a_E^*(\ell,m-1) \end{bmatrix} a_E(\ell,m) \tag{115}$$

$$\frac{d\mathbf{M}_z}{dr} = \frac{1}{8\pi\omega k^2} \sum_m m \left| a_E(\ell,m) \right|^2 \tag{116}$$

These equations show that for a general ℓth order electric multipole that consists of a superposition of different m values, only the z component of the angular momentum is relatively simple.

For a multipole with a single m value, M_x and M_y vanish, while a comparison of Eq. (116) and Eq. (105) shows that

$$\frac{dM_z}{dr} = \frac{m}{\omega} \frac{dU}{dr} \tag{117}$$

independent of r [40]. Experimentally, the photon can carry $\hbar$ units of angular momentum. Thus, during excitation the spin, orbital, or total angular momentum of the orbitsphere can change by zero or $\pm\ \hbar$. The electron transition rules arise from conservation of angular

momentum. The selection rules for multipole transitions between quantum states arise from conservation of total angular momentum and component angular momentum where the photon carries $\hbar$ of angular momentum.

For the electric dipole transition, the selection rules are

$$\Delta m = 0, \pm 1$$
$$\Delta m_s = 0 \tag{118}$$

O. Orbital and Spin Splitting

The ratio of the square of the angular momentum, M^2, to the square of the energy, U^2, for a pure ($\hbar$, m) multipole is [40]

$$\frac{M^2}{U^2} = \frac{m^2}{\omega^2} \tag{119}$$

The magnetic moment is defined as

$$\mu = \frac{\text{charge x angular momentum}}{\text{2 x mass}} \tag{120}$$

The radiation of a multipole of order ($\hbar$, m) carries $m\hbar$ units of the z component of angular momentum per photon of energy $\hbar\omega$. Thus, the z component of the angular momentum of the corresponding excited state electron orbitsphere is

$$L_z = m\hbar \tag{121}$$

Therefore,

$$\mu_z = \frac{em\hbar}{2m_e} = m\mu_B \tag{122}$$

where μ_B is the Bohr magneton. The orbital splitting energy is

$$E_{mag}^{orb} = m\mu_B \mathbf{B} \tag{123}$$

The spin and orbital splitting energies superimpose; thus, the principal excited state energy levels of the hydrogen atom are split by the energy $E_{mag}^{spin/orb}$.

$$E_{mag}^{spin/orb} = m\frac{e\hbar}{2m_e}\mathbf{B} + m_s g\frac{e\hbar}{m_e}\mathbf{B} \text{ where} \tag{124}$$

$n = 2,3,4,...$
$\ell = 1,2,...,n-1$
$m = -\ell,-\ell+1,...,0,...,+\ell$
$m_s = \pm\frac{1}{2}$

P. Resonant Line Shape and Width

The spectroscopic linewidth shown in Figure 17 arises from the classical rise-time band-width relationship, and the Lamb Shift is due to conservation of energy and linear momentum and arises from the radiation reaction force between the electron and the photon. It follows from the Poynting power theorem with spherical radiation that the transition probabilities are given by the ratio of power and the energy of the transition [41]. The transition probability in the case of the electric multipole moment is

$$\frac{1}{\tau} = \frac{power}{energy} \tag{125}$$

$$\tau = \frac{energy}{power}$$

$$\tau = \frac{[\hbar\omega]}{\left[\frac{2\pi c}{\left[(2l+1)!!\right]^2}\left(\frac{l+1}{l}\right)k^{2l+1}\left|Q_{lm}+Q_{lm}^{'}\right|^2\right]} = \frac{1}{2\pi}\left(\frac{h}{e^2}\right)\sqrt{\frac{\mu_0}{\varepsilon_0}}\frac{\left[(2l+1)!!\right]^2}{2\pi}\left(\frac{l}{l+1}\right)\left(\frac{l+3}{3}\right)^2\frac{1}{(kna_0)^{2l}\omega}$$

(126)

$$\mathbf{E}(\omega) \propto \int_0^\infty e^{-\alpha t} e^{-i\omega t} dt = \frac{1}{\alpha - i\omega} \tag{127}$$

The relationship between the rise-time and the band-width for exponential decay is

$$\tau\Gamma = \frac{1}{\pi} \tag{128}$$

The energy radiated per unit frequency interval is

$$\frac{dI(\omega)}{d\omega} = I_0 \frac{\Gamma}{2\pi} \frac{1}{\left(\omega - \omega_0 - \Delta\omega\right)^2 + \left(\Gamma / 2\right)^2} \tag{129}$$

Q. Lamb Shift

The Lamb Shift of the $^2P_{1/2}$ state of the hydrogen atom is due to conservation of linear momentum of the electron, atom, and photon. The electron component is

$$\Delta f = \frac{\Delta\omega}{2\pi} = \frac{E_{h\upsilon}}{h} = \frac{\left(E_{h\upsilon}\right)^2}{2h\mu_e c^2} = 1052.48\ MHz \tag{130}$$

where $E_{h\upsilon}$ is

$$E_{h\nu} = 13.5983\ eV\left(1 - \frac{1}{n^2}\right)\frac{3}{4\pi}\sqrt{\frac{3}{4}} - h\Delta f \tag{131}$$

$$h\Delta f <<< 10\ eV \tag{132}$$

Therefore,

$$E_{h\nu} = 13.5983\ eV\left(1 - \frac{1}{n^2}\right)\frac{3}{4\pi}\sqrt{\frac{3}{4}} \tag{133}$$

The atom component is

$$\Delta f = \frac{\Delta\omega}{2\pi} = \frac{E_{h\upsilon}}{h} = \frac{\left(E_{h\upsilon}\right)^2}{2hm_H c^2} = \frac{\left(13.5983\ eV\left(1-\frac{1}{n^2}\right)\left(1+\frac{1}{2}-\sqrt{\frac{3}{4}}\right)\right)^2}{2hm_H c^2} = 5.3839\ MHz \tag{134}$$

The sum of the components is

$$\Delta f = 1052.48\ MHz + 5.3839\ MHz = 1057.87\ MHz \tag{135}$$

The experimental Lamb Shift [42] is

$$\Delta f = 1057.862\ MHz \tag{136}$$

Other core results of QED can be replicated using closed-form equations containing fundamental constants only without involving renormalization and virtual particles. The results derived from Maxwell's equations and given in Chps. 2 and 29 of Ref. [7] are in remarkable agreement between the calculated and experimental values that are only limited by the accuracy of the fundamental constants.

R. Fine Structure (Spin-Orbital Coupling)

The fine structure energy is the Lamb-shifted relativistic interaction energy between the spin and orbital magnetic moments due to the corresponding angular momenta. The electron's motion in the hydrogen atom is always perpendicular to its radius; consequently, as shown in Sec. I.D.a, the electron's angular momentum of $\hbar$ given by Eq. (14) is invariant. The angular momentum of the photon given in the Photon Equations section (Sec. I.W) is $\left|\mathbf{m}\right| = \left|\frac{1}{8\pi}\mathrm{Re}\left[\mathbf{r}\times(\mathbf{E}\times\mathbf{B}^*)\right]\right| = \hbar$. It is conserved for the solutions for the resonant photons and excited state electron functions given in the Excited States section (Sec. I.L) and the Photon Equations section (Sec. I.W). Thus, the electrodynamic angular momentum and the inertial angular momentum are matched such that the correspondence principle holds. It follows from

the principle of conservation of angular momentum that $\frac{e}{m_e}$ of Eq. (50) is invariant as given in the Special Relativistic Correction to the Electron Radius section (Sec. I.D.a) and as shown previously [7]. In the case of spin-orbital coupling, the invariant $\hbar$ of spin angular momentum and orbital angular momentum each give rise to a corresponding invariant magnetic moment of a Bohr magneton, and their corresponding energies superimpose as given in the Orbital and Spin Splitting section (Sec. I.O). The interaction of the two magnetic moments gives rise to a relativistic spin-orbital coupling energy. The vector orientations of the momenta must be considered as well as the condition that flux must be linked by the electron in units of the magnetic flux quantum in order to conserve the invariant electron angular momentum of $\hbar$. The energy may be calculated with the additional conditions of the invariance of the electron's charge and mass to charge ratio $\frac{e}{m_e}$.

As shown at Eqs. (57-61) in the Electron g Factor section (Sec. I.G), flux must be linked by the electron orbitsphere in units of the magnetic flux quantum. The maximum projection of the rotating spin angular momentum of the electron onto an axis given by Eq. (55) is $\sqrt{\frac{3}{4}}\hbar$. Then, using the magnetic energy term of Eq. (60), the spin-orbital coupling energy $E_{s/o}$ is given by [7]

$$E_{s/o} = 2\frac{\alpha}{2\pi}\left(\frac{e\hbar}{2m_e}\right)\frac{\mu_0 e\hbar}{2\left(2\pi m_e\right)\left(\frac{r}{2\pi}\right)^3}\sqrt{\frac{3}{4}} = \frac{\alpha\pi\mu_0 e^2\hbar^2}{m_e^2 r^3}\sqrt{\frac{3}{4}} \tag{137}$$

In the case that $n = 2$, the radius given by Eq. (99) is $r = 2a_0$. The predicted energy difference between the ${}^2P_{3/2}$ and ${}^2P_{1/2}$ levels of the hydrogen atom, $E_{s/o}$, given by Eq. (137) is

$$E_{s/o} = \frac{\alpha\pi\mu_0 e^2\hbar^2}{8m_e^2 a_0^{\,3}}\sqrt{\frac{3}{4}} \tag{138}$$

As in the case of the $^2P_{1/2} \rightarrow {}^2S_{1/2}$ transition, the photon-momentum transfer for the $^2P_{3/2} \rightarrow {}^2P_{1/2}$ transition gives rise to a frequency shift derived after that of the Lamb shift with $\Delta m_\ell = -1$ included. The energy, E_{FS}, for the $^2P_{3/2} \rightarrow {}^2P_{1/2}$ transition called the fine structure splitting is given by

$$\begin{aligned} E_{FS} &= \frac{\alpha^5(2\pi)^2}{8} m_e c^2 \sqrt{\frac{3}{4}} + \left(13.5983\ eV\left(1-\frac{1}{2^2}\right)\right)^2 \left[\frac{\left(\frac{3}{4\pi}\left(1-\sqrt{\frac{3}{4}}\right)\right)^2}{2h\mu_e c^2} + \frac{\left(1+\left(1-\sqrt{\frac{3}{4}}\right)\right)^2}{2hm_H c^2}\right] \\ &= 4.5190\ X\ 10^{-5}\ eV + 1.75407\ X\ 10^{-7}\ eV \\ &= 4.53659\ X\ 10^{-5}\ eV \end{aligned} \tag{139}$$

where the first term corresponds to $E_{s/o}$ given by Eq. (138) expressed in terms of the mass energy of the electron using Eqs. (23.48a-23.48b) of Ref. [7] and the second and third terms correspond to the electron recoil and atom recoil, respectively. The energy of $4.53659\ X\ 10^{-5}\ eV$ corresponds to a frequency of $10,969.4\ MHz$ or a wavelength of $2.73298\ cm$. The experimental value of the $^2P_{3/2}$—$^2P_{1/2}$ transition frequency is $10,969.1\ MHz$ [42, 43]. The large natural widths of the hydrogen $2p$ levels limits the experimental accuracy; yet, given this limitation, the agreement between the theoretical and experimental fine structure is excellent.

S. Hyperfine Structure

The hyperfine structure of the hydrogen atom is calculated from the force balance

contribution between the electron and the proton [7]. The energy corresponds to the Stern-Gerlach and stored electric and magnetic energy changes. The total energy of the transition from antiparallel to parallel alignment, $\Delta E_{total}^{S/N}$, is given as the sum:

$$\begin{aligned}\Delta E_{total}^{S/N} &= -\mu_0\mu_B\mu_P\sqrt{\frac{3}{4}}\left(\frac{1}{r_+^3}+\frac{1}{r_-^3}\right)+\frac{-e^2}{8\pi\varepsilon_o}\left[\frac{1}{r_+}-\frac{1}{r_-}\right]+\left(-1-\left(\frac{2}{3}\right)^2-\frac{\alpha}{4}\right)4\pi\mu_o\mu_B^2\left(\frac{1}{r_+^3}-\frac{1}{r_-^3}\right)\\ &= -1.918365\ X\ 10^{-24}\ J+9.597048\ X\ 10^{-25}\ J+1.748861\ X\ 10^{-26}\ J\\ &= -9.411714\ X\ 10^{-25}\ J\end{aligned} \tag{140}$$

where

$$r = a_H \pm \frac{2\pi\alpha\ \mu_P}{ec}\sqrt{\frac{3}{4}} \tag{141}$$

The energy is expressed in terms of wavelength using the Planck relationship:

$$\lambda = \frac{hc}{\Delta E_{total}^{S/N}} = 21.10610\ cm \tag{142}$$

The experimental value from the hydrogen maser is $21.10611\ cm$ [44].

T. Muonium Hyperfine Structure Interval

The hyperfine structure of muonium is calculated from the force balance contribution between the electron and muon [7]. The energy corresponds to the Stern-Gerlach and stored electric and magnetic energy changes. The energy of the ground state ($1^2S_{1/2}$) hyperfine structure interval of muonium, $\Delta E\left(\Delta\nu_{Mu}\right)$, is given by the sum:

$$\begin{aligned}\Delta E\left(\Delta\nu_{Mu}\right) &= -\mu_0\mu_B\mu_\mu\sqrt{\frac{3}{4}}\left(\frac{1}{r_{2+}^3}+\frac{1}{r_{2-}^3}\right)+\frac{-e^2}{8\pi\varepsilon_o}\left[\frac{1}{r_{2+}}-\frac{1}{r_{2-}}\right]\\ &\quad+4\pi\mu_o\left(-1-\left(\frac{2}{3}\cos\frac{\pi}{3}\right)^2-\alpha\right)\left(\mu_B^2\left(\frac{1}{r_{2+}^3}-\frac{1}{r_{2-}^3}\right)+\mu_{B,\mu}^2\left(\frac{1}{r_{1+}^3}-\frac{1}{r_{1-}^3}\right)\right)\\ &= -6.02890320\ X\ 10^{-24}\ J+3.02903048\ X\ 10^{-24}\ J+4.23209178\ X\ 10^{-26}\ J+1.36122030\ X\ 10^{-28}\ J\\ &= -2.95741568\ X\ 10^{-24}\ J\end{aligned} \tag{143}$$

where

$$r_2 = a_\mu \pm \frac{2\pi\alpha\ \mu_\mu}{ec}\sqrt{\frac{3}{4}} \tag{144}$$

and

$$r_1 = \frac{a_\mu \pm \dfrac{2\pi\alpha\ \mu_\mu}{ec}\sqrt{\dfrac{3}{4}}}{\left(\dfrac{m_\mu}{m_e}\pm\dfrac{m_\mu e\alpha c}{2\hbar^2}\mu_0\ \mu_\mu\sqrt{\dfrac{3}{4}}\right)^{1/3}} \tag{145}$$

Using Planck's equation, the interval frequency, $\Delta\nu_{Mu}$, and wavelength, $\Delta\lambda_{Mu}$, are

$$\begin{aligned}\Delta\nu_{Mu} &= 4.46330328\ GHz\\ \Delta\lambda_{Mu} &= 6.71682919\ \text{cm}\end{aligned} \tag{146}$$

The experimental hyperfine structure interval of muonium is [45]

$$\Delta E\left(\Delta \nu_{Mu}\right) = -2.957415336\ X\ 10^{-24}\ J$$
$$\Delta \nu_{Mu} = 4.463302765(53)\ GHz\ \ (12\,ppm) \tag{147}$$
$$\Delta \lambda_{Mu} = 6.71682998\ \text{cm}$$

U. Positronium Hyperfine Structure

The leptons are at the same radius, and the positronium hyperfine interval is given by the sum of the Stern-Gerlach, $\Delta E_{\text{spin-spin}}$, and fine structure, $\Delta E_{s/o}(^3S_1 \rightarrow {}^1S_0)$, energies [7]. The hyperfine structure interval of positronium ($^3S_1 \rightarrow {}^1S_0$) is given by the sum:

$$\begin{aligned}\Delta E_{\text{Ps hyperfine}} &= \Delta E_{\text{spin-spin}} + \Delta E_{s/o}(^3S_1 \rightarrow {}^1S_0)\\ &= \frac{g\mu_o e^2\hbar^2}{8m_e^2\left(2a_0\right)^3} + \frac{3g\alpha^5\left(2\pi\right)^2}{8} m_e c^2 \sqrt{\frac{3}{4}}\\ &= \frac{g\alpha^5\left(2\pi\right)^2}{8} m_e c^2 \left(\frac{1}{8\pi\alpha} + \frac{3\sqrt{3}}{2}\right)\\ &= 8.41155110\ X\ 10^{-4}\ eV\end{aligned} \tag{148}$$

Using Planck's equation, the interval in frequency, $\Delta \upsilon$, is

$$\Delta \upsilon = \ 203.39041\ GHz \tag{149}$$

The experimental ground-state hyperfine structure interval is [46]

$$\begin{aligned}\Delta E_{\text{Ps hyperfine}}\left(\text{experimental}\right) &= 8.41143\ X\ 10^{-4}\ eV\\ \Delta \upsilon\left(\text{experimental}\right) &= 203.38910(74)\ GHz\ \ (3.6\,ppm)\end{aligned} \tag{150}$$

V. Excited States of Helium

The orbitsphere is a resonator cavity which traps single photons of discrete frequencies. In the ground state of the helium atom, both electrons are at $r_1 = r_2 = 0.567a_o$ as given by Eq. (179). When a photon is absorbed, one of the initially indistinguishable electrons called electron

1 moves to a smaller radius, and the other called electron 2 moves to a greater radius. As shown in Ref. [7], due to the relationship between the angular momentum, energy, and frequency given by Eq. (119), the radial electric field of the trapped photon has a quantized magnitude of a reciprocal integer and is given by Eq. (95). Since the field of electron 1 is equivalent to that of a point for $r > r_1$, the total central field for electron 2 is given by Eq. (96). The radii of electron 2 are determined from the force balance of the electric, magnetic, and centrifugal forces that corresponds to the minimum of energy of the system [7]. The excited-state energies are then given by the electric energies at these radii.

SINGLET EXCITED STATES WITH $\ell = 0$ ($1s^2 \rightarrow 1s^1(ns)^1$)

Force Balance Equation

$$\frac{m_e v^2}{r_2} = \frac{\hbar^2}{m_e r_2^3} = \frac{1}{n}\frac{e^2}{4\pi\varepsilon_o r_2^2} + \frac{2}{3}\frac{1}{n}\frac{\hbar^2}{2m_e r_2^3}\sqrt{s(s+1)} \tag{151}$$

Radius of electron 2

$$r_2 = \left[n - \frac{\sqrt{\frac{3}{4}}}{3} \right] a_{He} \qquad n = 2,3,4,... \tag{152}$$

The excited-state energy is the energy stored in the electric field, E_{ele}, which is the energy of electron 2 relative to the ionized electron at rest having zero energy:

$$E_{ele} = -\frac{1}{n}\frac{e^2}{8\pi\varepsilon_o r_2} \tag{153}$$

TRIPLET EXCITED STATES WITH $\ell = 0$ ($1s^2 \rightarrow 1s^1(ns)^1$)

Force Balance Equation

$$\frac{m_e v^2}{r_2} = \frac{\hbar^2}{m_e r_2^3} = \frac{1}{n}\frac{e^2}{4\pi\varepsilon_o r_2^2} + 2\frac{2}{3}\frac{1}{n}\frac{\hbar^2}{2m_e r_2^3}\sqrt{s(s+1)} \tag{154}$$

Radius of electron 2

$$r_2 = \left[n - \frac{2\sqrt{\frac{3}{4}}}{3} \right] a_{He} \qquad n = 2,3,4,... \tag{155}$$

SINGLET EXCITED STATES WITH $\ell \neq 0$

Force Balance Equation

$$\frac{m_e v^2}{r_2} = \frac{\hbar^2}{m_e r_2^3} = \frac{1}{n}\frac{e^2}{4\pi\varepsilon_o r_2^2} - \frac{1}{n}\frac{\frac{3}{2}}{(2\ell+1)!!}\left(\frac{\ell+1}{\ell}\right)^{1/2}\frac{1}{\ell+2}\frac{1}{2}\frac{\hbar^2}{m_e r^3}\left(\sqrt{s(s+1)} - \sqrt{\frac{\ell}{\ell+1}}\right) \tag{156}$$

Radius of electron 2

$$r_2 = \left[n + \frac{\frac{3}{4}}{(2\ell+1)!!}\frac{1}{\ell+2}\left(\frac{\ell+1}{\ell}\right)^{1/2}\left(\sqrt{\frac{3}{4}} - \sqrt{\frac{\ell}{\ell+1}}\right) \right] a_{He} \qquad n = 2,3,4,... \tag{157}$$

TRIPLET EXCITED STATES WITH $\ell \neq 0$

Force Balance Equation

$$\frac{m_e v^2}{r_2} = \frac{\hbar^2}{m_e r_2^3} = \frac{1}{n}\frac{e^2}{4\pi\varepsilon_o r_2^2} + \frac{1}{n}\frac{\frac{3}{2}}{(2\ell+1)!!}\left(\frac{\ell+1}{\ell}\right)^{1/2}\frac{1}{\ell+2}\frac{1}{2}\frac{\hbar^2}{m_e r^3}\left(2\sqrt{s(s+1)} - \sqrt{\frac{\ell}{\ell+1}}\right) \tag{158}$$

Radius of electron 2

$$r_2 = \left[n - \frac{\frac{3}{4}}{(2\ell+1)!!}\frac{1}{\ell+2}\left(\frac{\ell+1}{\ell}\right)^{1/2}\left(2\sqrt{\frac{3}{4}} - \sqrt{\frac{\ell}{\ell+1}}\right)\right]a_{He} \qquad n = 2,3,4,... \tag{159}$$

The combined energies of the various states of helium appear in Table III. A plot of the predicted and experimental energies of levels assigned by NIST [47] appears in Figure 18. For over 100 states, the r-squared value is 0.999994, and the typical average relative difference is about 5 significant figures which is within the error of the experimental data. The agreement is remarkable.

The hydrino states given in Sec II are strongly supported by the calculation of the helium excited states as well as the hydrogen excited states given in Sec. I.L since the electron-photon model is the same in both the excited states and in the lower-energy states of hydrogen except that the photon provides a central field of magnitude n in the hydrino case and $1/n$ in the excited-state case.

W. Photon Equations

The time-averaged angular-momentum density, $\mathbf{m}$, of an emitted photon is

$$\mathbf{m} = \int \frac{1}{8\pi c}\mathrm{Re}\left[\mathbf{r}\times(\mathbf{E}\times\mathbf{B}^*)\right]dx^4 = \hbar \tag{160}$$

A photon comprising a field-line pattern called a photon electric and magnetic vector field (e&mvf) similar to the orbitsphere is generated from two orthogonal great circle field lines shown in Figure 19 rather than two great circle current loops as in the case of the electron spin function.

The right-handed-circularly-polarized photon electric and magnetic vector field (RHCP photon-e&mvf) shown in Figure 20 is generated by the rotation of the basis elements comprising the great circle magnetic field line in the xz-plane and the great circle electric field line in the yz-plane about the $\left(\mathbf{i}_x, \mathbf{i}_y, 0\mathbf{i}_z\right)$-axis by $\frac{\pi}{2}$ corresponding to the output of the matrix given by Eq. (161).

E FIELD and H FIELD:

$$\begin{bmatrix} x' \\ y' \\ z' \end{bmatrix} = \begin{bmatrix} \frac{1}{2}+\frac{\cos\theta}{2} & \frac{1}{2}-\frac{\cos\theta}{2} & -\frac{\sin\theta}{\sqrt{2}} \\ \frac{1}{2}-\frac{\cos\theta}{2} & \frac{1}{2}+\frac{\cos\theta}{2} & \frac{\sin\theta}{\sqrt{2}} \\ \frac{\sin\theta}{\sqrt{2}} & -\frac{\sin\theta}{\sqrt{2}} & \cos\theta \end{bmatrix} \bullet \left(\begin{bmatrix} 0 \\ r_n \cos\phi \\ r_n \sin\phi \end{bmatrix}_{\text{Red}} + \begin{bmatrix} r_n \cos\phi \\ 0 \\ r_n \sin\phi \end{bmatrix}_{\text{Blue}} \right) \tag{161}$$

The left-handed-circularly-polarized photon electric and magnetic vector field (LHCP photon-e&mvf) is generated by the rotation of the basis elements comprising the great circle magnetic field line in the xz-plane and the great circle electric field line in the yz-plane about $\left(\mathbf{i}_x, -\mathbf{i}_y, 0\mathbf{i}_z\right)$-axis by $\frac{\pi}{2}$. A linearly polarized photon is the superposition of the right- and left-handed circularly polarized photons.

The field invariance under Gauss' Integral Law also applies to the fields of the photon-e&mvf [48] in the determination of the photon field observed in the laboratory frame as shown in Figure 21.

The relationship between the relativistic velocity and the electric field of a moving charge shown schematically in Figure 22.

From field pattern given by Eq. (161), the photon equation in the lab frame of a right-handed circularly polarized photon orbitsphere is

$$\mathbf{E} = \mathbf{E}_0 \left[\mathbf{x} + i\mathbf{y} \right] e^{-jk_z z} e^{-j\omega t} \tag{162}$$

$$\mathbf{H} = \left(\frac{\mathbf{E}_0}{\eta} \right) \left[\mathbf{y} - i\mathbf{x} \right] e^{-jk_z z} e^{-j\omega t} = \mathbf{E}_0 \sqrt{\frac{\varepsilon}{\mu}} \left[\mathbf{y} - i\mathbf{x} \right] e^{-jk_z z} e^{-j\omega t} \tag{163}$$

with a wavelength of

$$\lambda = 2\pi \frac{c}{\omega} \tag{164}$$

The relationship between the photon orbitsphere radius and wavelength is

$$2\pi r_0 = \lambda_0 \tag{165}$$

The electric field lines of a right-handed circularly polarized photon orbitsphere as seen along the axis of propagation in the lab inertial reference frame as it passes a fixed point is shown in Figure 23.

a. Spherical Wave

Photons superimpose, and the amplitude due to N photons is

$$E_{total} = \sum_{n=1}^{N} \frac{e^{-ik_r |\mathbf{r}-\mathbf{r}'|}}{4\pi \, |\, \mathbf{r} - \mathbf{r}' \,|} f(\theta, \phi) \tag{166}$$

In the far field, the emitted wave is a spherical wave

$$E_{total} = E_o \frac{e^{-ikr}}{r} \tag{167}$$

The Green Function is given as the solution of the wave equation. Thus, the superposition of photons gives the classical result. As r goes to infinity, the spherical wave becomes a plane wave. The double slit interference pattern is predicted classically as shown in Chps. 3 and 8 of Ref. [7]. From the equation of a photon, the wave-particle duality arises naturally. The energy is always given by Planck's equation; yet, an interference pattern is observed when photons add over time or space. The results also predict those of the Aspect experiment involving Bell's inequalities as shown in Chp. 37 of Ref. [7].

X. Equations of the Free Electron

a. Charge Density Function

The radius of an electron orbitsphere increases with the absorption of electromagnetic energy [49]. With the absorption of a photon of energy in excess of the ionization energy, the electron becomes ionized as a plane wave (spherical wave in the limit) with the de Broglie wavelength. The ionized electron traveling at constant velocity is nonradiative and is a two-dimensional surface having a total charge of e and a total mass of m_e. The nature of the free electron can be solved as a boundary value problem given by the projection of the orbitsphere into a plane that linearly propagates along an axis perpendicular to the plane where the velocity of the plane and the orbitsphere is given by

$$v = \frac{\hbar}{m_e \rho_0} \tag{168}$$

and the radius of the orbitsphere in spherical coordinates is equal to the radius of the free

electron in cylindrical coordinates ($\rho_0 = r_0$). The mass density function of a free electron shown in Figure 24 is a two-dimensional disk having the mass density distribution in the xy(ρ)-plane

$$\begin{aligned} \sigma_m(\rho,\phi,z) &= \frac{m_e}{\frac{2}{3}\pi\rho_0^3}\sqrt{\rho_0^2-\rho^2} = \frac{3}{2}\frac{m_e}{\pi\rho_0^2}\sqrt{1-\left(\frac{\rho}{\rho_0}\right)^2}\,\delta(z) \qquad \text{for } 0 \le \rho \le \rho_0 \\ \sigma_m(\rho,\phi,z) &= 0 \qquad\qquad \text{for } \rho_0 < \rho \end{aligned} \tag{169}$$

where $\frac{m_e}{\pi\rho_0^2}$ is the average mass density. The charge-density distribution, $\sigma_e(\rho,\phi,z)$, in the xy-plane is given by replacing m_e with e. The charge density distribution of the free electron has been confirmed experimentally [50, 51]. Researchers working at the Japanese National Laboratory for High Energy Physics (KEK) demonstrated that the charge of the free electron increases toward the particle's core and is symmetrical as a function of ϕ. In addition, the wave-particle duality arises naturally, and the result is consistent with scattering experiments from helium and the double split experiment which can be derived classically as shown in Chp. 8 of Ref. [7] with a simulation available at Ref. [19].

b. Current Density Function

The current-density function is the product of the charge-density function times the angular velocity function. In order to be stable over time, the free electron also possesses time harmonic charge motion in the xy-plane at a constant angular frequency. The magnitude of the angular velocity of the orbitsphere is given by Eq. (16). During ionization of the electron, the scalar sum of the magnitude of the angular momentum, $\hbar$, must be conserved. The current-density function of a free electron propagating with velocity v_z along the z-axis is given by the product of the charge density (Eq. (169) with e replacing m_e) and the constant angular velocity

such that the angular momentum of $\hbar$ is conserved. The projection of the constant angular velocity of the orbitsphere into the plane of the free electron gives the angular velocity

$$\omega = \frac{5}{2}\frac{\hbar}{m_e \rho_0^2} \tag{170}$$

From the mass density, σ_m, given by Eq. (169) and the angular frequency, ω, given by Eq. (170), the angular momentum-density function, $\mathbf{L}$ is

$$\mathbf{L}\mathbf{i}_z = \frac{m_e}{\frac{2}{3}\pi\rho_0^3}\sqrt{\rho_0^2 - \rho^2}\,\frac{5}{2}\frac{\hbar}{m_e\rho_0^2}\rho^2 \tag{171}$$

The total angular momentum of the free electron is given by integration over the two-dimensional disc having the angular-momentum density given by Eq. (171):

$$\begin{aligned}\mathbf{L}\mathbf{i}_z &= \int_0^{2\pi}\int_0^{\rho_0} \frac{m_e}{\frac{2}{3}\pi\rho_0^3}\sqrt{\rho_0^2 - \rho^2}\,\frac{5}{2}\frac{\hbar}{m_e\rho_0^2}\rho^2\,\rho d\rho d\phi \\ &= \hbar\mathbf{i}_z\end{aligned} \tag{172}$$

The current-density function of the free electron, $\mathbf{J}(\rho,\phi,z,t)$, is given by the product of the angular velocity ω and the charge-density function given by Eqs. (170) and (169) with replacement of m_e with e, respectively. The current-density function given by

$$\mathbf{J}(\rho,\phi,z,t) = \left[\frac{e}{\frac{2}{3}\pi\rho_0^3}\sqrt{\rho_0^2 - \rho^2}\,\frac{5}{2}\frac{\hbar}{m_e\rho_0^2}\,\mathbf{i}_\phi\right] + \frac{e\hbar}{m_e\rho_0}\delta(z - \frac{\hbar}{m_e\rho_0}t)\mathbf{i}_z \tag{173}$$

is shown in Figure 25.

The spacetime Fourier transform of Eq. (173) is [18, 52]

$$\frac{e}{\frac{4}{3}\pi\rho_0^3}\frac{\hbar}{m_e}\mathrm{sinc}(s\rho_0)+2\pi e\frac{\hbar}{m_e\rho_0}\delta(\omega-\mathbf{k}_z\bullet\mathbf{v}_z) \tag{174}$$

where $\mathrm{sinc}(s\rho_0)=\frac{\sin s\rho_0}{s\rho_0}$ and s is the wavenumber $\frac{2\pi}{\rho_0}$. For time harmonic motion corresponding to the electron parameters ω_0 and s_0, Eq. (93) is

$$2\pi\rho_0=\lambda_0 \tag{175}$$

When the radial projection of the velocity is c, $\mathbf{s}$ is the lightlike $\mathbf{s}^0$ wherein

$$\mathbf{s}\bullet\mathbf{v}=\mathbf{s}\bullet\mathbf{c}=\omega_0 \tag{176}$$

the relativistically corrected wavelength given by Eq. (32) is

$$\rho_0=\lambda_0 \tag{177}$$

Substitution of Eq. (177) into the sinc function results in the vanishing of the entire Fourier transform of the current-density function. Thus, spacetime harmonics of $\frac{\omega}{c}=k$ *or* $\frac{\omega}{c}\sqrt{\frac{\varepsilon}{\varepsilon_0}}=k$ do not exist. Radiation due to charge motion does not occur in any medium when this boundary condition is met.

c. Stern-Gerlach Experiment

The Stern-Gerlach experiment demonstrates that the magnetic moment of the electron can only be parallel or antiparallel to an applied magnetic field with a magnetic moment of one Bohr magneton. The presence of the magnetic field results in the excitation of a resonant Larmor precession by a photon carrying $\hbar$ of angular momentum. The mutually perpendicularly oriented $\hbar$ of angular momentum of each of the photon and free electron causes the vectors to mutually rotate about each other. The $\hbar$ of electron angular momentum on the z'-axis and the $\hbar$

of photon angular momentum on the x'-axis gives a resultant stationary projection of $\sqrt{2}\hbar$ onto the $\left(\mathbf{i}_x, 0\mathbf{i}_y, \mathbf{i}_z\right)$-axis or $\left(-\mathbf{i}_x, 0\mathbf{i}_y, \mathbf{i}_z\right)$-axis. The static projection of the resultant angular momentum onto the z-axis is $\hbar$ with a contribution of $\frac{\hbar}{2}$ from each of the intrinsic electron current and the photon.

Rotation of the plane-lamina disc having the azimuthal current equivalent to concentric circles given by Eq. (177) about the resultant rotational $\left(\mathbf{i}_x, 0\mathbf{i}_y, \mathbf{i}_z\right)$- or $\left(-\mathbf{i}_x, 0\mathbf{i}_y, \mathbf{i}_z\right)$-axes by 2π during a Larmor-precession period generates the equivalent of the momentum-density pattern of a component orbitsphere-cvf (o-cvf) called the primary o-cvf for each of the concentric circular current loops in the xy-plane (ρ-plane). The continuous progression of larger current loops along ρ generates a continuum of o-cvfs for $0 \le \rho \le \rho_0$ over a period that comprise two conical surfaces joined at the origin and facing in the opposite directions along the $\left(\mathbf{i}_x, 0\mathbf{i}_y, \mathbf{i}_z\right)$- or $\left(-\mathbf{i}_x, 0\mathbf{i}_y, \mathbf{i}_z\right)$-axis, the axis of rotation as shown in Figure 26.

The precessing electron can further interact with a resonant photon directed along the x-axis that rotates the z-axis-directed static projection of the resultant of $\hbar$ such that it flips to the opposite direction. A uniform spherical momentum density is formed over time by each circular current basis element at position ρ by combined Larmor and spin-flip rotations. The resulting spatial momentum density over a period interacts with the external applied magnetic field in a manner that is equivalent to that of orbitsphere function, $Y_0^{\,0}(\phi, \theta)$ shown in Figures 12 and 14 having a uniform momentum density on a spherical shell of radius ρ_0, a total sum of the magnitude of the angular momentum from the contributions from all of the infinitesimal points on the orbitsphere of $\hbar$, and $\mathbf{L}_z = \frac{\hbar}{2}$.

Since the projection of the intrinsic free electron angular momentum and that of the resonant photon that excites the Larmor precession onto the z-axis are both $\frac{\hbar}{2}$, the Larmor-excited free electron behaves equivalently to the bound electron. Flux must be linked in the same manner in units of the magnetic flux quantum, $\Phi_0 = \frac{h}{2e}$. Consequently, the g factor for the free electron is the same as that of the bound electron, and the energy of the transition between these states is that of the resonant photon given by

$$\Delta E_{mag}^{spin} = g\mu_B B$$

(See Chp. 3 of Ref. [7] for details of the derivations.)

Y. Two-Electron Atoms

Two electron atoms may be solved from a central force balance equation with the nonradiation condition. The force balance equation using Eq. (13) is

$$\frac{m_e}{4\pi r_2^2}\frac{v_2^2}{r_2} = \frac{m_e}{4\pi r_2^2}\frac{\hbar^2}{m_e r_2^3} = \frac{e}{4\pi r_2^2}\frac{(Z-1)e}{4\pi\varepsilon_o r_2^2} + \frac{1}{4\pi r_2^2}\frac{\hbar^2}{Zm_e r_2^3}\sqrt{s(s+1)} \tag{178}$$

which gives the radius of both electrons as

$$r_2 = r_1 = a_0\left(\frac{1}{Z-1} - \frac{\sqrt{s(s+1)}}{Z(Z-1)}\right);\ s = \frac{1}{2} \tag{179}$$

a. Ionization Energies Calculated using the Poynting Power Theorem

For helium, which has no electric field beyond r_1

$$Ionization\ Energy(He) = -E(electric) + E(magnetic)\left(1 - \frac{1}{2}\left(\left(\frac{2}{3}\cos\frac{\pi}{3}\right)^2 + \alpha\right)\right) \tag{180}$$

where,

$$E(electric) = -\frac{(Z-1)e^2}{8\pi\varepsilon_o r_1} \tag{181}$$

$$E(magnetic) = \frac{2\pi\mu_0 e^2\hbar^2}{m_e^2 r_1^3} = \frac{8\pi\mu_o\mu_B^2}{r_1^3} \tag{182}$$

For $3 \le Z$

$$Ionization\ Energy = -Electric\ Energy - \frac{1}{Z} Magnetic\ Energy \tag{183}$$

The energies of several two-electron atoms are given in Table IV. The exact solutions for one through twenty-electron atoms are given in Ref. [3] and Ref. [7].

Z. Elastic Electron Scattering from Helium Atoms

The aperture distribution function, $a(\rho,\phi,z)$, for the elastic scattering of an incident electron plane wave represented by $\pi(z)$ by a helium atom represented by

$$\frac{2}{4\pi(0.567a_o)^2}[\delta(r-0.567a_o)] \tag{184}$$

is given by the convolution of the plane wave with the helium atom function:

$$a(\rho,\phi,z) = \pi(z) \otimes \frac{2}{4\pi(0.567a_o)^2}[\delta(r-0.567a_o)] \tag{185}$$

The aperture function is

$$a(\rho,\phi,z) = \frac{2}{4\pi(0.567a_o)^2}\sqrt{(0.567a_o)^2 - z^2}\,\delta(r-\sqrt{(0.567a_o)^2 - z^2}) \tag{186}$$

a. Far Field Scattering (circular symmetry)

Applying Huygens' principle to a disturbance caused by the plane wave electron over the

helium atom as an aperture gives the amplitude of the far field or Fraunhofer diffraction pattern $F(s)$ as the Fourier Transform of the aperture distribution. The intensity I_1^{ed} is the square of the amplitude.

$$F(s)=\frac{2}{4\pi(0.567a_o)^2}2\pi\int_0^{\infty}\int_{-\infty}^{\infty}\sqrt{(0.567a_o)^2-z^2}\,\delta(\rho-\sqrt{(0.567a_o)^2-z^2})J_o(s\rho)e^{-iwz}\rho d\rho dz \qquad (187)$$

$$I_1^{ed}=F(s)^2$$

$$=I_e\left\{\left[\frac{2\pi}{(z_ow)^2+(z_os)^2}\right]^{\frac{1}{2}}\left\{2\left[\frac{z_os}{(z_ow)^2+(z_os)^2}\right]J_{3/2}\left[((z_ow)^2+(z_os)^2)^{1/2}\right]-\left[\frac{z_os}{(z_ow)^2+(z_os)^2}\right]^2 J_{5/2}\left[((z_ow)^2+(z_os)^2)^{1/2}\right]\right\}\right\}^2 \qquad (188)$$

$$s=\frac{4\pi}{\lambda}\sin\frac{\theta}{2};\ w=0\ (\textit{units of } \mathring{A}^{-1}) \qquad (189)$$

The experimental results of Bromberg [54], the extrapolated experimental data of Hughes [54], the small angle data of Geiger [55] and the semiexperimental results of Lassettre [54] for the elastic differential cross section for the elastic scattering of electrons by helium atoms is shown graphically in Figure 27. The elastic differential cross section as a function of angle numerically calculated by Khare [54] using the first Born approximation and first-order exchange approximation also appear in Figure 27. These results which are based on a quantum mechanical model are compared with experimentation [54, 55]. The closed-form function (Eqs. (188) and (189)) for the elastic differential cross section for the elastic scattering of electrons by helium atoms is shown graphically in Figure 28. The scattering amplitude function, $F(s)$ (Eq. (187), is shown as an insert. It is apparent from Figure 27 that the quantum mechanical calculations fail completely at predicting the experimental results at small scattering angles; whereas, there is

good agreement between Eq. (188) and the experimental results.

AA. One- Through Twenty-Electron Atoms

The physical approach based on Maxwell's equations was applied to multielectron atoms that were solved exactly [3, 7]. The classical predictions of the ionization energies were solved for the physical electrons comprising concentric orbitspheres ("bubble-like" charge-density functions) that are electrostatic and magnetostatic corresponding to a constant charge distribution and a constant current corresponding to spin angular momentum. Alternatively, the charge is a superposition of a constant and a dynamical component. In the latter case, charge density waves on the surface are time and spherically harmonic and correspond additionally to electron orbital angular momentum that superimposes the spin angular momentum.

Thus, the electrons of multielectron atoms all exist as orbitspheres of discrete radii which are given by r_n of the radial Dirac delta function, $\delta(r-r_n)$. These electron orbitspheres may be spin paired or unpaired depending on the force balance which applies to each electron. Ultimately, the electron configuration must be a minimum of energy. Minimum energy configurations are given by solutions to Laplace's equation. Electrons of an atom with the same principal and ℓ quantum numbers align parallel until each of the m_ℓ levels are occupied, and then pairing occurs until each of the m_ℓ levels contain paired electrons. The electron configuration for one through twenty-electron atoms that achieves an energy minimum is: 1s < 2s < 2p < 3s < 3p < 4s.

In each case, the corresponding force balance of the central Coulombic, paramagnetic, and diamagnetic forces was derived for each n-electron atom that was solved for the radius of each electron. The central Coulombic force was that of a point charge at the origin since the

electron charge-density functions are spherically symmetrical with a time dependence that was nonradiative. This feature eliminated the electron-electron repulsion terms and the intractable infinities of SQM and permitted general solutions. The ionization energies were obtained using the calculated radii in the determination of the Coulombic and any magnetic energies. The radii and ionization energies for all cases are given by equations having fundamental constants and each nuclear charge, Z, only. The predicted ionization energies and electron configurations given are in remarkable agreement with the experimental values known for 400 atoms and ions [3, 7].

a. General Equation for the Ionization Energies of Five Through Ten-Electron Atoms

As an example, for each n-electron atom having a central charge of Z times that of the proton and an electron configuration $1s^2 2s^2 2p^{n-4}$, there are two indistinguishable spin-paired electrons in an orbitsphere with radii r_1 and r_2 both given by:

$$r_1 = r_2 = a_o \left[\frac{1}{Z-1} - \frac{\sqrt{\frac{3}{4}}}{Z(Z-1)} \right] \tag{190}$$

two indistinguishable spin-paired electrons in an orbitsphere with radii r_3 and r_4 both given by:

$$r_4 = r_3 = \frac{\dfrac{a_0\left(1-\dfrac{\sqrt{\frac{3}{4}}}{Z}\right)}{\left((Z-3)-\left(\frac{1}{4}-\frac{1}{Z}\right)\dfrac{\sqrt{\frac{3}{4}}}{r_1}\right)} \pm a_o \sqrt{\dfrac{\left(1-\dfrac{\sqrt{\frac{3}{4}}}{Z}\right)^2}{\left((Z-3)-\left(\frac{1}{4}-\frac{1}{Z}\right)\dfrac{\sqrt{\frac{3}{4}}}{r_1}\right)^2} + 4\dfrac{\left[\dfrac{Z-3}{Z-2}\right] r_1 10\sqrt{\frac{3}{4}}}{\left((Z-3)-\left(\frac{1}{4}-\frac{1}{Z}\right)\dfrac{\sqrt{\frac{3}{4}}}{r_1}\right)}}}{2} \qquad (191)$$

r_1 *in units of* a_o

and $n-4$ electrons in an orbitsphere with radius r_n given by

$$r_n = \frac{\dfrac{a_0}{\left((Z-(n-1))-\left(\frac{A}{8}-\frac{B}{2Z}\right)\dfrac{\sqrt{3}}{r_3}\right)} \pm a_0 \sqrt{\left(\dfrac{1}{\left((Z-(n-1))-\left(\frac{A}{8}-\frac{B}{2Z}\right)\dfrac{\sqrt{3}}{r_3}\right)}\right)^2 + \dfrac{20\sqrt{3}\left(\left[\dfrac{Z-n}{Z-(n-1)}\right]\left(1-\dfrac{\sqrt{2}}{2}\right)r_3\right)}{\left((Z-(n-1))-\left(\frac{A}{8}-\frac{B}{2Z}\right)\dfrac{\sqrt{3}}{r_3}\right)}}}{2} \qquad (192)$$

r_3 *in units of* a_0

The parameter A given in Table V corresponds to the diamagnetic force, $\mathbf{F}_{diamagnetic}$:

$$\mathbf{F}_{diamagnetic} = -\sum_m \frac{(\ell+|m|)!}{(2\ell+1)(\ell-|m|)!}\frac{\hbar^2}{4m_e r_n^2 r_3}\sqrt{s(s+1)}\mathbf{i}_\mathbf{r} \qquad (193)$$

The parameter B given in Table V corresponds to the paramagnetic force, $\mathbf{F}_{mag\ 2}$:

$$\mathbf{F}_{mag\ 2} = \frac{1}{Z}\frac{\hbar^2}{m_e r_n^2 r_3}\sqrt{s(s+1)}\mathbf{i}_\mathbf{r} \qquad (194)$$

or

$$\mathbf{F}_{mag\ 2} = \frac{1}{Z}\frac{4\hbar^2}{m_e r_n^2 r_3}\sqrt{s(s+1)}\mathbf{i}_\mathbf{r} \tag{195}$$

depending on the negative or positive superposition of the spin and orbital angular momentum determined by the minimization of the total energy. The ionization energies for the n-electron atoms are given by the negative of the electric energy, $E(electric)$:

$$E(Ionization) = -Electric\ Energy = \frac{(Z-(n-1))e^2}{8\pi\varepsilon_o r_n} \tag{196}$$

The results of applying Eqs. (190-196) to determine the $1s^2 2s^2 2p^{n-4}$ -atom ionization energies for five through ten electron atoms are compared with the experimental results [35, 53] in Tables VI-XI.

The agreement between the experimental ionization energies and the classical predictions based on concentric dynamical orbitspheres ("bubble-like" charge-density functions) wherein the charge-density waves on the surface are time and spherically harmonic is remarkable. The classical shell model of atomic electrons is also being confirmed by studying electron dynamics using coherent short-pulse laser excitation [56-58].

AB. The Nature of the Chemical Bond of Hydrogen

The hydrogen molecule charge and current density functions, bond distance, and energies are solved from the Laplacian in ellipsoidal coordinates with the constraint of nonradiation.

$$(\eta-\zeta)R_\xi\frac{\partial}{\partial\xi}(R_\xi\frac{\partial\phi}{\partial\xi}) + (\zeta-\xi)R_\eta\frac{\partial}{\partial\eta}(R_\eta\frac{\partial\phi}{\partial\eta}) + (\xi-\eta)R_\zeta\frac{\partial}{\partial\zeta}(R_\zeta\frac{\partial\phi}{\partial\zeta}) = 0 \tag{197}$$

The force balance equation for the hydrogen molecule is

$$\frac{\hbar^2}{m_e a^2 b^2}D = \frac{e^2}{8\pi\varepsilon_o a b^2}D + \frac{\hbar^2}{2m_e a^2 b^2}D \tag{198}$$

where

$$D = \mathbf{r}(t) \cdot \mathbf{i}_\xi \tag{199}$$

is the time dependent distance from the origin to the tangent plane at a point on the ellipsoidal MO. Eq. (198) has the parametric solution

$$r(t) = \mathbf{i}a\cos\omega t + \mathbf{j}b\sin\omega t \tag{200}$$

when the semimajor axis, a, is

$$a = a_o \tag{201}$$

The internuclear distance, $2c'$, which is the distance between the foci is

$$2c' = \sqrt{2}a_o \tag{202}$$

The experimental internuclear distance is $\sqrt{2}a_o$. The semiminor axis is

$$b = \frac{1}{\sqrt{2}}a_o \tag{203}$$

The eccentricity, e, is

$$e = \frac{1}{\sqrt{2}} \tag{204}$$

a. The Energies of the Hydrogen Molecule

The potential energy of the two electrons in the central field of the protons at the foci is

$$V_e = \frac{-2e^2}{8\pi\varepsilon_o\sqrt{a^2-b^2}}\ln\frac{a+\sqrt{a^2-b^2}}{a-\sqrt{a^2-b^2}} = -67.836\ eV \tag{205}$$

The potential energy of the two protons is

$$V_p = \frac{e^2}{8\pi\varepsilon_o\sqrt{a^2-b^2}} = 19.242\ eV \tag{206}$$

The kinetic energy of the electrons is

$$T = \frac{\hbar^2}{2m_e a\sqrt{a^2-b^2}} \ln \frac{a+\sqrt{a^2-b^2}}{a-\sqrt{a^2-b^2}} = 33.918\ eV \tag{207}$$

The energy, V_m, of the magnetic force between the electrons is

$$V_m = \frac{-\hbar^2}{4m_e a\sqrt{a^2-b^2}} \ln \frac{a+\sqrt{a^2-b^2}}{a-\sqrt{a^2-b^2}} = -16.959\ eV \tag{208}$$

During bond formation, the electrons undergo a reentrant oscillatory orbit with vibration of the protons. The corresponding energy $\overline{E}_{osc}$ is the difference between the Doppler and average vibrational kinetic energies:

$$\overline{E}_{osc} = \overline{E}_D + \overline{E}_{Kvib} = \left(V_e + T + V_m + V_p\right)\sqrt{\frac{2\overline{E}_K}{Mc^2}} + \frac{1}{2}\hbar\sqrt{\frac{k}{\mu}} \tag{209}$$

The total energy is

$$E_T = V_e + T + V_m + V_p + \overline{E}_{osc} \tag{210}$$

$$E_T = -\frac{e^2}{8\pi\varepsilon_o a_0}\left[\left(2\sqrt{2} - \sqrt{2} + \frac{\sqrt{2}}{2}\right)\ln\frac{\sqrt{2}+1}{\sqrt{2}-1} - \sqrt{2}\right]\left[1 + \sqrt{\frac{2\hbar\sqrt{\frac{e^2}{4\pi\varepsilon_o a_0^3}}}{m_e c^2}}\right] - \frac{1}{2}\hbar\sqrt{\frac{k}{\mu}} = -31.689\ eV \tag{211}$$

The energy of two hydrogen atoms is

$$E(2H[a_H]) = -27.21\ eV \tag{212}$$

The bond dissociation energy, E_D, is the difference between the total energy of the corresponding hydrogen atoms (Eq. (212)) and E_T (Eq. (211)).

$$E_D = E(2H[a_H]) - E_T = 4.478\ eV \tag{213}$$

The experimental energy is $E_D = 4.478\ eV$. The calculated and experimental parameters of H_2, D_2, H_2^+, and D_2^+ from Ref. [4] and Chp. 12 of Ref. [7] are given in Table XII.

Despite the predictions of standard quantum mechanics that preclude the imaging of a molecule orbital, the full three-dimensional structure of the outer molecular orbital of N_2 has been recently tomographically reconstructed [59]. The charge-density surface observed is similar to that shown in Figure 29 for H_2 which is direct evidence that MO's electrons are not point-particle probability waves that have no form until they are "collapsed to a point" by measurement. Rather they are physical, two-dimensional equipotential charge density functions as derived herein.

II. Hydrino States

A. Extension of the Rydberg States to Lower Levels

For a spherical resonator cavity, the nonradiative boundary condition and the relationship between the electron and the photon give the "allowed" hydrogen energy states which are quantized as a function of the parameter n. That is the nonradiative boundary condition and the relationship between an allowed radius and the photon standing wave wavelength (Eq. (92)) gives rise to Eq. (93), the boundary condition for allowed radii and allowed electron wavelengths as a function of the parameter n. Each value of n corresponds to an allowed transition effected by a resonant photon which excites the transition in the orbitsphere resonator cavity. In addition to the traditional integer values (1, 2, 3,...,) of n, values of fractions are allowed by Eq. (93) which correspond to transitions with an increase in the central field and decrease in the radius of the orbitsphere. This occurs, for example, when the orbitsphere couples to another resonator cavity which can absorb energy. This is the absorption of an energy hole by the hydrogen atom.

The absorption of an energy hole destroys the balance between the centrifugal force and the increased central electric force. Consequently, the electron undergoes a transition to a stable lower energy state. Thus, the corresponding reaction from an initial energy state to a lower energy state requiring an energy hole is called a transition reaction.

From energy conservation, the energy hole of a hydrogen atom which excites resonator modes of radial dimensions $\frac{a_H}{m+1}$ is

$$m \cdot 27.2\ eV, \quad \text{where } m = 1, 2, 3, 4, ... \tag{214}$$

After resonant absorption of the energy hole, the radius of the orbitsphere, a_H, shrinks to $\frac{a_H}{m+1}$ and after t cycles of transition, the radius is $\frac{a_H}{mt+1}$. In other words, the radial ground state field can be considered as the superposition of Fourier components. The removal of negative Fourier components of energy $m \cdot 27.2\ eV$, where m is an integer increases the positive electric field inside the spherical shell by m times the charge of a proton. The resultant electric field is a time harmonic solution of Laplace's Equations in spherical coordinates. In this case, the radius at which force balance and nonradiation are achieved is $\frac{a_H}{m+1}$ where m is an integer. In decaying to this radius from the "ground" state, a total energy of $[(m+1)^2 - 1^2] X 13.6\ eV$ is released.

The increased-binding-energy hydrogen atom is called a *hydrino atom* having a binding energy of

$$Binding\ Energy = \frac{13.6\ eV}{n^2} \tag{215}$$

where

$$n = \frac{1}{2}, \frac{1}{3}, \frac{1}{4}, ..., \frac{1}{p} \tag{216}$$

and p is an integer greater than 1. Hydrino atoms are designated as $H\left[\frac{a_H}{p}\right]$ where a_H is the radius of the hydrogen atom. The potential energy diagram of the hydrogen is extended to lower Rydberg states as given in Figure 30.

The size of the electron orbitsphere as a function of potential energy is given in Figure 31.

B. Photonic Equation

As shown previously, the photonic equation must be a solution of Laplace's equation in spherical coordinates. The "trapped photon" field comprises an electric field which provides force balance and a nonradiative orbitsphere. Following the Maxwellian approach given for excited states given in the Sec. I.L (Eq. (95)), the solution to this boundary value problem of the radial photon electric field is given by

$$\mathbf{E}_{r\,photon\;n,l,m} = \frac{e\left(na_H\right)^{\ell}}{4\pi\varepsilon_o}\frac{1}{r^{(\ell+2)}}\left[-Y_0^0\left(\theta,\phi\right)+\frac{1}{n}\left[Y_0^0\left(\theta,\phi\right)+\mathrm{Re}\left\{Y_\ell^m\left(\theta,\phi\right)e^{i\omega_n t}\right\}\right]\right]\delta(r-r_n)$$

$$\omega_n = 0 \quad for\; m = 0 \tag{217}$$

$$n = \frac{1}{p}$$

$$p = 2,3,4,...$$

$$\ell = 1,2,..., p-1$$

$$m = -\ell, -\ell+1, ..., 0, ..., +\ell$$

The quantum numbers of the electron are p, ℓ, m (m_ℓ), and m_S as given in Secs. I.C and I.L wherein the principal quantum number of excited states is replaced by $n = \frac{1}{p}$.

C. Stability of the "Ground" and Hydrino States

For the below "ground" (fractional quantum number) energy states of the hydrogen atom, σ_{photon}, the two-dimensional surface charge due to the "trapped photon" at the electron orbitsphere, is given by Eqs. (217) and (94).

$$\sigma_{photon} = \frac{e}{4\pi(r_n)^2}\left[Y_0^0(\theta,\phi) - \frac{1}{n}\left[Y_0^0(\theta,\phi) + \mathrm{Re}\left\{ Y_\ell^m(\theta,\phi) e^{i\omega_n t} \right\} \right] \right] \delta(r - r_n) \quad n = 1, \frac{1}{2}, \frac{1}{3}, \frac{1}{4}, ..., \tag{218}$$

And, $\sigma_{electron}$, the two-dimensional surface charge of the electron orbitsphere is

$$\sigma_{electron} = \frac{-e}{4\pi(r_n)^2}\left[Y_0^0(\theta,\phi) + \mathrm{Re}\left\{ Y_\ell^m(\theta,\phi) e^{i\omega_n t} \right\} \right] \delta(r - r_n) \tag{219}$$

The superposition of σ_{photon} (Eq. (218)) and $\sigma_{electron}$, (Eq. (219)) where the spherical harmonic functions satisfy the conditions given in the Angular Function section (Sec. I.C) is a radial electric monopole represented by a delta function.

$$\sigma_{photon} + \sigma_{electron} = \frac{-e}{4\pi(r_n)^2}\left[\frac{1}{n} Y_0^0(\theta,\phi) + \left(1 + \frac{1}{n}\right) \mathrm{Re}\left\{ Y_\ell^m(\theta,\phi) e^{i\omega_n t} \right\} \right] \delta(r - r_n) \quad n = 1, \frac{1}{2}, \frac{1}{3}, \frac{1}{4}, ...,$$

In the case of lower-energy states, the superposition given by Eq. (220) involves integer charge (equivalent) only. Whereas, in the case of excited states, the superposition given by Eq. (105) involves the sum of a delta function with a fractional charge (radial monopole term) and two

delta functions of charge plus one and minus one which is a doublet function (radial dipole term). As given in Sec. I.D.b, these states having a radial delta function are nonradiative since spacetime harmonics of $\frac{\omega_n}{c} = k$ or $\frac{\omega_n}{c}\sqrt{\frac{\varepsilon}{\varepsilon_o}} = k$ for which the Fourier transform of the current-density function is nonzero do not exist.

D. Catalysts

Certain atoms or ions serve as catalysts to release energy from hydrogen to produce hydrinos. For example, He^+, Ar^+, and K are predicted to serve as catalysts since they meet the catalyst criterion—a chemical or physical process with an enthalpy change equal to an integer multiple of the potential energy of atomic hydrogen, $27.2\ eV$. This catalysis releases energy from the hydrogen atom with a commensurate decrease in size of the hydrogen atom, $r_n = na_H$. For example, the catalysis of $H(n=1)$ to $H(n=1/2)$ releases $40.8\ eV$, and the hydrogen radius decreases from a_H to $\frac{1}{2}a_H$ having binding energies given by Eqs. (215) and (216).

The excited energy states of atomic hydrogen are also given by Eq. (215) except that

$$n = 2, 3, 4, ... \tag{221}$$

The $n=1$ state is the "ground" state for "pure" photon transitions (the $n=1$ state can absorb a photon and go to an excited electronic state, but it cannot release a photon and go to a lower-energy electronic state). However, an electron transition from the ground state to a lower-energy state is possible by a nonradiative energy transfer such as multipole coupling or a resonant collision mechanism. These lower-energy states have fractional quantum numbers, $n = \frac{1}{\text{integer}}$.

Processes such as the hydrogen catalytic reaction that occur without photons and that

require collisions or nonradiative energy transfer are common. For example, the exothermic chemical reaction of $H + H$ to form H_2 does not occur with the emission of a photon. Rather, the reaction requires a collision with a third body, M, to remove the bond energy- $H + H + M \rightarrow H_2 + M^*$ [60]. The third body distributes the energy from the exothermic reaction, and the end result is the H_2 molecule and an increase in the temperature of the system. Some commercial phosphors are based on nonradiative energy transfer involving multipole coupling. For example, the strong absorption strength of Sb^{3+} ions along with the efficient nonradiative transfer of excitation from Sb^{3+} to Mn^{2+}, are responsible for the strong manganese luminescence from phosphors containing these ions [61].

It is well known that the electric field of an absorbed photon superimposes that of the proton such that the electron of H moves to a higher-energy excited state at a radius that is greater than that of the n=1 state. Similarly, in order to conserve energy, the resonant nonradiative energy transfer from H to the catalyst of $m \cdot 27.2\ eV$ results in an increased interaction between the electron and the central field that is equivalent to m+1 times that of a proton. The increased interaction then causes the radius to decrease with the further release of energy such as the further emission of lines with the energies of $q \cdot 13.6\ eV$ as reported previously [62-64]. These lines can be explained as electronic transitions to fractional Rydberg states of atomic hydrogen given by Eqs. (215) and (216) wherein the catalytic system involves helium ions because the second ionization energy of helium is $54.417\ eV$, which is equivalent to $2 \cdot 27.2\ eV$. In this case, $54.417\ eV$ is transferred nonradiatively from atomic hydrogen to He^+ which is resonantly ionized. The electron decays to the $n = 1/3$ state with the further release of $54.417\ eV$ which may be emitted as a photon. The catalysis reaction is

$$54.417\ eV + He^{+} + H\left[a_H\right] \rightarrow He^{2+} + e^{-} + H\left[\frac{a_H}{3}\right] + 108.8\ eV \tag{222}$$

$$He^{2+} + e^{-} \rightarrow He^{+} + 54.417\ eV \tag{223}$$

And, the overall reaction is

$$H\left[a_H\right] \rightarrow H\left[\frac{a_H}{3}\right] + 54.4\ eV + 54.4\ eV \tag{224}$$

Since the products of the catalysis reaction have binding energies of $m \cdot 27.2\ eV$, they may further serve as catalysts. Thus, further catalytic transitions may occur: $n = \frac{1}{3} \rightarrow \frac{1}{4}$, $\frac{1}{4} \rightarrow \frac{1}{5}$, and so on.

Since the reactions given by Eqs. (222-224) involve two steps of energy release, it may be written as follows:

$$54.417\ eV + He^{+} + H\left[a_H\right] \rightarrow He^{2+} + e^{-} + H*\left[\frac{a_H}{3}\right] + 54.4\ eV \tag{225}$$

$$H*\left[\frac{a_H}{3}\right] \rightarrow H\left[\frac{a_H}{3}\right] + 54.4\ eV \tag{226}$$

$$He^{2+} + e^{-} \rightarrow He^{+} + 54.417\ eV \tag{227}$$

And, the overall reaction is

$$H\left[a_H\right] \rightarrow H\left[\frac{a_H}{3}\right] + 54.4\ eV + 54.4\ eV \tag{228}$$

wherein $H*\left[\frac{a_H}{3}\right]$ has the radius of the hydrogen atom and a central field equivalent to 3 times that of a proton and $H\left[\frac{a_H}{3}\right]$ is the corresponding stable state with the radius of 1/3 that of H.

H is the lightest atom; thus, it is the most probable fast species in collisional energy

exchange from the H intermediate (e.g. $H*\left[\frac{a_H}{3}\right]$). Additionally, H is unique with regard to $H*\left[\frac{a_H}{p}\right]$ in that all are these species are energy states of hydrogen with corresponding harmonic de Broglie wavelengths. Thus, the cross section for H excitation by a nonradiative energy transfer to form fast H is predicted to be large since it is a resonant process. Efficient energy transfer can occur by through-space mechanisms which are common such as dipole-dipole interactions as described by Förster's theory [65-69]. Consequently, in addition to radiation, a resonant transfer to form fast H may occur, and the emission of $H\left(n=3\right)$ from fast $H\left(n=1\right)$ atoms excited by collisions with the background H_2 may occur. Extraordinary (>100 eV) Balmer α line broadening is observed consistent with predictions [70-73].

E. Data

The data from a broad spectrum of investigational techniques strongly and consistently indicates that hydrogen can exist in lower-energy states then previously thought possible. The predicted reaction involves a resonant, nonradiative energy transfer from otherwise stable atomic hydrogen to a catalyst capable of accepting the energy. The product is $H\left(1/p\right)$, fractional Rydberg states of atomic hydrogen wherein $n=\frac{1}{2},\frac{1}{3},\frac{1}{4},...,\frac{1}{p}$; ($p\leq 137$ is an integer) replaces the well known parameter $n=\text{integer}$ in the Rydberg equation for hydrogen excited states. These atomic products react to more stable hydride ions $H^-\left(1/p\right)$ in novel hydride compounds and lower-energy molecular hydrogen $H_2\left(1/p\right)$.

A new chemically generated or assisted plasma source based on the resonant energy

transfer mechanism (rt-plasma) between atomic hydrogen and certain catalysts has been developed that may be a new power source. One such source operates by incandescently heating a hydrogen dissociator and a catalyst to provide atomic hydrogen and gaseous catalyst, respectively, such that the catalyst reacts with the atomic hydrogen to produce a plasma. It was extraordinary that intense extreme ultraviolet (EUV) emission was observed by Mills et al. [74-79] at low temperatures (e.g. $\approx 10^3\ K$) and an extraordinary low field strength of about 1-2 V/cm from atomic hydrogen and certain atomized elements or certain gaseous ions which singly or multiply ionize at integer multiples of the potential energy of atomic hydrogen, $27.2\ eV$. A number of independent experimental observations confirm that the rt-plasma is due to a novel reaction of atomic hydrogen which produces as chemical intermediates, hydrogen in fractional quantum states that are at lower energies than the traditional "ground" ($n = 1$) state. Power is released [63, 74, 80-82], and the final reaction products are novel hydride compounds [74, 82-88] or lower-energy molecular hydrogen [82, 85]. The supporting data include EUV spectroscopy [62-64, 72, 75-79, 82-85, 89-90], characteristic emission from catalysts and the hydride ion products [76, 78, 82-84, 89-90], lower-energy hydrogen emission [62-64, 82, 85], chemically formed plasmas [74-79, 82-84, 89-90], extraordinary (>100 eV) Balmer α line broadening [70-76, 78, 83, 89-90], population inversion of H lines [89-91], elevated electron temperature [63, 70, 71], anomalous plasma afterglow duration [79], power generation [63, 74, 80-82], and analysis of novel chemical compounds [74, 82, 85-88].

III. Conclusion

SQM has never dealt with the nature of fundamental particles. Rather, it postulates the impossible situation that they occupy no volume; yet are everywhere at once. In contrast, using

the classical wave equation with the constraint of nonradiation based on Maxwell's equations, CQM gives closed-form physical solutions for the electron in atoms, the free electron, and excited states which match the observations. With these solutions, conjugate parameters can be solved for the first time, and atomic theory is at last made predictive and intuitive. Application of Maxwell's equations precisely predicts hundreds of fundamental spectral observations in exact equations with no adjustable parameters (fundamental constants only). Moreover, unification of atomic and large scale physics, the ultimate objective of natural theory, is enabled. The result gives a natural relationship between Maxwell's equations, special relativity, and general relativity. CQM holds over a scale of spacetime of 85 orders of magnitude—it correctly predicts the nature of the universe from the scale of the quarks to that of the cosmos.

In this paper, a summary of the results of CQM [2-11] was presented. (The details of the derivations are given in Ref. [7].) Specifically, CQM gives closed form solutions for the atom including the stability of the $n = 1$ state and the instability of the excited states, the equation of the photon and electron in excited states, the equation of the free electron, and photon which predict the wave particle duality behavior of particles and light. The current and charge density functions of the electron may be directly physically interpreted. For example, spin angular momentum results from the motion of negatively charged mass moving systematically, and the equation for angular momentum, $\mathbf{r} \times \mathbf{p}$, can be applied directly to the wave function (a current density function) that describes the electron. The magnetic moment of a Bohr magneton, Stern Gerlach experiment, g factor, Lamb shift, resonant line width and shape, selection rules, correspondence principle, wave particle duality, excited states, reduced mass, rotational energies, and momenta, orbital and spin splitting, spin-orbital coupling (fine structure), Knight shift, and spin-nuclear coupling (hyperfine structure), muonium hyperfine structure interval, ionization

energies of multielectron atoms, elastic electron scattering from helium atoms, and the nature of the chemical bond are derived in closed form equations based on Maxwell's equations. The calculations agree with experimental observations.

For any kind of wave advancing with limiting velocity and capable of transmitting signals, the equation of front propagation is the same as the equation for the front of a light wave. By applying this condition to electromagnetic and gravitational fields at particle production, the Schwarzschild metric (SM) is derived from the classical wave equation which modifies general relativity to include conservation of spacetime (See Ref. [7], Chp. 23 and footnote 7 of Chp. 23), in addition to momentum and matter/energy. The result gives a natural relationship between Maxwell's equations, special relativity, and general relativity. It gives gravitation from the atom to the cosmos. The universe is time harmonically oscillatory in matter energy and spacetime expansion and contraction with a minimum radius that is the gravitational radius. In closed form equations with fundamental constants only, CQM gives the deflection of light by stars, the precession of the perihelion of Mercury, the particle masses, the Hubble constant, the age of the universe, the observed acceleration of the expansion, the power of the universe, the power spectrum of the universe, the microwave background temperature, the uniformity of the microwave background radiation at 2.7 K with the microkelvin spatial variation observed by the DASI, the observed violation of the GZK cutoff, the mass density, the large scale structure of the universe, and the identity of dark matter which matches the criteria for the structure of galaxies. In a special case wherein the gravitational potential energy density of a blackhole equals that of the Planck mass, matter converts to energy and spacetime expands with the release of a gamma ray burst. The singularity in the SM is eliminated.

The Maxwellian approach allows to the solution of previously intractable problems such

as the equations of the masses of fundamental particles. Exemplary relations between fundamental particles are shown in Table XIII.

It successfully predicted the mass of the top quark before it was reported and correctly predicted the acceleration of the expansion of the universe before it was observed [94]. It further predicts the existence of new states of hydrogen that are lower in energy than the n=1 state that represents a new energy source and a new field of chemistry that has far reaching technological implications in power generation, materials, lighting, and lasers. The existence of such states has been confirmed by the data presented in over 60 published journal articles and over 50 independent tests reports and articles [95].

Having presented the theory of CQM, the misunderstandings and errors of a critique by Rathke [1] were then addressed. Rathke missed the use of the stability to radiation as the constraint to solve the nature of the bound electron. The requirement that the electron equation of motion obeys a two-dimensional wave equation arises from the constraint that the bound electron does not radiate according to Maxwell's equations. It does not arise from a Bohr-type condition or some wave-particle duality notion. Nothing is waving including probability.

The angular charge-density wave functions given by Eq. (31) are solutions of the two-dimensional wave equation plus time. Rathke has copied the two-dimensional wave equation incorrectly and reversed the sign of the time differential. His other comments about incurable failures are made moot by this careless error.

The equations of motion are the same in all frames. Only the radius is corrected due to relative motion. The equations are relativistically invariant. The azimuthal motion is an inertial frame as supported by many experiments. The correctness of the relativistic radius correction is confirmed by the remarkable agreement between predictions and experiments on numerous

experimental observables such as the electron g factor, the invariance of the electron magnetic moment of μ_B and angular momentum of $\hbar$, the Lamb shift, the fine structure and hyperfine structure of the hydrogen atom, the hyperfine structure intervals of positronium and muonium and the relativistically corrected ionization energies of one- and two-electron atoms.

In contradiction to Rathke's claim that excited states can not be solved by CQM, the excited states of hydrogen and now helium are given in closed-form equations with fundamental constants only. These results are derived from Maxwell's equations based on the physical process of excitation of the electron state by the photon. These results can not be reproduced by SQM. Even for the hydrogen excited states, the SQM methodology involves no physics and is arguably simply another form of the Rydberg formula to which it reduces. It is not predictive and is has many consequences that are not in agreement with observations [2-11].

Hydrino states are predicted from Maxwell's equations in an analogous manner as the excited states. The equations of the excited states and hydrino states and the mechanism for their formation are given in contradiction to Rathke's claim. The data including an independent replication under NIAC [96] overwhelmingly demonstrates their existence and the exothermic reaction of their formation.

References

1. A. Rathke, New J. Phys. **7**, 127 (2005).

2. R. L. Mills, Phys. Essays **16**, 433 (2003).

3. R. L. Mills, Phys. Essays **18**, 321 (2005).

4. R. L. Mills, Physics Essays **17**, 342 (2004).

5. R. L. Mills, "Maxwell's Equations and QED: Which is Fact and Which is Fiction," Physics Essays, **25**, 225 (2006).

6. R. L. Mills, "Exact Classical Quantum Mechanical Solution for Atomic Helium Which Predicts Conjugate Parameters from a Unique Solution for the First Time," in press, posted with speadsheets at http://www.blacklightpower.com/theory/theory.shtml..

7. R. Mills, *The Grand Unified Theory of Classical Quantum Mechanics*; April 2007 Edition, posted at http://www.blacklightpower.com/theory/bookdownload.shtml.

8. R. L. Mills, Annales de la Fondation Louis de Broglie, **30**, 129 (2005).

9. R. L. Mills, Int. J. Hydrogen Energy **27**, 565 (2002).

10. R. L. Mills, Int. J. Hydrogen Energy **26**, 1059 (2001).

11. R. L Mills, Int. J. of Hydrogen Energy **25**, 1171 (2000).

12. P. Pearle, Foundations Phys. **7**, 931 (1977).

13. V. F. Weisskopf, Rev. Mod. Phys. **21**, 305 (1949).

14. A. Einstein, B. Podolsky, N. Rosen, Phys. Rev. **47**, 777 (1935).

15. H. Wergeland, "The Klein Paradox Revisited", *Old and New Questions in Physics, Cosmology, Philosophy, and Theoretical Biology*, A. van der Merwe, Editor (Plenum Press, New York, 1983), pp. 503-515.

16. F. Laloë, Am. J. Phys. **69** (6), 655 (2001).

17. F. Dyson, Am. J. Phys. **58**, 209 (1990).

18. H. A. Haus, Am. J. Phys. **54**, 1126 (1986).

19. http://www.blacklightpower.com/theory/theory.shtml.

20. F. Bueche, *Introduction to Physics for Scientists and Engineers*, 2nd Edition, (McGraw-Hill, 1975), pp. 352-353.

21. D. A. McQuarrie, *Quantum Chemistry*, (University Science Books, Mill Valley, CA, 1983), pp. 206-225.

22. P. Sprangle and A. T. Drobot, IEEE Trans. Microwave Theor. Tech. **25**, 528 (1977).

23. J. Daboul and J. H. D. Jensen, Z. Physik **265**, 455 (1973).

24. T. A. Abbott and D. J. Griffiths, Am. J. Phys. **53**, 1203 (1985).

25. G. Goedecke, Phys. Rev. **135B**, 281 (1964).

26. J. D. Jackson, *Classical Electrodynamics*, 2nd Edition (John Wiley & Sons, New York, 1975), pp. 739-779.

27. D. A. McQuarrie, *Quantum Chemistry*, (University Science Books, Mill Valley, CA, 1983), pp. 238-241.

28. R. C. Weast, *CRC Handbook of Chemistry and Physics*, 68th Edition, (CRC Press, Boca Raton, Florida, 1987-88), p. F-186 to p. F-187.

29. R. S. Van Dyck, Jr., P. Schwinberg, H. Dehmelt, Phys. Rev. Lett. **59**, 26 (1987).

30. P. J. Mohr, B. N. Taylor, "CODATA recommended values of the fundamental physical constants: 1998," Rev. Mod. Phys. **72**(2), 376-378, 474 (2000).

31. G. P. Lepage, "Theoretical advances in quantum electrodynamics," International Conference on Atomic Physics, Atomic Physics; Proceedings, Singapore, World Scientific, Vol. 7, (1981), pp. 297-311.

32. E. R. Williams, P. T. Olsen, Phys. Rev. Lett. **42**, 1575 (1979).

33. K. v. Klitzing, G. Dorda, M. Pepper, Phys. Rev. Lett. **45**, 494 (1980).

34. H. Margenau, G. M. Murphy, *The Mathematics of Chemistry and Physics*, 2nd Edition, (D. Van Nostrand Company, Inc., New York, 1956), pp. 363-367.

35. C. E. Moore, "Ionization Potentials and Ionization Limits Derived from the Analyses of Optical Spectra," Nat. Stand. Ref. Data Ser.-Nat. Bur. Stand. (U.S.), No. 34, 1970.

36. D. R. Lide, *CRC Handbook of Chemistry and Physics*, 79th Edition, (CRC Press, Boca Raton, Florida, 1998-9), p. 10-175 to p. 10-177.

37. http://physics.nist.gov/PhysRefData/ASD/levels_form.html.

38. A. Gumberidze, et al., Phys. Rev. Letts., **94**, 223001 (2005).

39. M. Mizushima, *Quantum Mechanics of Atomic Spectra and Atomic Structure*, (W.A. Benjamin, Inc., New York, 1970), p.17.

40. J. D. Jackson, *Classical Electrodynamics*, 2nd Edition, (John Wiley & Sons, New York, 1975), pp. 739-752.

41. J. D. Jackson, *Classical Electrodynamics*, 2nd Edition, (John Wiley & Sons, New York, 1975), pp. 758-763.

42. P. J. Mohr, B. N. Taylor, "CODATA recommended values of the fundamental physical constants: 1998," Rev. Mod. Phys. **72**(2), 371 (2000).

43. P. J. Mohr, B. N. Taylor, "CODATA recommended values of the fundamental physical constants: 1998," Rev. Mod. Phys. **72**(2), 418 (2000).

44. P. J. Mohr, B. N. Taylor, "CODATA recommended values of the fundamental physical constants: 1998," Rev. Mod. Phys. **72**(2), 418-419 (2000).

45. W. Liu, et al., Phys. Rev. Letts. **82**, 711 (1999).

46. M. W. Ritter, P. O. Egan, V. W. Hughes, K. A. Woodle, Phys. Rev. A **30**, 1331 (1984).

47. NIST Atomic Spectra Database, www.physics.nist.gov/cgi-bin/AtData/display.ksh.

48. E. M. Purcell, *Electricity and Magnetism*, (McGraw-Hill, New York, 1965), pp. 156-167.

49. D. B. Clark, J. Chem. Ed. **68**, 454 (1991).

50. J. Gribbin, "More to electrons that meets the eye," New Scientist, January 25, (1997), p. 15.

51. I. Levine, et al., Phys. Rev. Lett. **78**, 424 (1997).

52. R. N. Bracewell, *The Fourier Transform and Its Applications*, (McGraw-Hill Book Company, New York, 1978), pp. 248-249.

53. R. C. Weast, *CRC Handbook of Chemistry and Physics*, 58th Edition, (CRC Press, West Palm Beach, FL, 1977), p. E-68.

54. P. J. Bromberg, J. Chem. Phys. **50**, 3906 (1969).

55. J. Geiger, *Zeitschrift fur Physik*, **175**, 530 (1963).

56. S. N. Pisharody, R. R. Jones, Science **303**, 813 (2004).

57. C. R. Stroud, Science **303**, 778 (2004).

58. H. Maeda, D. V. L. Norum, T. F. Gallagher, Science. **307**, 1757 (2005).

59. J. Itatani, et al., Nature, **432**, 867 (2004).

60. N. V. Sidgwick, *The Chemical Elements and Their Compounds*, Volume I, (Clarendon Press, Oxford, 1950), p.17.

61. M. D. Lamb, *Luminescence Spectroscopy*, (Academic Press, London, 1978), p. 68.

62. R. L. Mills, P. Ray, J. Phys. D, Appl. Phys. **36**, 1535 (2003).

63. R. L. Mills, P. Ray, B. Dhandapani, M. Nansteel, X. Chen, J. He, J Mol. Struct. **643**(1-3), 43 (2002).

64. R. Mills, P. Ray, Int. J. Hydrogen Energy **27**, 301 (2002).

65. F. Wilkinson, "Intramolecular Electronic Energy Transfer Between Organic Molecules," *Luminescence in Chemistry*, E. J. Bowen, Editor, (D. Van Nostrand Co. Ltd., London, 1968), Chapter 8, pp. 154-182.

66. H. Morawetz, Science **240**, 172 (1988).

67. O. Schnepp, M. Levy, J. Am. Chem. Soc. **84**, 172 (1962).

68. F. Wilkinson, *Luminescence in Chemistry*, E. J. Bowen, Editor, (D. Van Nostrand Co. Ltd., London, 1968), pp. 155-182.

69. Th. Förster, *Comparative Effects of Radiation*, Report of a Conference held at the University of Puerto Rico, San Juan, February 15-19, (1960), sponsored by the National Academy of Sciences; National Research Council, Edited by Milton Burton, J. S. Kirby-Smith, and John L. Magee, John Wiley & Sons, Inc., New York, (1960), pp. 300-325.

70. R. L. Mills, P. Ray, B. Dhandapani, R. M. Mayo, J. He, J. Appl. Phys. **92**, 7008 (2002).

71. R. L. Mills, P. Ray, B. Dhandapani, J. He, IEEE Trans. Plasma Sci. **31**, 338 (2003).

72. R. L. Mills, P. Ray, New J. Phys. **4**, 22.1 (2002).

73. J. Phillips, C. Chen, "Evidence of Energetic Reaction Between Helium and Hydrogen Species in RF Generated Plasmas," submitted.

74. R. Mills, P. Ray, B. Dhandapani, W. Good, P. Jansson, M. Nansteel, J. He, A. Voigt, Eur. Phys. J. Appl. Phys. **28**, 83 (2004).

75. R. Mills and M. Nansteel, P. Ray, IEEE Trans. Plasma Sci. **30**, 639 (2002).

76. R. Mills and M. Nansteel, P. Ray, New J. Phys. **4**, 70.1 (2002).

77. R. Mills, J. Dong, Y. Lu, Int. J. Hydrogen Energy **25**, 919 (2000).

78. R. Mills, M. Nansteel and P. Ray, J. Plasma Phys. **69**, 131 (2003).

79. H. Conrads, R. Mills, Th. Wrubel, Plasma Sources Sci. Technol. **12**, 389 (2003).

80. J. Phillips, R. L. Mills, X. Chen, J. Appl. Phys. 96, 3095 (2004).

81. R. L. Mills, X. Chen, P. Ray, J. He, B. Dhandapani, Thermochim. Acta **406**/1-2, 35 (2003).

82. R. Mills, J. He, Z. Chang, W. Good, Y. Lu, B. Dhandapani, Int. J. Hydrogen Energy **32**, 2573 (2007).

83. R. L. Mills, P. Ray, Int. J. Hydrogen Energy **28**, 825, (2003).

84. R. Mills, Int. J. Hydrogen Energy **26**, 1041 (2001).

85. R. L. Mills, Y. Lu, M. Nansteel, J. He, A. Voigt, B. Dhandapani, "Energetic Catalyst-Hydrogen Plasma Reaction as a Potential New Energy Source," Division of Fuel Chemistry, Session: Chemistry of Solid, Liquid, and Gaseous Fuels, 227th American Chemical Society National Meeting, March 28-April 1, 2004, Anaheim, CA.

86. R. Mills, B. Dhandapani, M. Nansteel, J. He, T. Shannon, A. Echezuria, Int. J. Hydrogen Energy **26**, 339 (2001).

87. R. Mills, B. Dhandapani, N. Greenig, J. He, Int. J. Hydrogen Energy **25**, 1185 (2000).

88. R. Mills, B. Dhandapani, M. Nansteel, J. He, A. Voigt, Int. J. Hydrogen Energy **26**, 965 (2001).

89. R. Mills, P. Ray, R. M. Mayo, IEEE Trans. Plasma Sci. **31**, 236 (2003).

90. R. L. Mills, P. Ray, J. Phys. D, Appl. Phys. **36**, 1504 (2003).

91. R. Mills, P. Ray, R. M. Mayo, Appl. Phys. Lett. **82**, 1679 (2003).

92. K. Hagiwara et al., Phys. Rev. D 66, 010001 (2002); http://pdg.lbl.gov/2002/s035.pdf.

93. P. J. Mohr and B. N. Taylor, "CODATA recommended values of the fundamental physical constants: 1998," Rev. Mod. Phys. **72**(2), 351 (2000).

94. R. Mills, *The Grand Unified Theory of Classical Quantum Mechanics*; 1995 Edition, ISBN 0-9635171-1-2, Library of Congress Card Number 94-077780.

95. http://www.blacklightpower.com/

96. A. J. Marchese, P. M. Jansson, J. L. Schmalzel, “The BlackLight Rocket Engine,” Phase I Final Report, NASA Institute for Advanced Concepts Phase I, May 1-November 30, 2002, http://www.niac.usra.edu/files/studies/final_report/pdf/752Marchese.pdf.

Table I. Relativistic ionization energies for some one-electron atoms.

One e Atom	Z	β (Eq. (1.267) of Ref. [7])	Theoretical Ionization Energies (eV) (Eq. (1.272) of Ref. [7])	Experimental Ionization Energies (eV) [a]	Relative Difference between Experimental and Calculated [b]
H	1	0.00730	13.59847	13.59844	-0.000002
He^{+}	2	0.01459	54.41826	54.41778	-0.000009
Li^{2+}	3	0.02189	122.45637	122.45429	-0.000017
Be^{3+}	4	0.02919	217.72427	217.71865	-0.000026
B^{4+}	5	0.03649	340.23871	340.2258	-0.000038
C^{5+}	6	0.04378	490.01759	489.99334	-0.000049
N^{6+}	7	0.05108	667.08834	667.046	-0.000063
O^{7+}	8	0.05838	871.47768	871.4101	-0.000078
F^{8+}	9	0.06568	1103.220	1103.1176	-0.000093
Ne^{9+}	10	0.07297	1362.348	1362.1995	-0.000109
Na^{10+}	11	0.08027	1648.910	1648.702	-0.000126
Mg^{11+}	12	0.08757	1962.945	1962.665	-0.000143
Al^{12+}	13	0.09486	2304.512	2304.141	-0.000161
Si^{13+}	14	0.10216	2673.658	2673.182	-0.000178

P^{14+}	15	0.10946	3070.451	3069.842	-0.000198
S^{15+}	16	0.11676	3494.949	3494.1892	-0.000217
Cl^{16+}	17	0.12405	3947.228	3946.296	-0.000236
Ar^{17+}	18	0.13135	4427.363	4426.2296	-0.000256
K^{18+}	19	0.13865	4935.419	4934.046	-0.000278
Ca^{19+}	20	0.14595	5471.494	5469.864	-0.000298
Sc^{20+}	21	0.15324	6035.681	6033.712	-0.000326
Ti^{21+}	22	0.16054	6628.064	6625.82	-0.000339
V^{22+}	23	0.16784	7248.745	7246.12	-0.000362
Cr^{23+}	24	0.17514	7897.827	7894.81	-0.000382
Mn^{24+}	25	0.18243	8575.426	8571.94	-0.000407
Fe^{25+}	26	0.18973	9281.650	9277.69	-0.000427
Co^{26+}	27	0.19703	10016.63	10012.12	-0.000450
Ni^{27+}	28	0.20432	10780.48	10775.4	-0.000471
Cu^{28+}	29	0.21162	11573.34	11567.617	-0.000495
Zn^{29+}	30	0.21892	12395.35	12388.93	-0.000518
Ga^{30+}	31	0.22622	13246.66	13239.49	-0.000542
Ge^{31+}	32	0.23351	14127.41	14119.43	-0.000565
As^{32+}	33	0.24081	15037.75	15028.62	-0.000608
Se^{33+}	34	0.24811	15977.86	15967.68	-0.000638
Kr^{35+}	36	0.26270	17948.05	17936.21	-0.000660
Rb^{36+}	37	0.27000	18978.49	18964.99	-0.000712

Mo^{41+}	42	0.30649	24592.04	24572.22	-0.000807
Xe^{53+}	54	0.39406	41346.76	41299.7	-0.001140
U^{91+}	92	0.67136	132279.32	131848.5	-0.003268

[a] From theoretical calculations, interpolation of H isoelectronic and Rydberg series, and experimental data [35-38].

[b] (Experimental-theoretical)/experimental.

Table II. Calculated energies (non-relativistic; no spin-orbit interaction; no electronic spin/nuclear spin interaction) and ionization energies for the hydrogen atom in the ground state and some excited states.

n	Z	Calculated r_n [a] (a_H)	Calculated Kinetic Energy[b] (eV)	Calculated Potential Energy[c] (eV)	Calculated Ionization Energy[d] (eV)	Experimental Ionization Energy[e] (eV)
1	1	1.000	13.598	-27.196	13.598	13.595
2	$\frac{1}{2}$	2.000	3.400	-6.799	3.400	3.393
3	$\frac{1}{3}$	3.000	1.511	-3.022	1.511	1.511
5	$\frac{1}{5}$	5.000	0.544	-1.088	0.544	0.544
10	$\frac{1}{10}$	10.000	0.136	-0.272	0.136	0.136

[a] from Eq. (99)

[b] from $T=-\frac{1}{2}V$

[c] from Eq. (85)

[d] from Eq. (102)

[e] experimental

Table III. Calculated and experimental energies of states of helium.

n	ℓ	r_1 (a_{He})	r_2 (a_{He})	Term Symbol	E_{ele} CQM He I Energy Levels (eV)	NIST He I Energy Levels [d] (eV)	Difference CQM-NIST (eV)	Relative Difference (CQM-NIST)
1	0	0.56699	0.566987	$1s^2\ ^1S$	-24.58750	-24.58741	-0.000092	0.0000038
2	0	0.506514	1.42265	$1s2s\ ^3S$	-4.78116	-4.76777	-0.0133929	0.0028090
2	0	0.501820	1.71132	$1s2s\ ^1S$	-3.97465	-3.97161	-0.0030416	0.0007658
2	1	0.500571	1.87921	$1s2p\ ^3P^0_2$	-3.61957	-3.6233	0.0037349	-0.0010308
2	1	0.500571	1.87921	$1s2p\ ^3P^0_1$	-3.61957	-3.62329	0.0037249	-0.0010280
2	1	0.500571	1.87921	$1s2p\ ^3P^0_0$	-3.61957	-3.62317	0.0036049	-0.0009949
2	1	0.499929	2.01873	$1s2p\ ^1P^0$	-3.36941	-3.36936	-0.0000477	0.0000141
3	0	0.500850	2.42265	$1s3s\ ^3S$	-1.87176	-1.86892	-0.0028377	0.0015184
3	0	0.500302	2.71132	$1s3s\ ^1S$	-1.67247	-1.66707	-0.0054014	0.0032401
3	1	0.500105	2.87921	$1s3p\ ^3P^0_2$	-1.57495	-1.58031	0.0053590	-0.0033911
3	1	0.500105	2.87921	$1s3p\ ^3P^0_1$	-1.57495	-1.58031	0.0053590	-0.0033911
3	1	0.500105	2.87921	$1s3p\ ^3P^0_0$	-1.57495	-1.58027	0.0053190	-0.0033659
3	2	0.500011	2.98598	$1s3d\ ^3D_3$	-1.51863	-1.51373	-0.0049031	0.0032391

3	2	0.500011	2.98598	$1s3d\ ^3D_2$	-1.51863	-1.51373	-0.0049031	0.0032391
3	2	0.500011	2.98598	$1s3d\ ^3D_1$	-1.51863	-1.51373	-0.0049031	0.0032391
3	2	0.499999	3.00076	$1s3d\ ^1D$	-1.51116	-1.51331	0.0021542	-0.0014235
3	1	0.499986	3.01873	$1s3p\ ^1P^0$	-1.50216	-1.50036	-0.0017999	0.0011997
4	0	0.500225	3.42265	$1s4s\ ^3S$	-0.99366	-0.99342	-0.0002429	0.0002445
4	0	0.500088	3.71132	$1s4s\ ^1S$	-0.91637	-0.91381	-0.0025636	0.0028054
4	1	0.500032	3.87921	$1s4p\ ^3P^0_2$	-0.87671	-0.87949	0.0027752	-0.0031555
4	1	0.500032	3.87921	$1s4p\ ^3P^0_1$	-0.87671	-0.87949	0.0027752	-0.0031555
4	1	0.500032	3.87921	$1s4p\ ^3P^0_0$	-0.87671	-0.87948	0.0027652	-0.0031442
4	2	0.500003	3.98598	$1s4d\ ^3D_3$	-0.85323	-0.85129	-0.0019398	0.0022787
4	2	0.500003	3.98598	$1s4d\ ^3D_2$	-0.85323	-0.85129	-0.0019398	0.0022787
4	2	0.500003	3.98598	$1s4d\ ^3D_1$	-0.85323	-0.85129	-0.0019398	0.0022787
4	2	0.500000	4.00076	$1s4d\ ^1D$	-0.85008	-0.85105	0.0009711	-0.0011411
4	3	0.500000	3.99857	$1s4f\ ^3F^0_3$	-0.85054	-0.85038	-0.0001638	0.0001926
4	3	0.500000	3.99857	$1s4f\ ^3F^0_4$	-0.85054	-0.85038	-0.0001638	0.0001926
4	3	0.500000	3.99857	$1s4f\ ^3F^0_2$	-0.85054	-0.85038	-0.0001638	0.0001926
4	3	0.500000	4.00000	$1s4f\ ^1F^0$	-0.85024	-0.85037	0.0001300	-0.0001529
4	1	0.499995	4.01873	$1s4p\ ^1P^0$	-0.84628	-0.84531	-0.0009676	0.0011446
5	0	0.500083	4.42265	$1s5s\ ^3S$	-0.61519	-0.61541	0.0002204	-0.0003582
5	0	0.500035	4.71132	$1s5s\ ^1S$	-0.57750	-0.57617	-0.0013253	0.0023002

5	1	0.500013	4.87921	$1s5p\ ^3P^0_2$	-0.55762	-0.55916	0.0015352	-0.0027456
5	1	0.500013	4.87921	$1s5p\ ^3P^0_1$	-0.55762	-0.55916	0.0015352	-0.0027456
5	1	0.500013	4.87921	$1s5p\ ^3P^0_0$	-0.55762	-0.55915	0.0015252	-0.0027277
5	2	0.500001	4.98598	$1s5d\ ^3D_3$	-0.54568	-0.54472	-0.0009633	0.0017685
5	2	0.500001	4.98598	$1s5d\ ^3D_2$	-0.54568	-0.54472	-0.0009633	0.0017685
5	2	0.500001	4.98598	$1s5d\ ^3D_1$	-0.54568	-0.54472	-0.0009633	0.0017685
5	2	0.500000	5.00076	$1s5d\ ^1D$	-0.54407	-0.54458	0.0005089	-0.0009345
5	3	0.500000	4.99857	$1s5f\ ^3F^0_3$	-0.54431	-0.54423	-0.0000791	0.0001454
5	3	0.500000	4.99857	$1s5f\ ^3F^0_4$	-0.54431	-0.54423	-0.0000791	0.0001454
5	3	0.500000	4.99857	$1s5f\ ^3F^0_2$	-0.54431	-0.54423	-0.0000791	0.0001454
5	3	0.500000	5.00000	$1s5f\ ^1F^0$	-0.54415	-0.54423	0.0000764	-0.0001404
5	4	0.500000	4.99988	$1s5g\ ^3G_4$	-0.54417	-0.54417	0.0000029	-0.0000054
5	4	0.500000	4.99988	$1s5g\ ^3G_5$	-0.54417	-0.54417	0.0000029	-0.0000054
5	4	0.500000	4.99988	$1s5g\ ^3G_3$	-0.54417	-0.54417	0.0000029	-0.0000054
5	4	0.500000	5.00000	$1s5g\ ^1G$	-0.54415	-0.54417	0.0000159	-0.0000293
5	1	0.499998	5.01873	$1s5p\ ^1P^0$	-0.54212	-0.54158	-0.0005429	0.0010025
6	0	0.500038	5.42265	$1s6s\ ^3S$	-0.41812	-0.41838	0.0002621	-0.0006266
6	0	0.500016	5.71132	$1s6s\ ^1S$	-0.39698	-0.39622	-0.0007644	0.0019291
6	1	0.500006	5.87921	$1s6p\ ^3P^0_2$	-0.38565	-0.38657	0.0009218	-0.0023845
6	1	0.500006	5.87921	$1s6p\ ^3P^0_1$	-0.38565	-0.38657	0.0009218	-0.0023845

6	1	0.500006	5.87921	$1s6p\ ^3P^0_0$	-0.38565	-0.38657	0.0009218	-0.0023845
6	2	0.500001	5.98598	$1s6d\ ^3D_3$	-0.37877	-0.37822	-0.0005493	0.0014523
6	2	0.500001	5.98598	$1s6d\ ^3D_2$	-0.37877	-0.37822	-0.0005493	0.0014523
6	2	0.500001	5.98598	$1s6d\ ^3D_1$	-0.37877	-0.37822	-0.0005493	0.0014523
6	2	0.500000	6.00076	$1s6d\ ^1D$	-0.37784	-0.37813	0.0002933	-0.0007757
6	3	0.500000	5.99857	$1s6f\ ^3F^0_3$	-0.37797	-0.37793	-0.0000444	0.0001176
6	3	0.500000	5.99857	$1s6f\ ^3F^0_4$	-0.37797	-0.37793	-0.0000444	0.0001176
6	3	0.500000	5.99857	$1s6f\ ^3F^0_2$	-0.37797	-0.37793	-0.0000444	0.0001176
6	3	0.500000	6.00000	$1s6f\ ^1F^0$	-0.37788	-0.37793	0.0000456	-0.0001205
6	4	0.500000	5.99988	$1s6g\ ^3G_4$	-0.37789	-0.37789	-0.0000023	0.0000060
6	4	0.500000	5.99988	$1s6g\ ^3G_5$	-0.37789	-0.37789	-0.0000023	0.0000060
6	4	0.500000	5.99988	$1s6g\ ^3G_3$	-0.37789	-0.37789	-0.0000023	0.0000060
6	4	0.500000	6.00000	$1s6g\ ^1G$	-0.37788	-0.37789	0.0000053	-0.0000140
6	5	0.500000	5.99999	$1s6h\ ^3H^0_4$	-0.37789	-0.37788	-0.0000050	0.0000133
6	5	0.500000	5.99999	$1s6h\ ^3H^0_5$	-0.37789	-0.37788	-0.0000050	0.0000133
6	5	0.500000	5.99999	$1s6h\ ^3H^0_6$	-0.37789	-0.37788	-0.0000050	0.0000133
6	5	0.500000	6.00000	$1s6h\ ^1H^0$	-0.37788	-0.37788	-0.0000045	0.0000119
6	1	0.499999	6.01873	$1s6p\ ^1P^0$	-0.37671	-0.37638	-0.0003286	0.0008730
7	0	0.500019	6.42265	$1s7s\ ^3S$	-0.30259	-0.30282	0.0002337	-0.0007718
7	0	0.500009	6.71132	$1s7s\ ^1S$	-0.28957	-0.2891	-0.0004711	0.0016295

7	1	0.500003	6.87921	$1s7p\ ^3P^0_2$	-0.28250	-0.28309	0.0005858	-0.0020692
7	1	0.500003	6.87921	$1s7p\ ^3P^0_1$	-0.28250	-0.28309	0.0005858	-0.0020692
7	1	0.500003	6.87921	$1s7p\ ^3P^0_0$	-0.28250	-0.28309	0.0005858	-0.0020692
7	2	0.500000	6.98598	$1s7d\ ^3D_3$	-0.27819	-0.27784	-0.0003464	0.0012468
7	2	0.500000	6.98598	$1s7d\ ^3D_2$	-0.27819	-0.27784	-0.0003464	0.0012468
7	2	0.500000	6.98598	$1s7d\ ^3D_1$	-0.27819	-0.27784	-0.0003464	0.0012468
7	2	0.500000	7.00076	$1s7d\ ^1D$	-0.27760	-0.27779	0.0001907	-0.0006864
7	3	0.500000	6.99857	$1s7f\ ^3F^0_3$	-0.27769	-0.27766	-0.0000261	0.0000939
7	3	0.500000	6.99857	$1s7f\ ^3F^0_4$	-0.27769	-0.27766	-0.0000261	0.0000939
7	3	0.500000	6.99857	$1s7f\ ^3F^0_2$	-0.27769	-0.27766	-0.0000261	0.0000939
7	3	0.500000	7.00000	$1s7f\ ^1F^0$	-0.27763	-0.27766	0.0000306	-0.0001102
7	4	0.500000	6.99988	$1s7g\ ^3G_4$	-0.27763	-0.27763	-0.0000043	0.0000155
7	4	0.500000	6.99988	$1s7g\ ^3G_5$	-0.27763	-0.27763	-0.0000043	0.0000155
7	4	0.500000	6.99988	$1s7g\ ^3G_3$	-0.27763	-0.27763	-0.0000043	0.0000155
7	4	0.500000	7.00000	$1s7g\ ^1G$	-0.27763	-0.27763	0.0000004	-0.0000016
7	5	0.500000	6.99999	$1s7h\ ^3H^0_5$	-0.27763	-0.27763	0.0000002	-0.0000009
7	5	0.500000	6.99999	$1s7h\ ^3H^0_6$	-0.27763	-0.27763	0.0000002	-0.0000009
7	5	0.500000	6.99999	$1s7h\ ^3H^0_4$	-0.27763	-0.27763	0.0000002	-0.0000009
7	5	0.500000	7.00000	$1s7h\ ^1H^0$	-0.27763	-0.27763	0.0000006	-0.0000021
7	6	0.500000	7.00000	$1s7\ i^3I_5$	-0.27763	-0.27762	-0.0000094	0.0000339

7	6	0.500000	7.00000	$1s7i\ ^3I6$	-0.27763	-0.27762	-0.0000094	0.0000339
7	6	0.500000	6.78349	$1s7i\ ^3I_7$	-0.27763	-0.27762	-0.0000094	0.0000339
7	6	0.500000	7.00000	$1s7i\ ^1I$	-0.27763	-0.27762	-0.0000094	0.0000338
7	1	0.500000	7.01873	$1s7p\ ^1P^0$	-0.27689	-0.27667	-0.0002186	0.0007900
8	0	0.500011	7.42265	$1s8s\ ^3S$	-0.22909	-0.22928	0.0001866	-0.0008139
8	0	0.500005	7.71132	$1s8s\ ^1S$	-0.22052	-0.2202	-0.0003172	0.0014407
9	0	0.500007	8.42265	$1s9s\ ^3S$	-0.17946	-0.17961	0.0001489	-0.0008291
9	0	0.500003	8.71132	$1s9s\ ^1S$	-0.17351	-0.1733	-0.0002141	0.0012355
10	0	0.500004	9.42265	$1s10s\ ^3S$	-0.14437	-0.1445	0.0001262	-0.0008732
10	0	0.500002	9.71132	$1s10s\ ^1S$	-0.14008	-0.13992	-0.0001622	0.0011594
11	0	0.500003	10.42265	$1s11s\ ^3S$	-0.11866	-0.11876	0.0001037	-0.0008734
11	0	0.500001	10.71132	$1s11s\ ^1S$	-0.11546	-0.11534	-0.0001184	0.0010268
						Avg.	**-0.000112**	**0.0000386**

Table IV. Relativistically corrected ionization energies for some two-electron atoms.

2 e Atom	Z	r_1 (a_o) [a]	Electric Energy [b] (eV)	Magnetic Energy [c] (eV)	Velocity (m/s) [d]	γ^* [e]	Theoretical Ionization Energies [f] (eV)	Experimental Ionization Energies [g] (eV)	Relative Error [h]
He	2	0.566987	23.996467	0.590536	3.85845E+06	1.000021	24.58750	24.58741	-0.000004
Li^{+}	3	0.35566	76.509	2.543	6.15103E+06	1.00005	75.665	75.64018	-0.0003
Be^{2+}	4	0.26116	156.289	6.423	8.37668E+06	1.00010	154.699	153.89661	-0.0052
B^{3+}	5	0.20670	263.295	12.956	1.05840E+07	1.00016	260.746	259.37521	-0.0053
C^{4+}	6	0.17113	397.519	22.828	1.27836E+07	1.00024	393.809	392.087	-0.0044
N^{5+}	7	0.14605	558.958	36.728	1.49794E+07	1.00033	553.896	552.0718	-0.0033
O^{6+}	8	0.12739	747.610	55.340	1.71729E+07	1.00044	741.023	739.29	-0.0023
F^{7+}	9	0.11297	963.475	79.352	1.93649E+07	1.00057	955.211	953.9112	-0.0014
Ne^{8+}	10	0.10149	1206.551	109.451	2.15560E+07	1.00073	1196.483	1195.8286	-0.0005
Na^{9+}	11	0.09213	1476.840	146.322	2.37465E+07	1.00090	1464.871	1465.121	0.0002
Mg^{10+}	12	0.08435	1774.341	190.652	2.59364E+07	1.00110	1760.411	1761.805	0.0008
Al^{11+}	13	0.07778	2099.05	243.13	2.81260E+07	1.00133	2083.15	2085.98	0.0014
Si^{12+}	14	0.07216	2450.98	304.44	3.03153E+07	1.00159	2433.13	2437.63	0.0018
P^{13+}	15	0.06730	2830.11	375.26	3.25043E+07	1.00188	2810.42	2816.91	0.0023
S^{14+}	16	0.06306	3236.46	456.30	3.46932E+07	1.00221	3215.09	3223.78	0.0027
Cl^{15+}	17	0.05932	3670.02	548.22	3.68819E+07	1.00258	3647.22	3658.521	0.0031
Ar^{16+}	18	0.05599	4130.79	651.72	3.90705E+07	1.00298	4106.91	4120.8857	0.0034

K^{17+}	19	0.05302	4618.77	767.49	4.12590E+07	1.00344	4594.25	4610.8	0.0036
Ca^{18+}	20	0.05035	5133.96	896.20	4.34475E+07	1.00394	5109.38	5128.8	0.0038
Sc^{19+}	21	0.04794	5676.37	1038.56	4.56358E+07	1.00450	5652.43	5674.8	0.0039
Ti^{20+}	22	0.04574	6245.98	1195.24	4.78241E+07	1.00511	6223.55	6249	0.0041
V^{21+}	23	0.04374	6842.81	1366.92	5.00123E+07	1.00578	6822.93	6851.3	0.0041
Cr^{22+}	24	0.04191	7466.85	1554.31	5.22005E+07	1.00652	7450.76	7481.7	0.0041
Mn^{23+}	25	0.04022	8118.10	1758.08	5.43887E+07	1.00733	8107.25	8140.6	0.0041
Fe^{24+}	26	0.03867	8796.56	1978.92	5.65768E+07	1.00821	8792.66	8828	0.0040
Co^{25+}	27	0.03723	9502.23	2217.51	5.87649E+07	1.00917	9507.25	9544.1	0.0039
Ni^{26+}	28	0.03589	10235.12	2474.55	6.09529E+07	1.01022	10251.33	10288.8	0.0036
Cu^{27+}	29	0.03465	10995.21	2750.72	6.31409E+07	1.01136	11025.21	11062.38	0.0034

[a] From Eq. (179).

[b] From Eq. (181).

[c] From Eq. (182).

[d] From Eq. (7.31) of Ref. [7].

[e] From Eq. (32) with $\gamma^* = \frac{r_n'}{r_n}$, and the velocity given by Eq. (7.31) of Ref. [7].

[f] From Eqs. (180) and (183) with $E(electric)$ of Eq. (181) relativistically corrected by γ^* according to Eq. (1.251) of Ref. [7] except that the electron-nuclear electrodynamic relativistic factor corresponding to the reduced mass of Eqs. (1.213-1.223) was not included.

[g] From theoretical calculations for ions Ne^{8+} to Cu^{28+} [35, 53].

[h] (Experimental-theoretical)/experimental.

Table V. Summary of the parameters of five through ten-electron atoms.

Atom Type	Electron Configuration	Ground State Term [a]	Orbital Arrangement of 2p Electrons (2p state)	Diamagnetic Force Factor A [b]	Paramagnetic Force Factor B [c]
Neutral 5 e Atom *B*	$1s^2 2s^2 2p^1$	$^2P^0_{1/2}$	$\underline{\uparrow}\ \ \underline{\ \ }\ \ \underline{\ \ }$ 1 0 -1	2	0
Neutral 6 e Atom *C*	$1s^2 2s^2 2p^2$	$^3P_0$	$\underline{\uparrow}\ \ \underline{\uparrow}\ \ \underline{\ \ }$ 1 0 -1	$\frac{2}{3}$	0
Neutral 7 e Atom *N*	$1s^2 2s^2 2p^3$	$^4S^0_{3/2}$	$\underline{\uparrow}\ \ \underline{\uparrow}\ \ \underline{\uparrow}$ 1 0 -1	$\frac{1}{3}$	1
Neutral 8 e Atom *O*	$1s^2 2s^2 2p^4$	$^3P_2$	$\underline{\uparrow\downarrow}\ \ \underline{\uparrow}\ \ \underline{\uparrow}$ 1 0 -1	1	2
Neutral 9 e Atom *F*	$1s^2 2s^2 2p^5$	$^2P^0_{3/2}$	$\underline{\uparrow\downarrow}\ \ \underline{\uparrow\downarrow}\ \ \underline{\uparrow}$ 1 0 -1	$\frac{2}{3}$	3
Neutral 10 e Atom *Ne*	$1s^2 2s^2 2p^6$	$^1S_0$	$\underline{\uparrow\downarrow}\ \ \underline{\uparrow\downarrow}\ \ \underline{\uparrow\downarrow}$ 1 0 -1	0	3
5 e Ion	$1s^2 2s^2 2p^1$	$^2P^0_{1/2}$	$\underline{\uparrow}\ \ \underline{\ \ }\ \ \underline{\ \ }$ 1 0 -1	$\frac{5}{3}$	1
6 e Ion	$1s^2 2s^2 2p^2$	$^3P_0$	$\underline{\uparrow}\ \ \underline{\uparrow}\ \ \underline{\ \ }$ 1 0 -1	$\frac{5}{3}$	4

7 e Ion	$1s^2 2s^2 2p^3$	${}^4S^0_{3/2}$	$\underset{1}{\uparrow}\ \underset{0}{\uparrow}\ \underset{-1}{\uparrow}$	$\frac{5}{3}$	6
8 e Ion	$1s^2 2s^2 2p^4$	${}^3P_2$	$\underset{1}{\uparrow\downarrow}\ \underset{0}{\uparrow}\ \underset{-1}{\uparrow}$	$\frac{5}{3}$	6
9 e Ion	$1s^2 2s^2 2p^5$	${}^2P^0_{3/2}$	$\underset{1}{\uparrow\downarrow}\ \underset{0}{\uparrow\downarrow}\ \underset{-1}{\uparrow}$	$\frac{5}{3}$	9
10 e Ion	$1s^2 2s^2 2p^6$	${}^1S_0$	$\underset{1}{\uparrow\downarrow}\ \underset{0}{\uparrow\downarrow}\ \underset{-1}{\uparrow\downarrow}$	$\frac{5}{3}$	12

[a] The theoretical ground state terms match those given by NIST [47].

[b] Eq. (193).

[c] Eqs. (194) and (195).

Table VI. Ionization energies for some five-electron atoms.

5 e Atom	Z	r_1 (a_o) [a]	r_3 (a_o) [b]	r_5 (a_o) [c]	Theoretical Ionization Energies [d] (eV)	Experimental Ionization Energies [e] (eV)	Relative Error [f]
B	5	0.20670	1.07930	1.67000	8.30266	8.29803	-0.00056
C^{+}	6	0.17113	0.84317	1.12092	24.2762	24.38332	0.0044
N^{2+}	7	0.14605	0.69385	0.87858	46.4585	47.44924	0.0209
O^{3+}	8	0.12739	0.59020	0.71784	75.8154	77.41353	0.0206
F^{4+}	9	0.11297	0.51382	0.60636	112.1922	114.2428	0.0179
Ne^{5+}	10	0.10149	0.45511	0.52486	155.5373	157.93	0.0152
Na^{6+}	11	0.09213	0.40853	0.46272	205.8266	208.5	0.0128
Mg^{7+}	12	0.08435	0.37065	0.41379	263.0469	265.96	0.0110
Al^{8+}	13	0.07778	0.33923	0.37425	327.1901	330.13	0.0089
Si^{9+}	14	0.07216	0.31274	0.34164	398.2509	401.37	0.0078
P^{10+}	15	0.06730	0.29010	0.31427	476.2258	479.46	0.0067
S^{11+}	16	0.06306	0.27053	0.29097	561.1123	564.44	0.0059
Cl^{12+}	17	0.05932	0.25344	0.27090	652.9086	656.71	0.0058
Ar^{13+}	18	0.05599	0.23839	0.25343	751.6132	755.74	0.0055
K^{14+}	19	0.05302	0.22503	0.23808	857.2251	861.1	0.0045
Ca^{15+}	20	0.05035	0.21308	0.22448	969.7435	974	0.0044
Sc^{16+}	21	0.04794	0.20235	0.21236	1089.1678	1094	0.0044
Ti^{17+}	22	0.04574	0.19264	0.20148	1215.4975	1221	0.0045

V^{18+}	23	0.04374	0.18383	0.19167	1348.7321	1355	0.0046
Cr^{19+}	24	0.04191	0.17579	0.18277	1488.8713	1496	0.0048
Mn^{20+}	25	0.04022	0.16842	0.17466	1635.9148	1644	0.0049
Fe^{21+}	26	0.03867	0.16165	0.16724	1789.8624	1799	0.0051
Co^{22+}	27	0.03723	0.15540	0.16042	1950.7139	1962	0.0058
Ni^{23+}	28	0.03589	0.14961	0.15414	2118.4690	2131	0.0059
Cu^{24+}	29	0.03465	0.14424	0.14833	2293.1278	2308	0.0064

Table VII. Ionization energies for some six-electron atoms.

6 e Atom	Z	r_1 (a_o) [a]	r_3 (a_o) [b]	r_6 (a_o) [c]	Theoretical Ionization Energies [d] (eV)	Experimental Ionization Energies [e] (eV)	Relative Error [f]
C	6	0.17113	0.84317	1.20654	11.27671	11.2603	-0.0015
N^{+}	7	0.14605	0.69385	0.90119	30.1950	29.6013	-0.0201
O^{2+}	8	0.12739	0.59020	0.74776	54.5863	54.9355	0.0064
F^{3+}	9	0.11297	0.51382	0.63032	86.3423	87.1398	0.0092
Ne^{4+}	10	0.10149	0.45511	0.54337	125.1986	126.21	0.0080
Na^{5+}	11	0.09213	0.40853	0.47720	171.0695	172.18	0.0064
Mg^{6+}	12	0.08435	0.37065	0.42534	223.9147	225.02	0.0049
Al^{7+}	13	0.07778	0.33923	0.38365	283.7121	284.66	0.0033
Si^{8+}	14	0.07216	0.31274	0.34942	350.4480	351.12	0.0019
P^{9+}	15	0.06730	0.29010	0.32081	424.1135	424.4	0.0007
S^{10+}	16	0.06306	0.27053	0.29654	504.7024	504.8	0.0002
Cl^{11+}	17	0.05932	0.25344	0.27570	592.2103	591.99	-0.0004
Ar^{12+}	18	0.05599	0.23839	0.25760	686.6340	686.1	-0.0008
K^{13+}	19	0.05302	0.22503	0.24174	787.9710	786.6	-0.0017
Ca^{14+}	20	0.05035	0.21308	0.22772	896.2196	894.5	-0.0019
Sc^{15+}	21	0.04794	0.20235	0.21524	1011.3782	1009	-0.0024
Ti^{16+}	22	0.04574	0.19264	0.20407	1133.4456	1131	-0.0022
V^{17+}	23	0.04374	0.18383	0.19400	1262.4210	1260	-0.0019

Cr^{18+}	24	0.04191	0.17579	0.18487	1398.3036	1396	-0.0017
Mn^{19+}	25	0.04022	0.16842	0.17657	1541.0927	1539	-0.0014
Fe^{20+}	26	0.03867	0.16165	0.16899	1690.7878	1689	-0.0011
Co^{21+}	27	0.03723	0.15540	0.16203	1847.3885	1846	-0.0008
Ni^{22+}	28	0.03589	0.14961	0.15562	2010.8944	2011	0.0001
Cu^{23+}	29	0.03465	0.14424	0.14970	2181.3053	2182	0.0003

Table VIII. Ionization energies for some seven-electron atoms.

7 e Atom	Z	r_1 (a_o) [a]	r_3 (a_o) [b]	r_7 (a_o) [c]	Theoretical Ionization Energies [d] (eV)	Experimental Ionization Energies [e] (eV)	Relative Error [f]
N	7	0.14605	0.69385	0.93084	14.61664	14.53414	-0.0057
O^{+}	8	0.12739	0.59020	0.78489	34.6694	35.1173	0.0128
F^{2+}	9	0.11297	0.51382	0.67084	60.8448	62.7084	0.0297
Ne^{3+}	10	0.10149	0.45511	0.57574	94.5279	97.12	0.0267
Na^{4+}	11	0.09213	0.40853	0.50250	135.3798	138.4	0.0218
Mg^{5+}	12	0.08435	0.37065	0.44539	183.2888	186.76	0.0186
Al^{6+}	13	0.07778	0.33923	0.39983	238.2017	241.76	0.0147
Si^{7+}	14	0.07216	0.31274	0.36271	300.0883	303.54	0.0114
P^{8+}	15	0.06730	0.29010	0.33191	368.9298	372.13	0.0086
S^{9+}	16	0.06306	0.27053	0.30595	444.7137	447.5	0.0062
Cl^{10+}	17	0.05932	0.25344	0.28376	527.4312	529.28	0.0035
Ar^{11+}	18	0.05599	0.23839	0.26459	617.0761	618.26	0.0019
K^{12+}	19	0.05302	0.22503	0.24785	713.6436	714.6	0.0013
Ca^{13+}	20	0.05035	0.21308	0.23311	817.1303	817.6	0.0006
Sc^{14+}	21	0.04794	0.20235	0.22003	927.5333	927.5	0.0000
Ti^{15+}	22	0.04574	0.19264	0.20835	1044.8504	1044	-0.0008
V^{16+}	23	0.04374	0.18383	0.19785	1169.0800	1168	-0.0009
Cr^{17+}	24	0.04191	0.17579	0.18836	1300.2206	1299	-0.0009

Mn^{18+}	25	0.04022	0.16842	0.17974	1438.2710	1437	-0.0009
Fe^{19+}	26	0.03867	0.16165	0.17187	1583.2303	1582	-0.0008
Co^{20+}	27	0.03723	0.15540	0.16467	1735.0978	1735	-0.0001
Ni^{21+}	28	0.03589	0.14961	0.15805	1893.8726	1894	0.0001
Cu^{22+}	29	0.03465	0.14424	0.15194	2059.5543	2060	0.0002

Table IX. Ionization energies for some eight-electron atoms.

8 e Atom	Z	r_1 (a_o) [a]	r_3 (a_o) [b]	r_8 (a_o) [c]	Theoretical Ionization Energies [d] (eV)	Experimental Ionization Energies [e] (eV)	Relative Error [f]
O	8	0.12739	0.59020	1.00000	13.60580	13.6181	0.0009
F^{+}	9	0.11297	0.51382	0.7649	35.5773	34.9708	-0.0173
Ne^{2+}	10	0.10149	0.45511	0.6514	62.6611	63.45	0.0124
Na^{3+}	11	0.09213	0.40853	0.5592	97.3147	98.91	0.0161
Mg^{4+}	12	0.08435	0.37065	0.4887	139.1911	141.27	0.0147
Al^{5+}	13	0.07778	0.33923	0.4338	188.1652	190.49	0.0122
Si^{6+}	14	0.07216	0.31274	0.3901	244.1735	246.5	0.0094
P^{7+}	15	0.06730	0.29010	0.3543	307.1791	309.6	0.0078
S^{8+}	16	0.06306	0.27053	0.3247	377.1579	379.55	0.0063
Cl^{9+}	17	0.05932	0.25344	0.2996	454.0940	455.63	0.0034
Ar^{10+}	18	0.05599	0.23839	0.2782	537.9756	538.96	0.0018
K^{11+}	19	0.05302	0.22503	0.2597	628.7944	629.4	0.0010
Ca^{12+}	20	0.05035	0.21308	0.2434	726.5442	726.6	0.0001
Sc^{13+}	21	0.04794	0.20235	0.2292	831.2199	830.8	-0.0005
Ti^{14+}	22	0.04574	0.19264	0.2165	942.8179	941.9	-0.0010
V^{15+}	23	0.04374	0.18383	0.2051	1061.3351	1060	-0.0013
Cr^{16+}	24	0.04191	0.17579	0.1949	1186.7691	1185	-0.0015
Mn^{17+}	25	0.04022	0.16842	0.1857	1319.1179	1317	-0.0016

Fe^{18+}	26	0.03867	0.16165	0.1773	1458.3799	1456	-0.0016
Co^{19+}	27	0.03723	0.15540	0.1696	1604.5538	1603	-0.0010
Ni^{20+}	28	0.03589	0.14961	0.1626	1757.6383	1756	-0.0009
Cu^{21+}	29	0.03465	0.14424	0.1561	1917.6326	1916	-0.0009

Table X. Ionization energies for some nine-electron atoms.

9 e Atom	Z	r_1 (a_o) [a]	r_3 (a_o) [b]	r_9 (a_o) [c]	Theoretical Ionization Energies [d] (eV)	Experimental Ionization Energies [e] (eV)	Relative Error [f]
F	9	0.11297	0.51382	0.78069	17.42782	17.42282	-0.0003
Ne^{+}	10	0.10149	0.45511	0.64771	42.0121	40.96328	-0.0256
Na^{2+}	11	0.09213	0.40853	0.57282	71.2573	71.62	0.0051
Mg^{3+}	12	0.08435	0.37065	0.50274	108.2522	109.2655	0.0093
Al^{4+}	13	0.07778	0.33923	0.44595	152.5469	153.825	0.0083
Si^{5+}	14	0.07216	0.31274	0.40020	203.9865	205.27	0.0063
P^{6+}	15	0.06730	0.29010	0.36283	262.4940	263.57	0.0041
S^{7+}	16	0.06306	0.27053	0.33182	328.0238	328.75	0.0022
Cl^{8+}	17	0.05932	0.25344	0.30571	400.5466	400.06	-0.0012
Ar^{9+}	18	0.05599	0.23839	0.28343	480.0424	478.69	-0.0028
K^{10+}	19	0.05302	0.22503	0.26419	566.4968	564.7	-0.0032
Ca^{11+}	20	0.05035	0.21308	0.24742	659.8992	657.2	-0.0041
Sc^{12+}	21	0.04794	0.20235	0.23266	760.2415	756.7	-0.0047
Ti^{13+}	22	0.04574	0.19264	0.21957	867.5176	863.1	-0.0051
V^{14+}	23	0.04374	0.18383	0.20789	981.7224	976	-0.0059
Cr^{15+}	24	0.04191	0.17579	0.19739	1102.8523	1097	-0.0053

Mn^{16+}	25	0.04022	0.16842	0.18791	1230.9038	1224	-0.0056
Fe^{17+}	26	0.03867	0.16165	0.17930	1365.8746	1358	-0.0058
Co^{18+}	27	0.03723	0.15540	0.17145	1507.7624	1504.6	-0.0021
Ni^{19+}	28	0.03589	0.14961	0.16427	1656.5654	1648	-0.0052
Cu^{20+}	29	0.03465	0.14424	0.15766	1812.2821	1804	-0.0046

Table XI. Ionization energies for some ten-electron atoms.

10 e Atom	Z	r_1 (a_o) [a]	r_3 (a_o) [b]	r_{10} (a_o) [c]	Theoretical Ionization Energies [d] (eV)	Experimental Ionization Energies [e] (eV)	Relative Error [f]
Ne	10	0.10149	0.45511	0.63659	21.37296	21.56454	0.00888
Na^{+}	11	0.09213	0.40853	0.560945	48.5103	47.2864	-0.0259
Mg^{2+}	12	0.08435	0.37065	0.510568	79.9451	80.1437	0.0025
Al^{3+}	13	0.07778	0.33923	0.456203	119.2960	119.992	0.0058
Si^{4+}	14	0.07216	0.31274	0.409776	166.0150	166.767	0.0045
P^{5+}	15	0.06730	0.29010	0.371201	219.9211	220.421	0.0023
S^{6+}	16	0.06306	0.27053	0.339025	280.9252	280.948	0.0001
Cl^{7+}	17	0.05932	0.25344	0.311903	348.9750	348.28	-0.0020
Ar^{8+}	18	0.05599	0.23839	0.288778	424.0365	422.45	-0.0038
K^{9+}	19	0.05302	0.22503	0.268844	506.0861	503.8	-0.0045
Ca^{10+}	20	0.05035	0.21308	0.251491	595.1070	591.9	-0.0054
Sc^{11+}	21	0.04794	0.20235	0.236251	691.0866	687.36	-0.0054
Ti^{12+}	22	0.04574	0.19264	0.222761	794.0151	787.84	-0.0078
V^{13+}	23	0.04374	0.18383	0.210736	903.8853	896	-0.0088
Cr^{14+}	24	0.04191	0.17579	0.19995	1020.6910	1010.6	-0.0100
Mn^{15+}	25	0.04022	0.16842	0.19022	1144.4276	1134.7	-0.0086
Fe^{16+}	26	0.03867	0.16165	0.181398	1275.0911	1266	-0.0072
Co^{17+}	27	0.03723	0.15540	0.173362	1412.6783	1397.2	-0.0111

Ni^{18+}	28	0.03589	0.14961	0.166011	1557.1867	1541	-0.0105
Cu^{19+}	29	0.03465	0.14424	0.159261	1708.6139	1697	-0.0068
Zn^{20+}	30	0.03349	0.13925	0.153041	1866.9581	1856	-0.0059

Table XII. The Maxwellian closed-form calculated and experimental parameters of H_2, D_2, H_2^+ and D_2^+.

Parameter	Calculated	Experimental	Eqs.[a]
H_2 Bond Energy	4.478 eV	4.478 eV	12.251
D_2 Bond Energy	4.556 eV	4.556 eV	12.253
H_2^+ Bond Energy	2.654 eV	2.651 eV	12.220
D_2^+ Bond Energy	2.696 eV	2.691 eV	12.222
H_2 Total Energy	31.677 eV	31.675 eV	12.247
D_2 Total Energy	31.760 eV	31.760 eV	12.248
H_2 Ionization Energy	15.425 eV	15.426 eV	12.249
D_2 Ionization Energy	15.463 eV	15.466 eV	12.250
H_2^+ Ionization Energy	16.253 eV	16.250 eV	12.218
D_2^+ Ionization Energy	16.299 eV	16.294 eV	12.219
H_2^+ Magnetic Moment	$9.274\ X\ 10^{-24}\ JT^{-1}$ μ_B	$9.274\ X\ 10^{-24}\ JT^{-1}$ μ_B	14.1-14.7
Absolute H_2 Gas-Phase NMR Shift	-28.0 ppm	-28.0 ppm	12.362
H_2 Internuclear Distance[b]	0.748 Å $\sqrt{2}a_o$	0.741 Å	12.238
D_2 Internuclear Distance[b]	0.748 Å $\sqrt{2}a_o$	0.741 Å	12.238
H_2^+ Internuclear Distance[c]	1.058 Å $2a_o$	1.06 Å	12.207

D_2^+ Internuclear Distance[b]	1.058 Å	1.0559 Å	12.207
	$2a_o$		
H_2 Vibrational Energy	0.517 eV	0.516 eV	12.259
D_2 Vibrational Energy	0.371 eV	0.371 eV	12.264
H_2 $\omega_e x_e$	120.4 cm^{-1}	121.33 cm^{-1}	12.261
D_2 $\omega_e x_e$	60.93 cm^{-1}	61.82 cm^{-1}	12.265
H_2^+ Vibrational Energy	0.270 eV	0.271 eV	12.228
D_2^+ Vibrational Energy	0.193 eV	0.196 eV	12.232
H_2 J=1 to J=0 Rotational Energy[b]	0.0148 eV	0.01509 eV	14.45
D_2 J=1 to J=0 Rotational Energy[b]	0.00741 eV	0.00755 eV	14.37-14.45
H_2^+ J=1 to J=0 Rotational Energy[c]	0.00740 eV	0.00739 eV	14.49
D_2^+ J=1 to J=0 Rotational Energy[b]	0.00370 eV	0.003723 eV	14.37-14.43, 14.49

[a] Ref. [7].

[b] The internuclear distances are not corrected for the reduction due to $\overline{E}_{osc}$.

[c] The internuclear distances are not corrected for the increase due to $\overline{E}_{osc}$.

Table XIII. The relations between the lepton masses and neutron to electron mass ratio are given in terms of the dimensionless fine structure constant α only.

$$\frac{m_\mu}{m_e} = \left(\frac{\alpha^{-2}}{2\pi}\right)^{\frac{2}{3}} \frac{\left(1+2\pi\frac{\alpha^2}{2}\right)}{\left(1+\frac{\alpha}{2}\right)} = 206.76828 \qquad (206.76827)^{\text{a}}$$

$$\frac{m_\tau}{m_\mu} = \left(\frac{\alpha^{-1}}{2}\right)^{\frac{2}{3}} \frac{\left(1+\frac{\alpha}{2}\right)}{\left(1-4\pi\alpha^2\right)} = 16.817 \qquad (16.817)$$

$$\frac{m_\tau}{m_e} = \left(\frac{\alpha^{-3}}{4\pi}\right)^{\frac{2}{3}} \frac{\left(1+2\pi\frac{\alpha^2}{2}\right)}{\left(1-4\pi\alpha^2\right)} = 3477.2 \qquad (3477.3)$$

$$\frac{m_N}{m_e} = \frac{12\pi^2}{1-\alpha}\sqrt{\frac{\sqrt{3}}{\alpha}} \frac{\left(1+2\pi\frac{\alpha^2}{2}\right)}{\left(1-2\pi\frac{\alpha^2}{2}\right)} = 1838.67 \qquad (1838.68)$$

[a] Experimental according to the 1998 CODATA and the Particle Data Group [92-93].

Figure Captions

Figure 1. The orbitsphere is a two dimensional spherical shell of zero thickness with the Bohr radius of the hydrogen atom, $r = a_H$. It is nonradiative, a minimum-energy surface, and extremely stable in that the balanced forces correspond to a pressure of twenty million atmospheres.

Figure 2. The electric fields of a proton, a bound electron, and a hydrogen atom corresponding to a minimum energy and no electron self interaction where the bubble-like geometry of the orbitsphere requires the central field of the proton.

Figure 3. The orbital function modulates the constant (spin) function. (shown for t = 0; three-dimensional view)

Figure 4. The current on the great circle in the y'z'-plane moves counter clockwise and the current on the great circle in the x'z'-plane moves clockwise. The xyz-system is the laboratory frame, and the orthogonal-current-loop basis set is rigid with respect to the x'y'z'-system that rotates about the $\left(\mathbf{i}_x, \mathbf{i}_y, 0\mathbf{i}_z\right)$-axis by π radians to generate the elements of the first component of the orbitsphere-cvf. The angular momentum of the orthogonal great circle current loops in the x'y'-plane that is evenly distributed over the surface is $\frac{\hbar}{2\sqrt{2}}$.

Figure 5. The current pattern of the orbitsphere-cvf component of STEP ONE shown with 6 degree increments of θ from the perspective of looking along the z-axis. The yz-plane great circle current loop that served as a basis element that was initially in the yz-plane is shown as red.

Figure 6. The current pattern of the orbitsphere-cvf component of STEP ONE shown with 6 degree increments of θ from the perspective of looking along the z-axis. The great circle

current loop that served as a basis element that was initially in the xz-plane is shown as red.

Figure 7. The current on the great circle in the plane that bisects the x'y'-quadrant and is parallel to the z'-axis moves clockwise, and the current on the great circle in the x'y'-plane moves counter clockwise. Rotation of the great circles about the $\left(-\frac{1}{\sqrt{2}}\mathbf{i}_x, \frac{1}{\sqrt{2}}\mathbf{i}_y, \mathbf{i}_z\right)$-axis by π radians generates the elements of the second component of the orbitsphere-cvf. The angular momentum of the orthogonal great circle current loops in the plane along the $\left(-\frac{1}{\sqrt{2}}\mathbf{i}_x, \frac{1}{\sqrt{2}}\mathbf{i}_y, \mathbf{i}_z\right)$- and z-axes is $\frac{\hbar}{2\sqrt{2}}$ corresponding to each of the z and -xy-components of magnitude $\frac{\hbar}{4}$.

Figure 8. The current pattern of the orbitsphere-cvf component of STEP TWO shown with 6 degree increments of θ from the perspective of looking along the z-axis. The great circle current loop that served as a basis element that was initially in the plane that bisects the xy-quadrant and was parallel to the z-axis is shown as red.

Figure 9. The current pattern of the orbitsphere-cvf component of STEP TWO shown with 6 degree increments of θ from the perspective of looking along the z-axis. The great circle current loop that served as a basis element that was initially in the xy-plane is shown as red.

Figure 10A-C. The current pattern of the orbitsphere-cvf shown with 6 degree increments of θ from the perspective of looking along the z-axis, x-axis, and y-axis, respectively.

Figure 11. The trajectory of the resultant angular momentum vector of the orthogonal great circle current loops of magnitude $\frac{\hbar}{2\sqrt{2}}$ during Step One (yellow vectors) gives $\mathbf{L}_z = \frac{\hbar}{4}$. The resultant angular momentum vector of the orthogonal great circle current loops of magnitude $\frac{\hbar}{2\sqrt{2}}$ of Step Two (black vector) is stationary, and the projections of the resultant vector for Step

Two are $\mathbf{L}_{xy} = \frac{\hbar}{4}$ and $\mathbf{L}_z = \frac{\hbar}{4}$.

Figure 12. The orbitsphere $Y_0^0(\theta,\phi)$ is by the convolution operator with the orbitsphere-cvf as the basis element. The bound electron is a two dimensional spherical shell of zero thickness with the Bohr radius of the hydrogen atom, $r = a_H$, having angular momentum components of $\mathbf{L}_{xy} = \frac{\hbar}{4}$ and $\mathbf{L}_z = \frac{\hbar}{2}$.

Figure 13. The current pattern of the secondary component orbitsphere-cvf given by Eq. (26) and shown with 6 degree increments of θ from the perspective of looking along the z-axis. The great circle current loop that served as a basis element that was initially in the yz-plane is shown as red.

Figure 14. A representation of the uniform current pattern of the $Y_0^0(\phi,\theta)$ orbitsphere shown with 30 degree increments ($N = M = 12$ in Eq. (27)) of the angle to generate the orbitsphere current-vector field corresponding to Eq. (26) and 30 degree increments of the rotation of this basis element about the $\left(\mathbf{i}_\mathbf{x},\mathbf{i}_\mathbf{y},0\mathbf{i}_\mathbf{z}\right)$-axis corresponding to Eq. (25). The great circle current loop that served as a basis element that was initially in the plane along the $\left(\mathbf{i}_\mathbf{x},-\mathbf{i}_\mathbf{y},0\mathbf{i}_\mathbf{z}\right)$- and z-axes of each secondary component orbitsphere-cvf is shown as red. The perspective is transverse to the z-axis.

Figure 15. The normalized radius as a function of the velocity due to relativistic contraction.

Figure 16A. The two-dimensional cut-away representation of the magnetic field of an electron orbitsphere. The field is a dipole outside the orbitsphere and uniform inside the orbitsphere.

Figure 16B. The three-dimensional cut-away representation of the magnetic field of an electron orbitsphere. The field is a dipole outside the orbitsphere and uniform inside the orbitsphere.

Figure 17. Broadening of the spectral line due to the rise-time and shifting of the spectral line due to the radiative reaction. The resonant line shape has width Γ. The level shift is $\Delta\omega$.

Figure 18. Comparison of CQM and NIST Values for He I Energy Levels.

Figure 19. The Cartesian coordinate system wherein the first great circle magnetic field line lies initially in the xz-plane, and the second great circle electric field line lies initially in the yz-plane.

Figure 20. The field-line pattern given by Eq. (161) from three orthogonal perspectives of a RHCP photon-e&mvf corresponding to the first great circle magnetic field line and the second great circle electric field line shown with 6 degree increments of the angle θ. (Electric field lines red; Magnetic field lines blue).

Figure 21. An observer at the origin of his frame with the photon-e&mvf stationary in its own frame propagating at light-speed c relative to the observer along its z-axis ($z_{photon-e\&mvf}$) that is collinear to the z-axis of the observer, $z_{laboratory}$.

Figure 22. The electric field of a moving point charge ($v = \frac{4}{5}c$).

Figure 23. The electric field lines of a right-handed circularly polarized photon-e&mvf as seen along the axis of propagation in the lab inertial reference frame as it passes a fixed point.

Figure. 24. The angular-momentum-axis view of the magnitude of the continuous mass (charge)-density function in the xy-plane of a polarized free electron propagating along the z-axis and the side view of this electron. For the polarized electron, the angular momentum axis is aligned along the direction of propagation, the z-axis.

Figure. 25. The magnitude plotted along the z-axis of the mass (charge)-density function of the free electron traveling at $10^5\ m/s$ relative to the observer. From Eq. (7), the radius of the xy-plane-lamina disc is $1.16\,X\,10^{-9}\ m$, and from Eq. (169), the maximum mass density and charge

density at $\rho = 0$ are $3.25\,X\,10^{-13}\ kg/m^2$ and $0.0571\ \mathrm{C}/m^2$, respectively. The corresponding current-density function, J, is given by the product of the charge density and constant angular velocity. From Eq. (173), the maximum current density at $\rho = 0$ is $1.23\,X\,10^{13}\ Am^{-2}$.

Figure 26. A view of one of the two conical surfaces formed by rotation of the plane-lamina disc comprised of concentric great circles about the $(\mathbf{i}_x, 0\mathbf{i}_y, \mathbf{i}_z)$-axis that join at the origin and face in the opposite directions along the axis of rotation, the $(\mathbf{i}_x, 0\mathbf{i}_y, \mathbf{i}_z)$-axis.

Figure 27. The experimental results for the elastic differential cross section for the elastic scattering of electrons by helium atoms and a Born approximation prediction.

Figure 28. The closed form function (Eqs. (188) and (189)) for the elastic differential cross section for the elastic scattering of electrons by helium atoms. The scattering amplitude function, $F(s)$ (Eq. (187), is shown as an insert.

Figure 29. **A**. Prolate spheroid MO. **B**. Prolate spheroid parameters of molecules and molecular ions where a is the semimajor axis, $2a$ is the total length of the molecule or molecular ion along the principal axis, $b = c$ is the semiminor axis, $2b = 2c$ is the total width of the molecule or molecular ion along the minor axis, c' is the distance from the origin to a focus (nucleus), $2c'$ is the internuclear distance, and the protons are at the foci.

Figure 30. Potential Energy well of a Hydrogen Atom.

Figure 31. Quantized sizes of hydrogen atoms where n is an integer for excited states and $n = 1/p$. for hydrino states where p is an integer.

Figure 1.

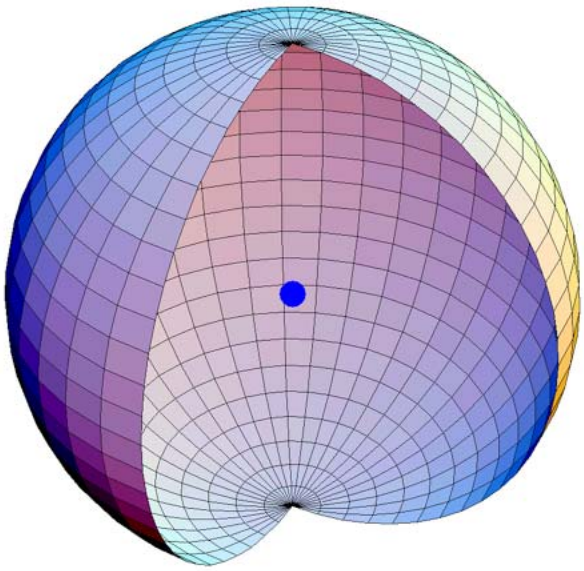

Figure 2.

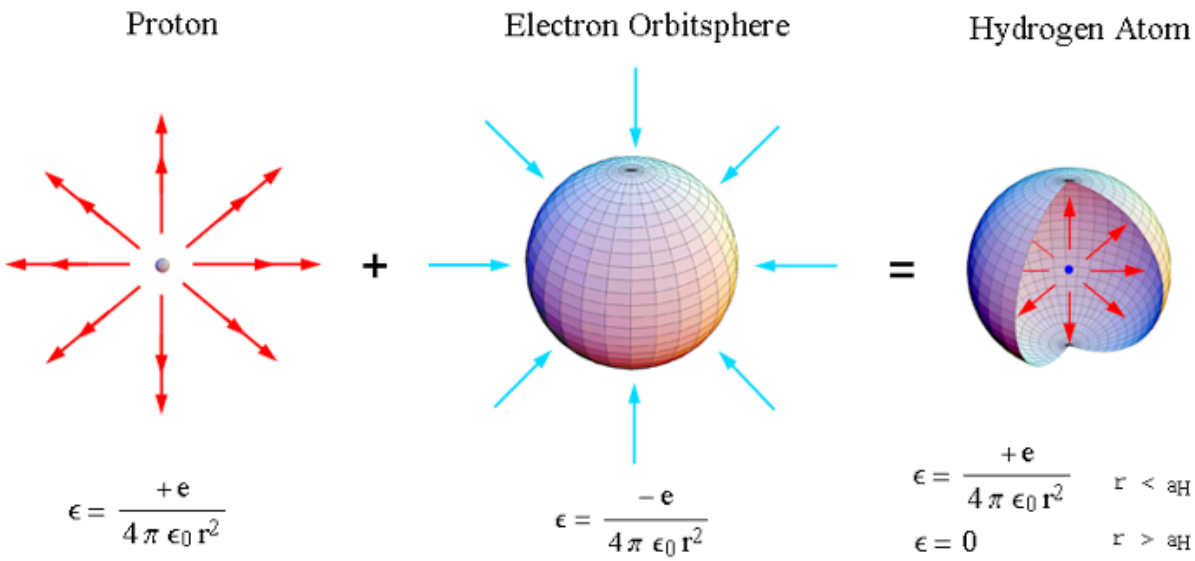
Proton
Electron Orbitsphere
Hydrogen Atom
+
=
$\epsilon = \frac{+e}{4\pi\epsilon_0 r^2}$
$\epsilon = \frac{-e}{4\pi\epsilon_0 r^2}$
$\epsilon = \frac{+e}{4\pi\epsilon_0 r^2}$ $r < a_H$
$\epsilon = 0$ $r > a_H$

Figure 3.

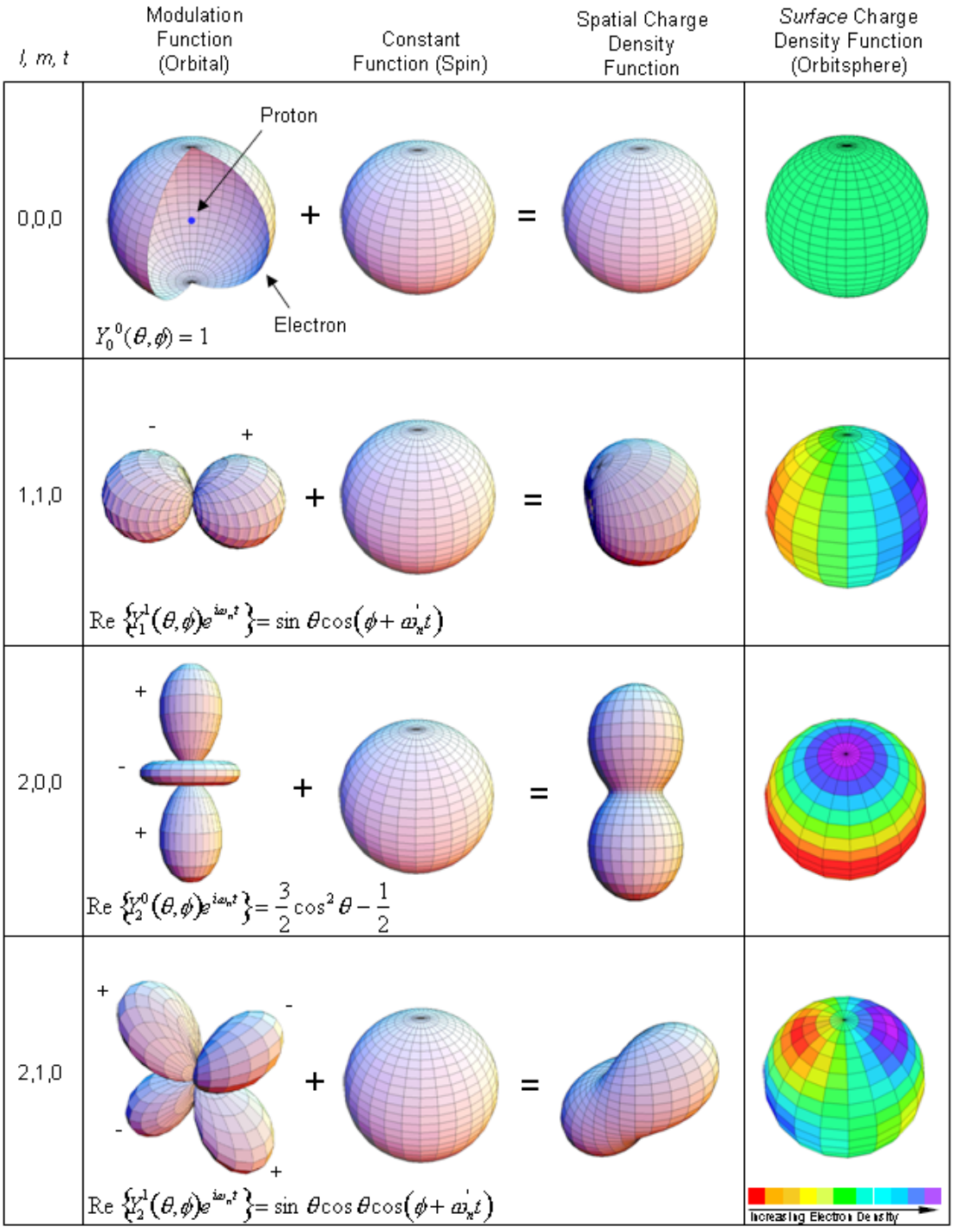
l, m, t
Modulation Function (Orbital)
Constant Function (Spin)
Spatial Charge Density Function
Surface Charge Density Function (Orbitsphere)
0,0,0
Proton
Electron
$Y_0^0(\theta,\phi) = 1$
1,1,0
$\mathrm{Re}\left\{Y_1^1(\theta,\phi)e^{i\omega_n t}\right\} = \sin\theta\cos\left(\phi + \omega_n' t\right)$
2,0,0
$\mathrm{Re}\left\{Y_2^0(\theta,\phi)e^{i\omega_n t}\right\} = \frac{3}{2}\cos^2\theta - \frac{1}{2}$
2,1,0
$\mathrm{Re}\left\{Y_2^1(\theta,\phi)e^{i\omega_n t}\right\} = \sin\theta\cos\theta\cos\left(\phi + \omega_n' t\right)$
Increasing Electron Density

Figure 4.

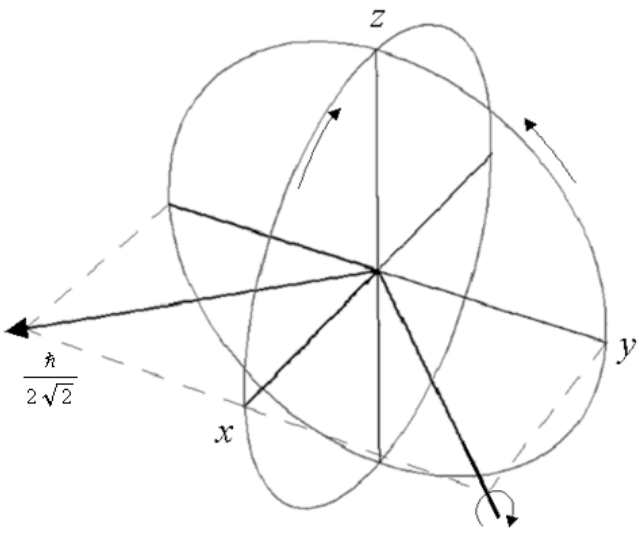

Figure 5.

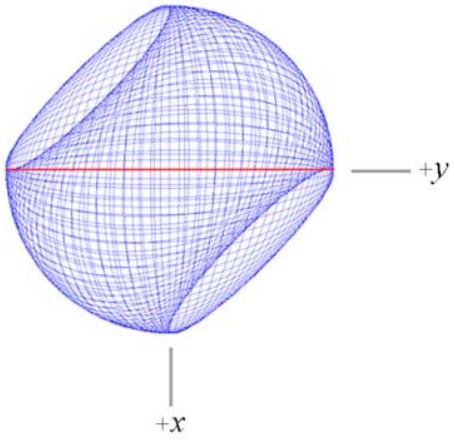

Figure 6.

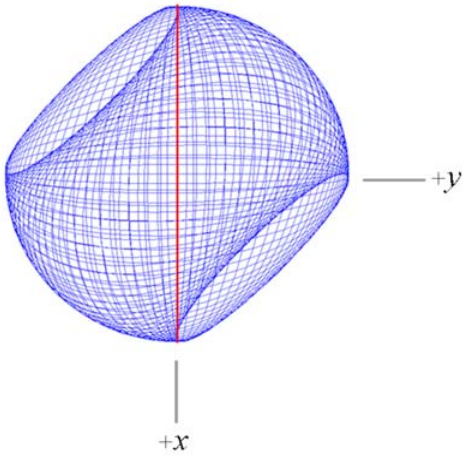

Figure 7.

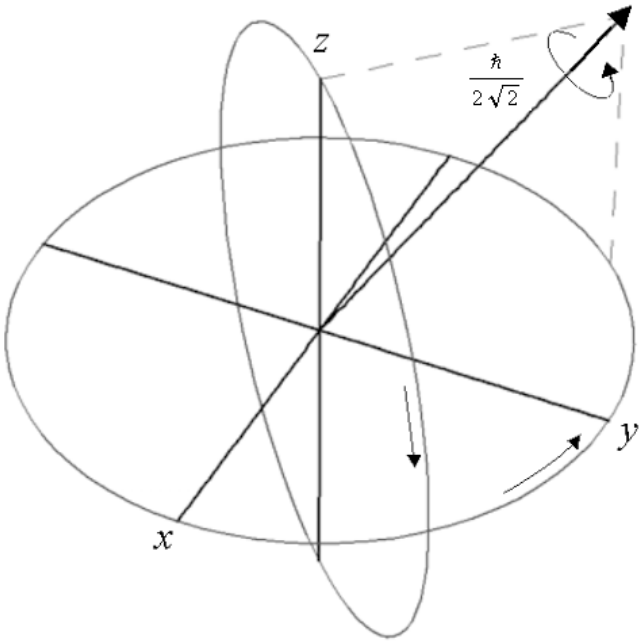

Figure 8.

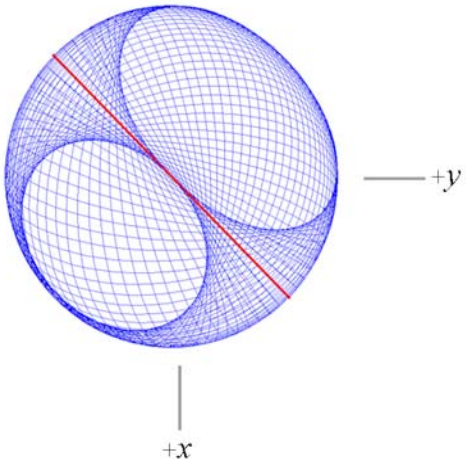

Figure 9.

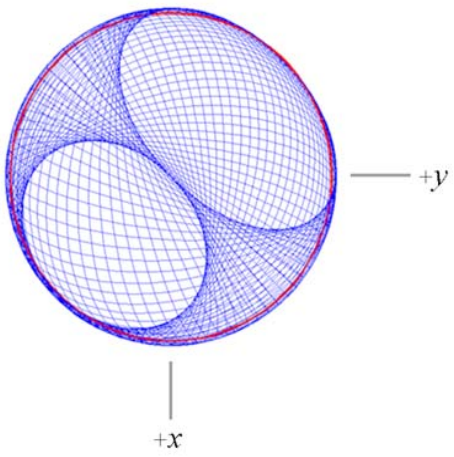

Figure 10A-C.

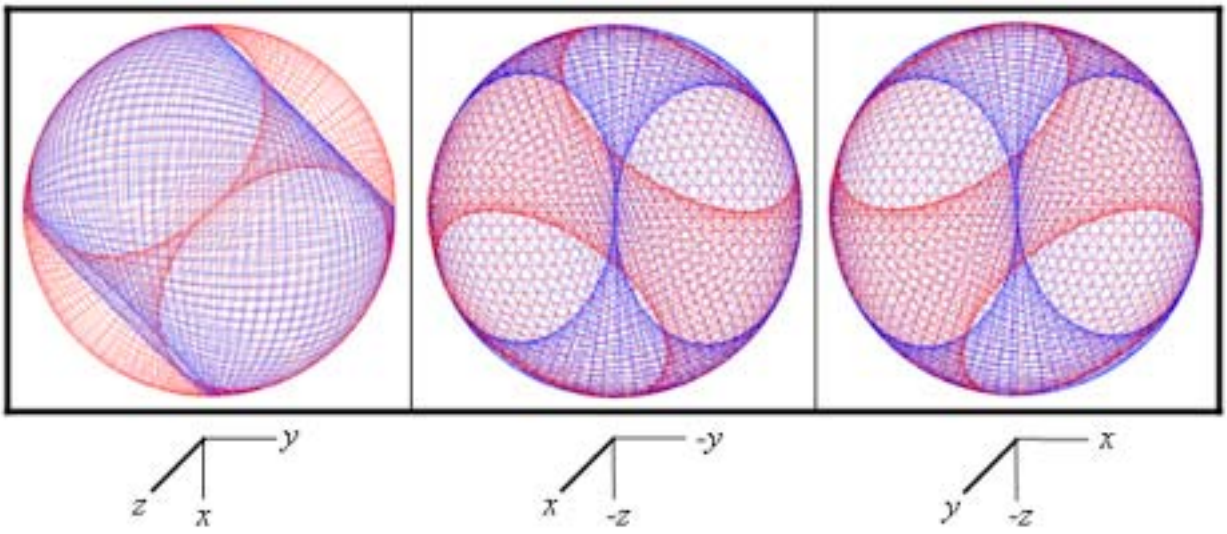

Figure 11.

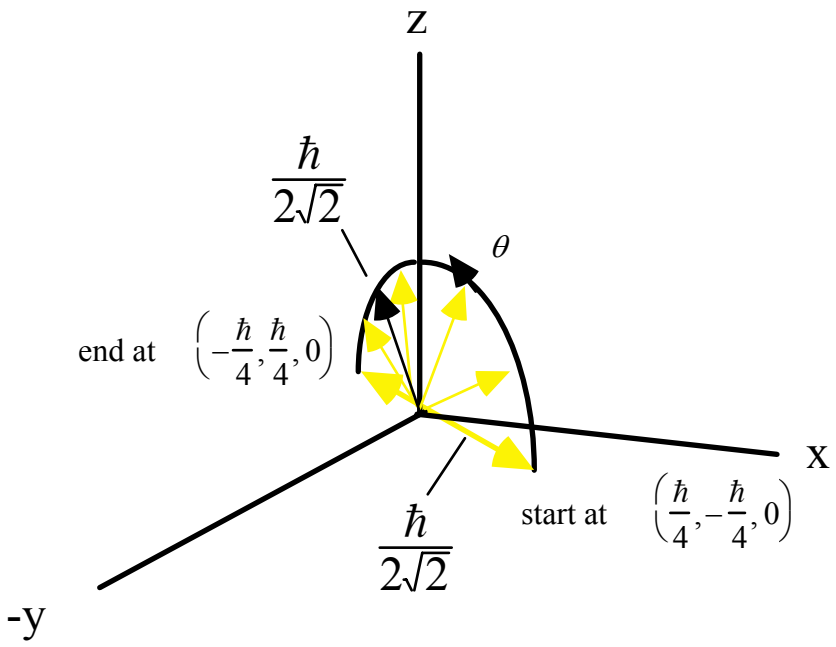
z
$\frac{\hbar}{2\sqrt{2}}$
θ
end at $\left(-\frac{\hbar}{4},\frac{\hbar}{4},0\right)$
x
start at $\left(\frac{\hbar}{4},-\frac{\hbar}{4},0\right)$
$\frac{\hbar}{2\sqrt{2}}$
-y

Figure 12.

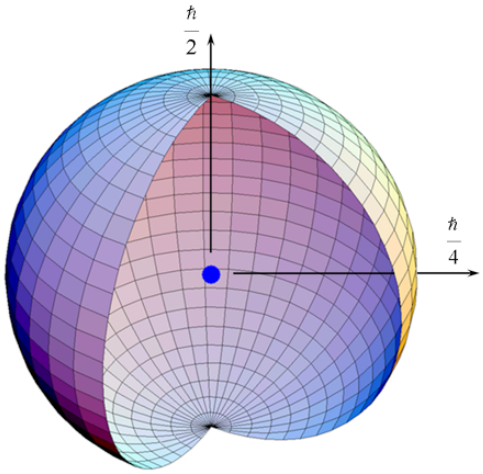

Figure 13.

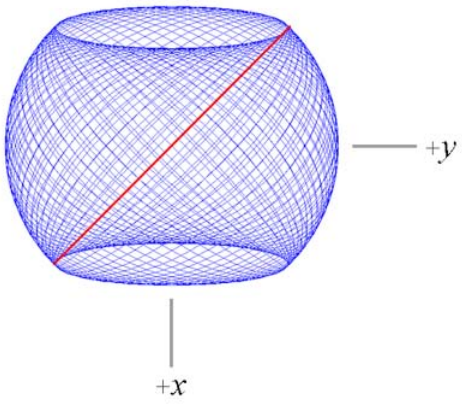

Figure 14.

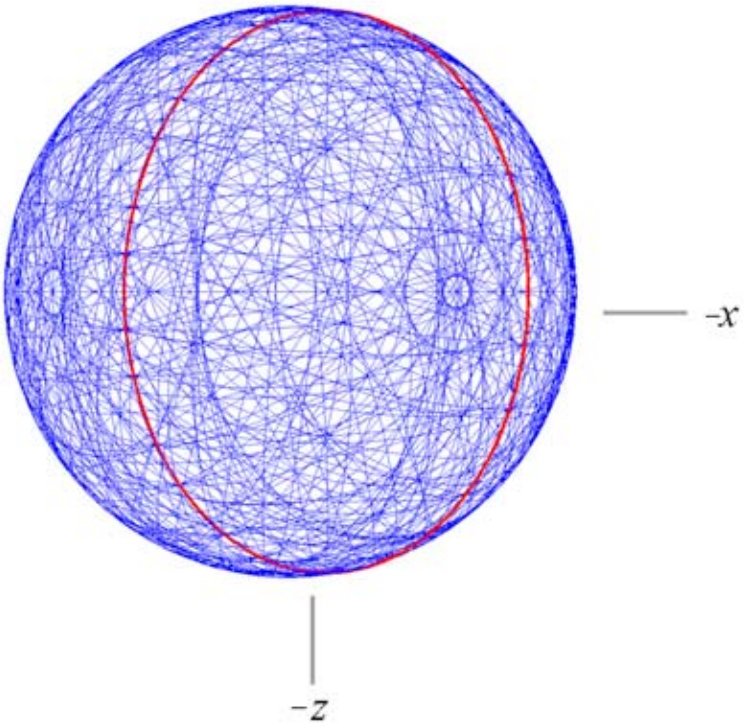

Figure 15.

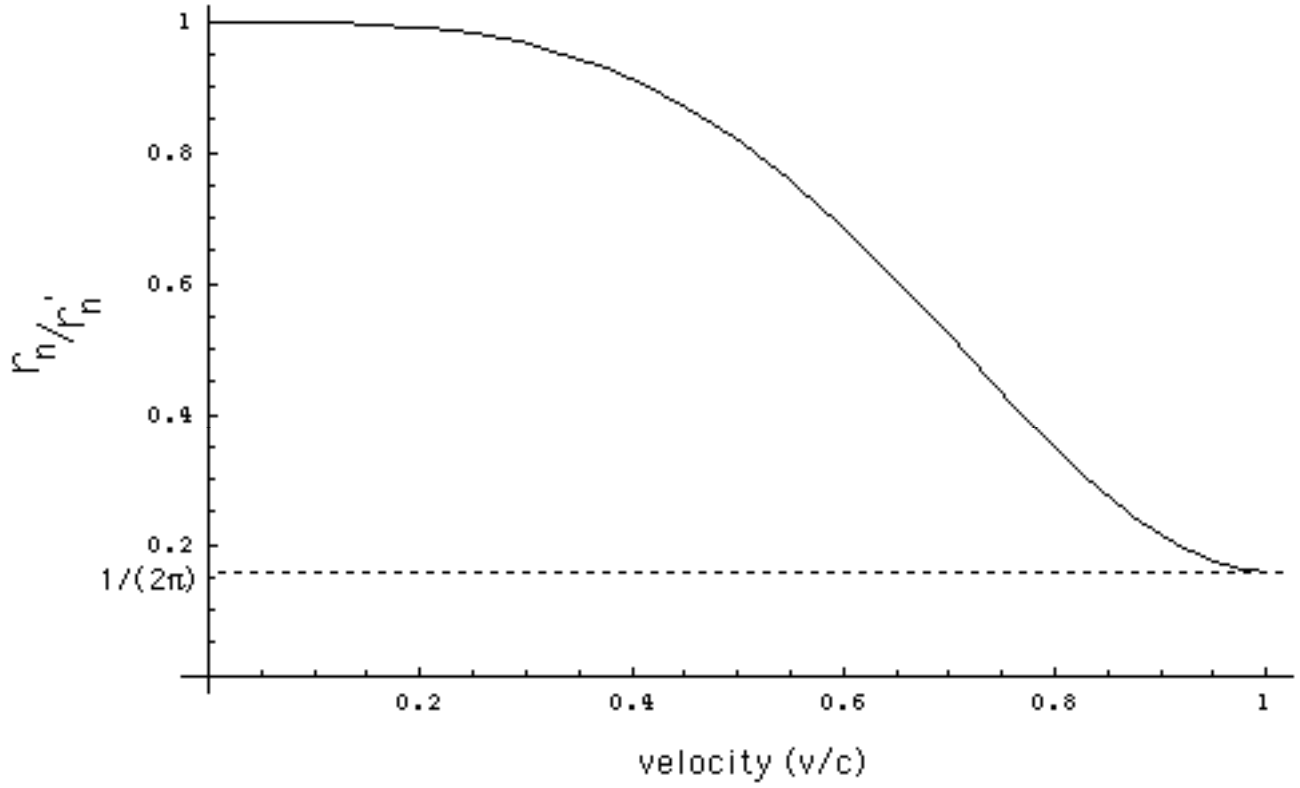

Figure 16A.

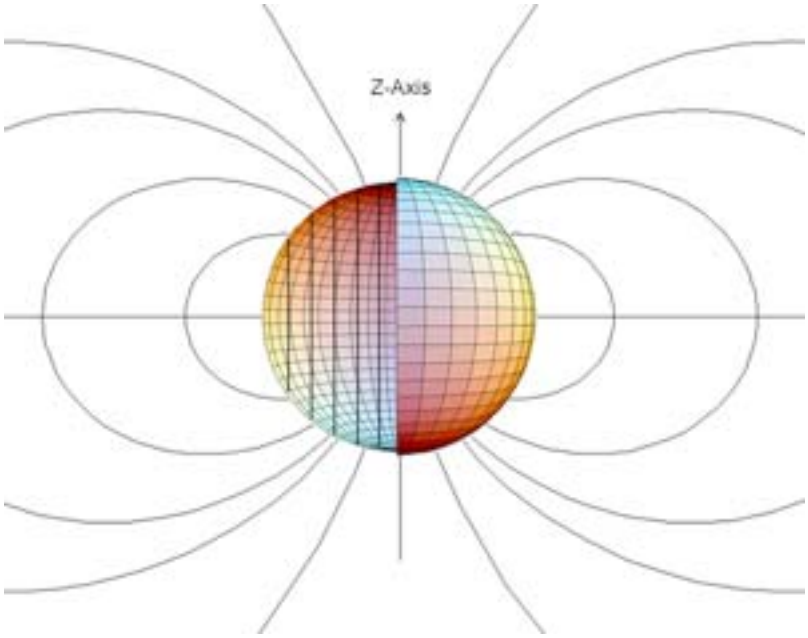

Figure 16B.

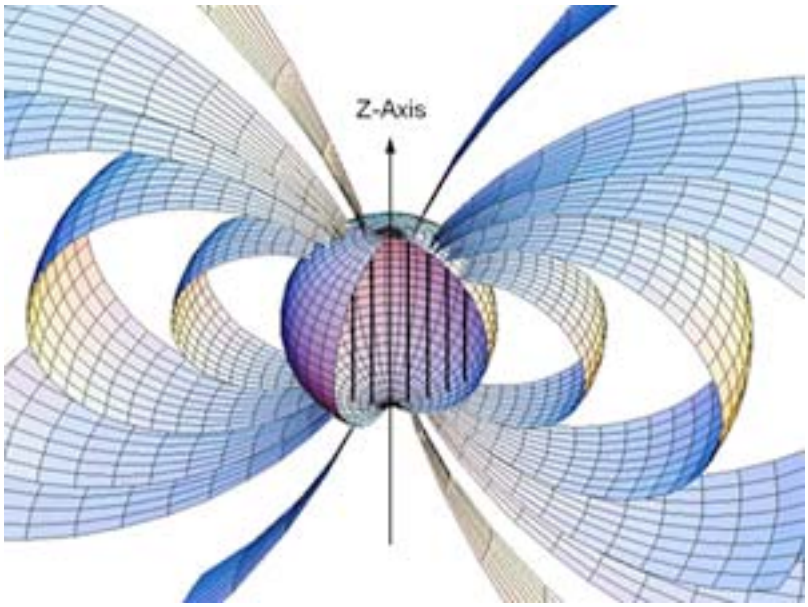

Figure 17.

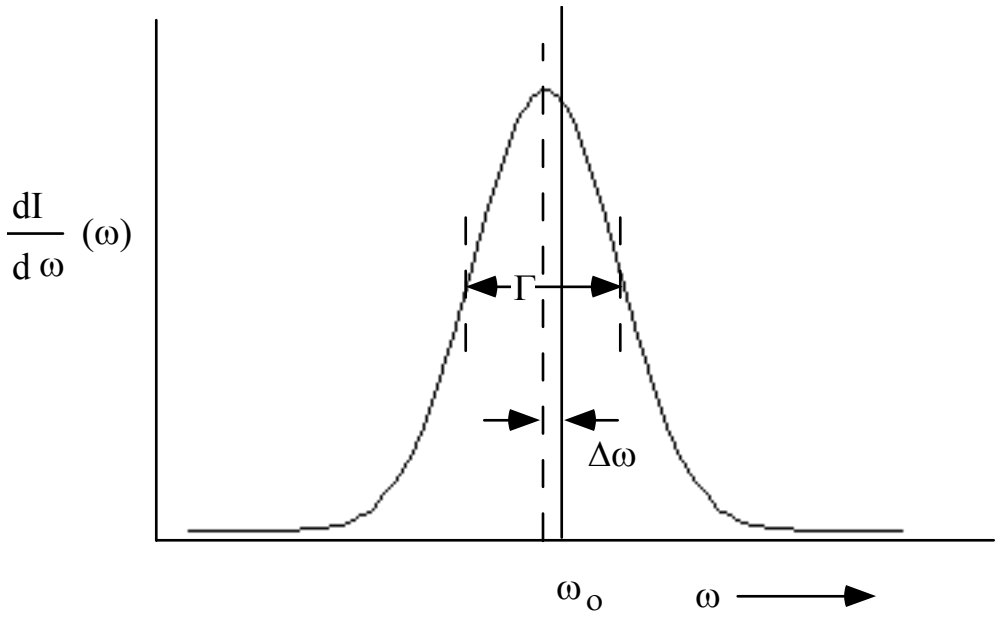

Figure 18.

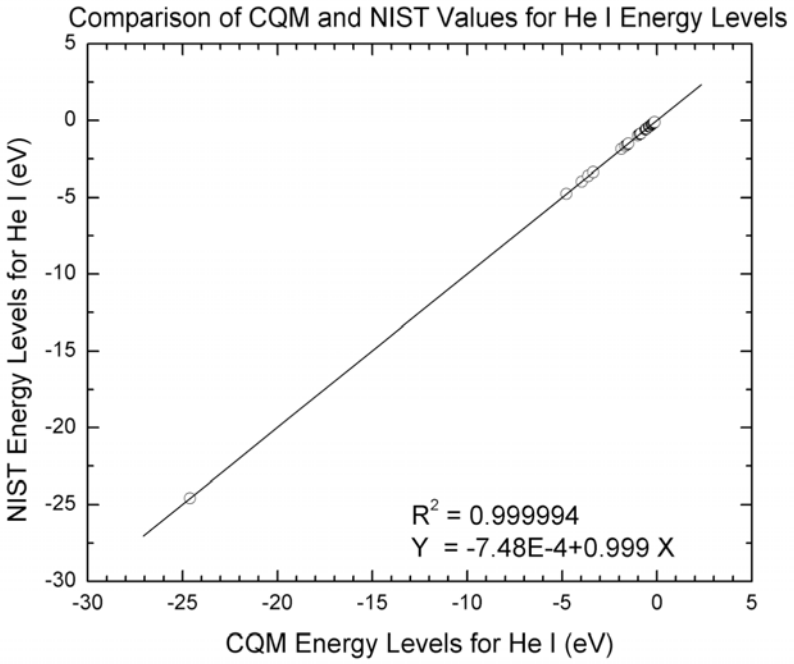
Comparison of CQM and NIST Values for He I Energy Levels
NIST Energy Levels for He I (eV)
CQM Energy Levels for He I (eV)
5
0
-5
-10
-15
-20
-25
-30
-30
-25
-20
-15
-10
-5
0
5
R2 = 0.999994
Y = -7.48E-4+0.999 X

Figure 19.

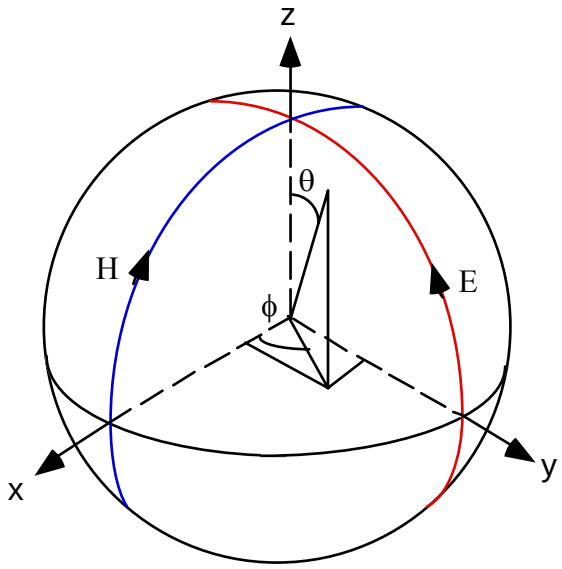

Figure 20.

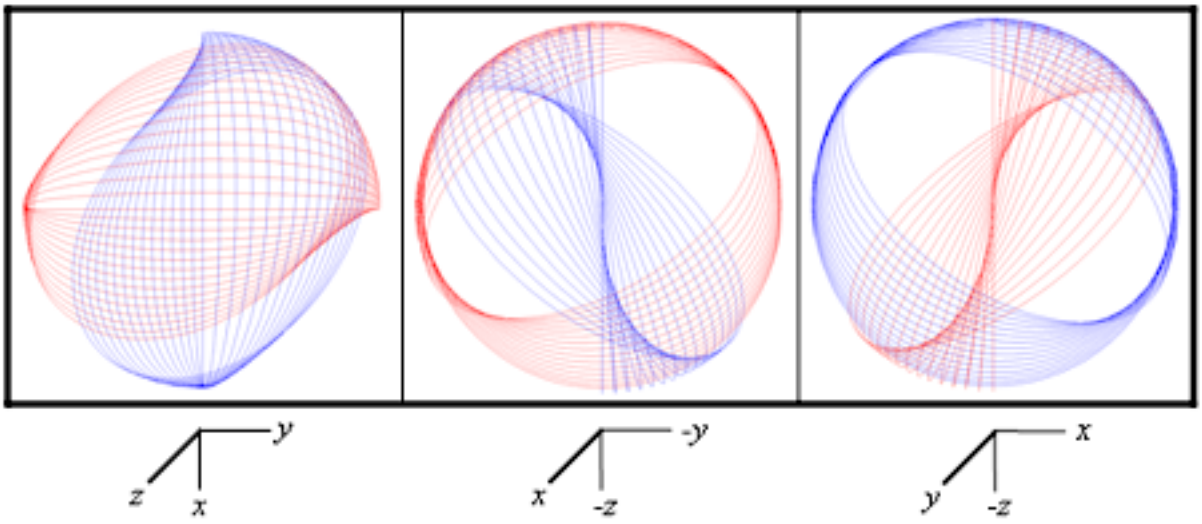

Figure 21.

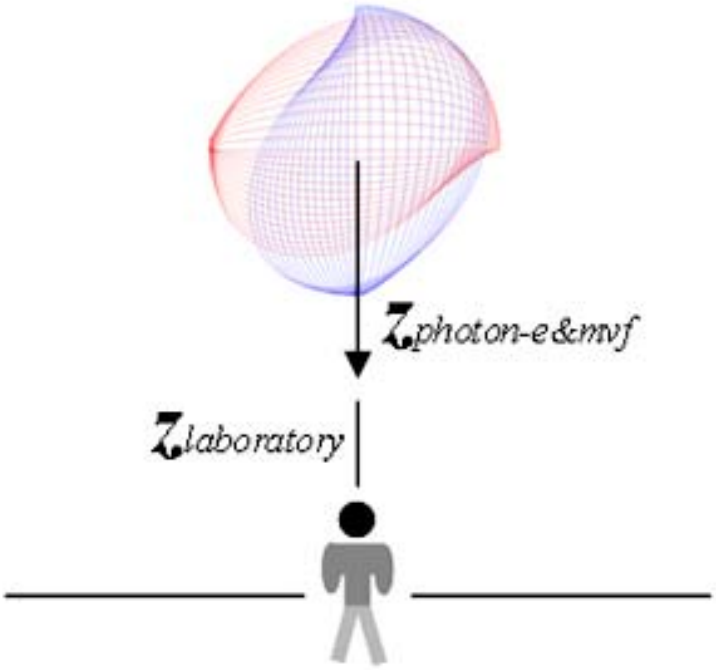

Figure 22.

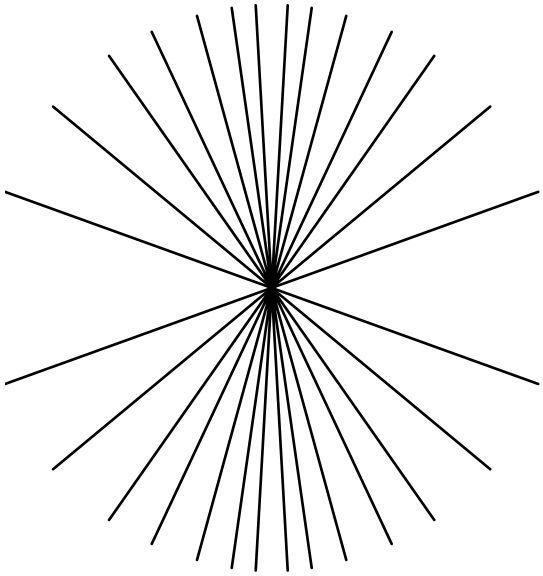

Figure 23.

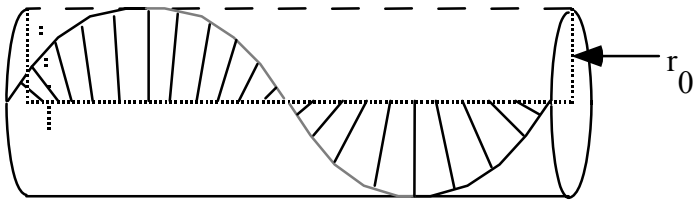

$$2 \pi r_0 = \lambda_0$$

Figure. 24.

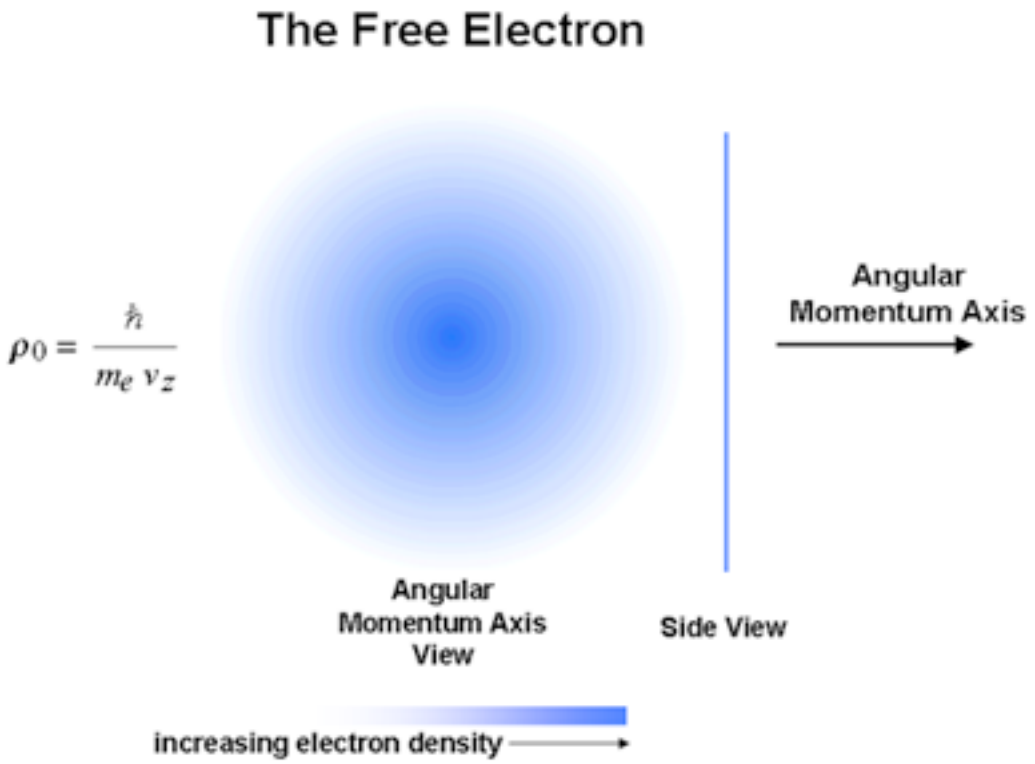
The Free Electron
$\rho_0 = \frac{\hbar}{m_e v_z}$
Angular
Momentum Axis
Angular
Momentum Axis
View
Side View
increasing electron density

Figure. 25.

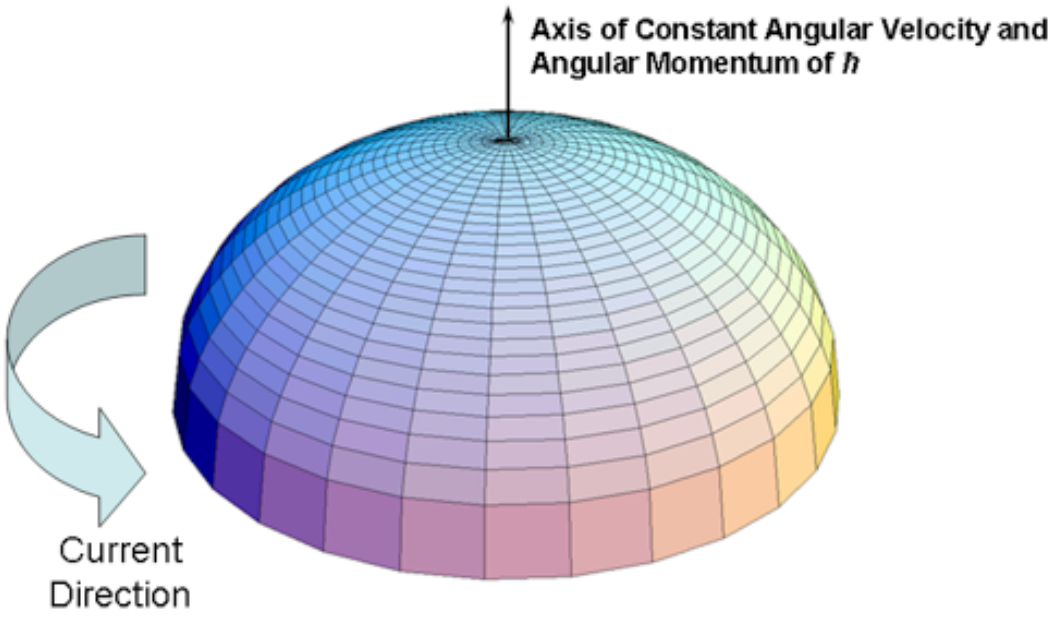
Axis of Constant Angular Velocity and
Angular Momentum of h
Current
Direction

Figure 26.

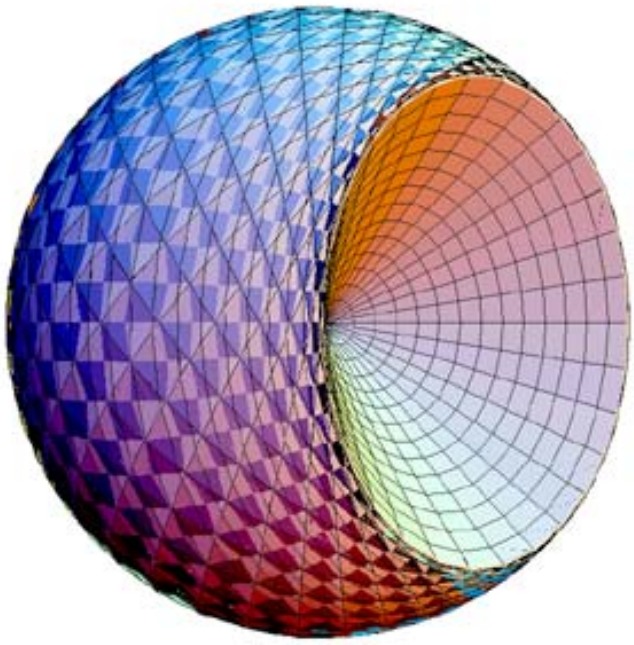

Figure 27.

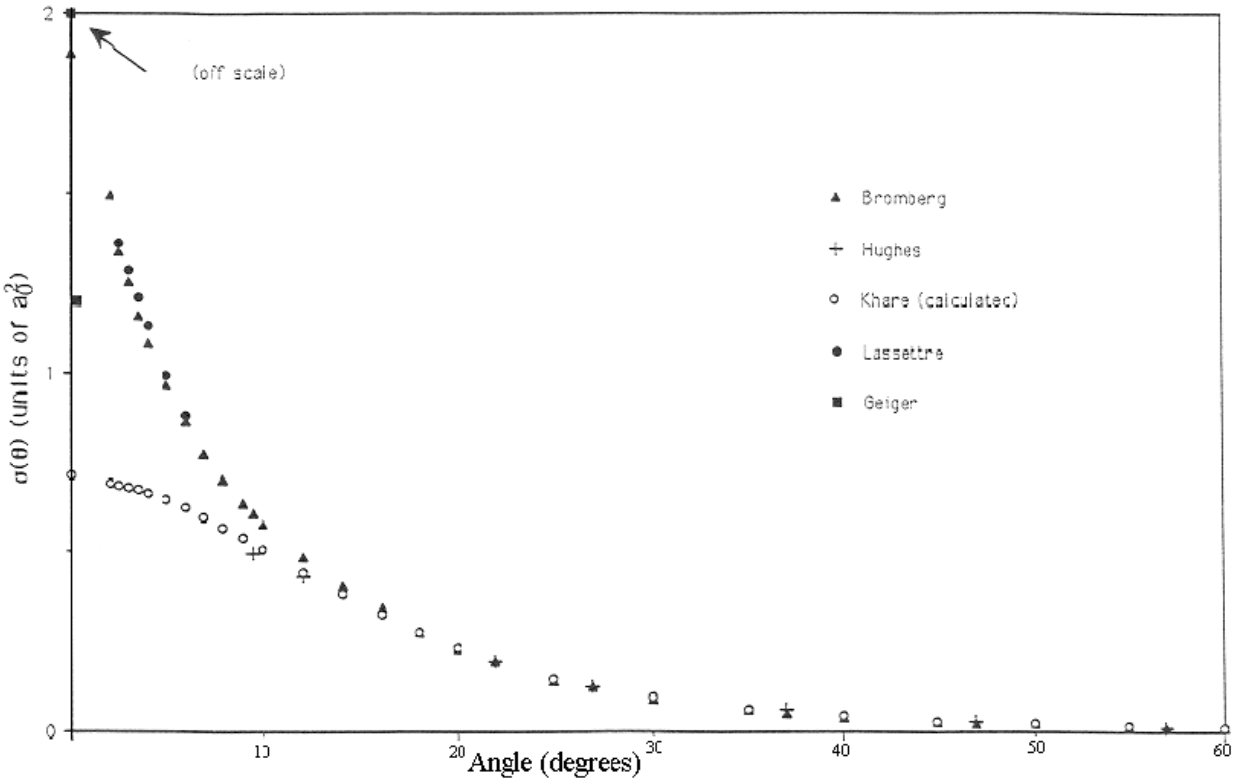
(off scale)
Bromberg
Hughes
Khare (calculated)
Lassettre
Geiger
σ(θ) (units of a0²)
Angle (degrees)
0
1
2
10
20
30
40
50
60

Figure 28.

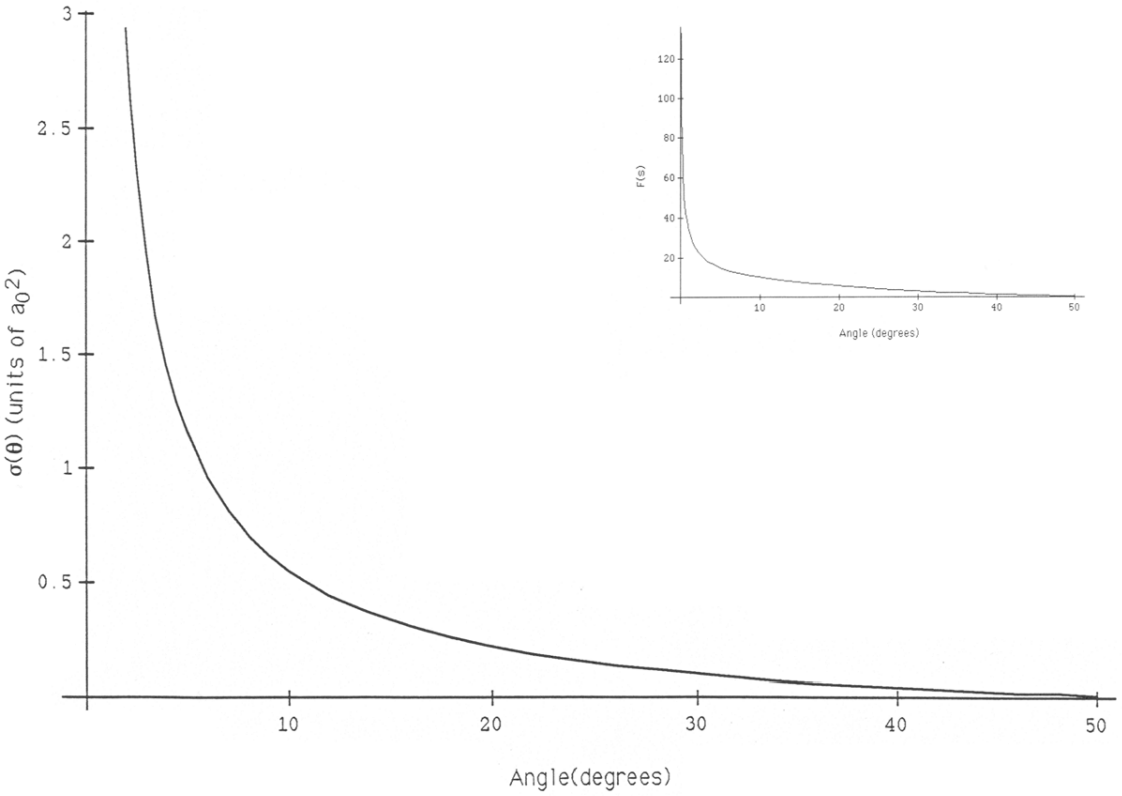

Figure 29.

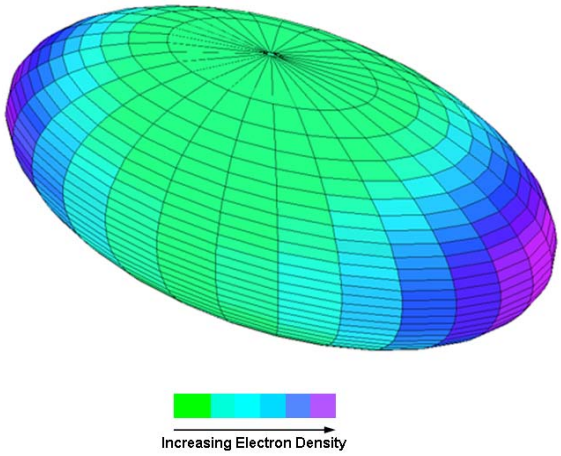

A

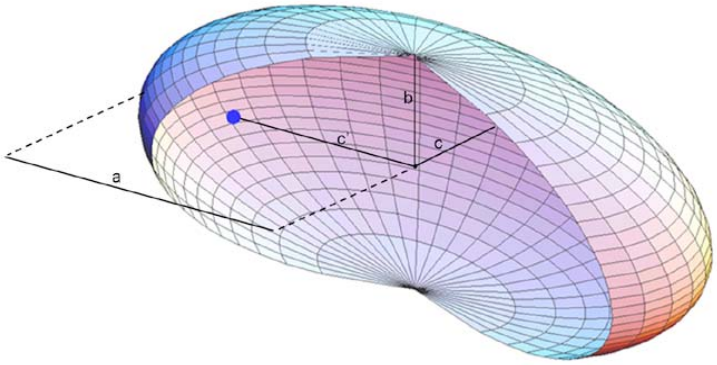

B

Figure 30.

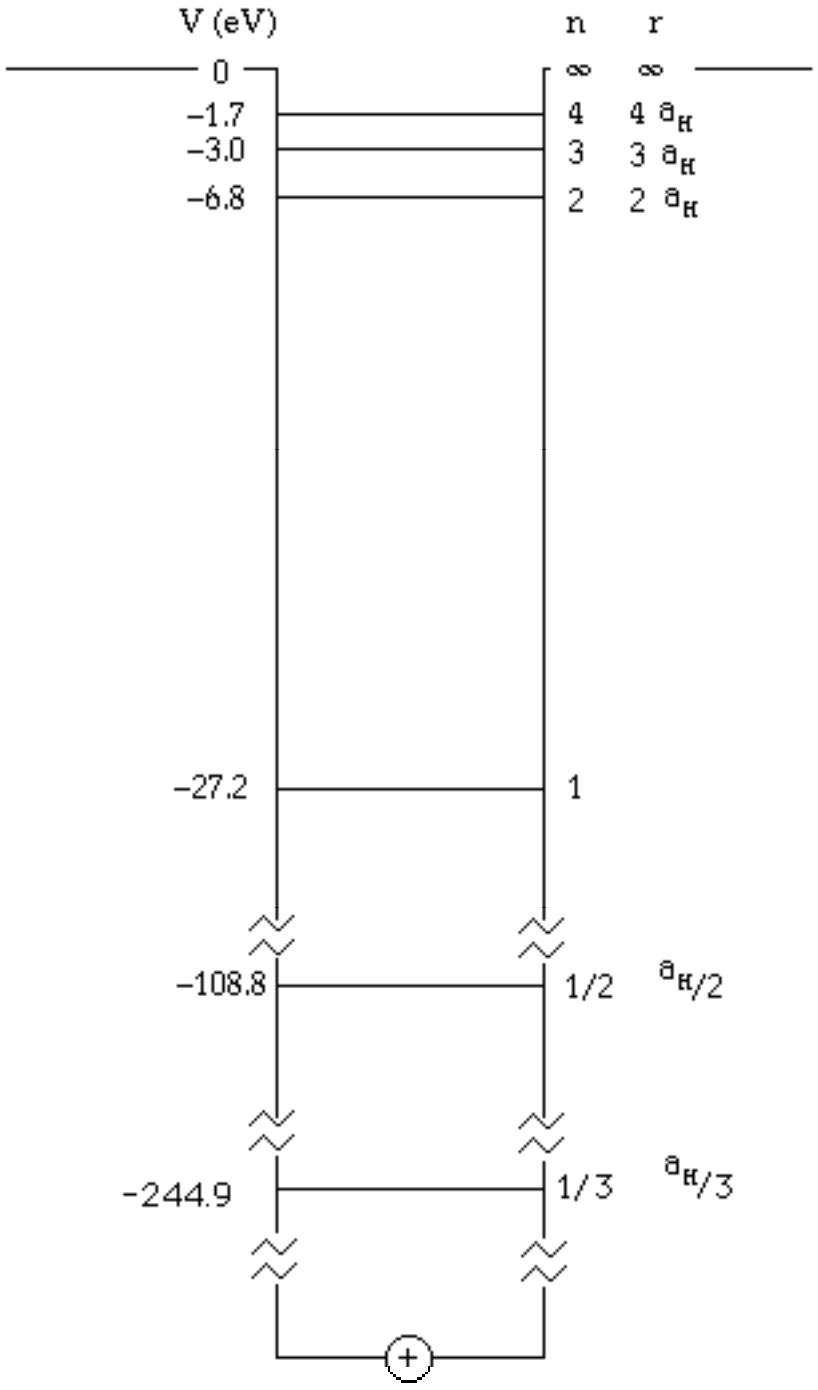

Figure 31.

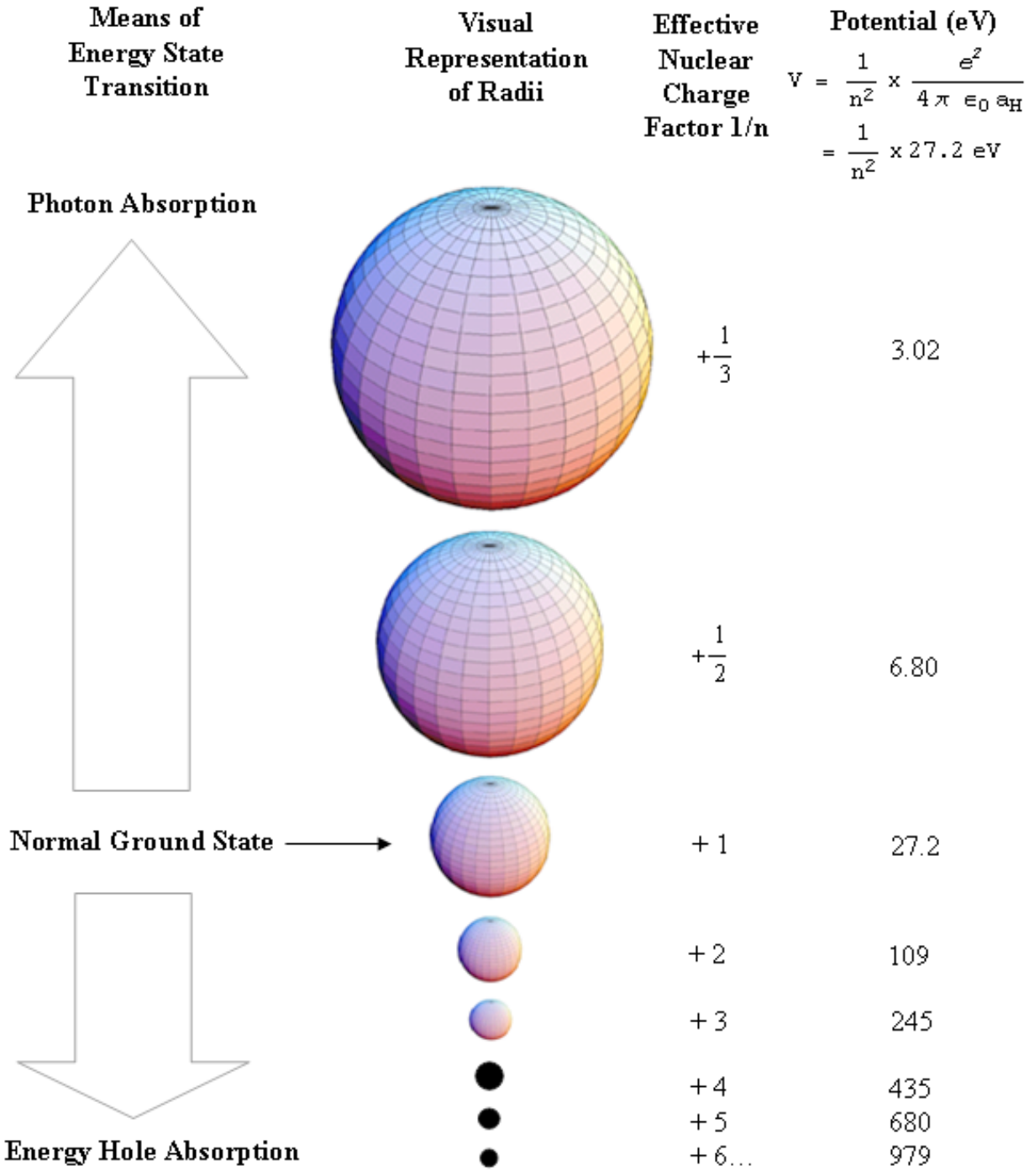
Means of Energy State Transition
Visual Representation of Radii
Effective Nuclear Charge Factor 1/n
Potential (eV)
$V = \frac{1}{n^2} \times \frac{e^2}{4\pi\ \epsilon_0\ a_H} = \frac{1}{n^2} \times 27.2\ eV$
Photon Absorption
Normal Ground State
Energy Hole Absorption
$+\frac{1}{3}$
3.02
$+\frac{1}{2}$
6.80
+1
27.2
+2
109
+3
245
+4
435
+5
680
+6...
979